POLITECNICO DI TORINO

Department of Structural, Geotechnical and Building Engineering

Master's Degree in Civil Engineering – Structures

IMPLEMENTATION OF A FINITE ELEMENT BASED MATLAB PROGRAM FOR THE BUCKLING ANALYSIS OF THIN-WALLED BEAMS WITH APPLICATION TO HIGH-RISE BUILDING STRUCTURES

Supervisors:

Prof. Giuseppe Lacidogna

Dr. Gianfranco Piana

Candidate:

Livia Bellogrado

A.Y. 2024 – 2025

To *Gianluca*,

with whom I shared not only the study,
but also the passion, determination and
dreams that have brought us here.

TABLE OF CONTENTS

ABSTRACT

In civil, mechanical and aerospace engineering, structural stability is an important issue when concerning open, thin-walled elements; for example C, L or Z profiles. These components are commonly found in lightweight structures due to their high strength-to-weight ratio, and can be subjected to buckling phenomena regarding local, distortional and global stability.

This thesis focuses on the global buckling of open thin-walled beams, with the main objective of implementing a Matlab code with an effective and versatile one-dimensional finite element formulation of literature. The Thesis combines theoretical formulations together with analytical and numerical modelling.

Firstly, the general concepts of structural stability and elastic buckling are recalled, discussing different types of bifurcation. Then, Vlasov's theory for open thin-walled sections is summarized. Also, the Finite Element Method (FEM) was introduced as a general and powerful tool to model behavior of beams subjected to various loading conditions and boundary conditions.

As an original contribution, a Matlab code was implemented to analyze elastic buckling of open thin-walled profiles by exploiting a finite element formulation of literature which uses exact or approximated interpolating functions. This code aims at being an open tool allowing to get quick solutions and to be easily embedded into more general Matlab codes.

In the last part of the Thesis, the analysis was extended to tall buildings, providing a global view of the effects due to wind and seismic loads, also considering the correlation between the global stability and local buckling of a structural element.

The results obtained by the formulation implemented were compared with others available in literature or with those obtained with a commercial finite element program.

The program implemented allows for the global elastic buckling analysis of straight beams with open cross-section under different loading and boundary conditions.

Tapered beams can be analyzed by connecting a discrete sequence of segments of uniform cross-section each, but with different sections from segment to segment.

Possible future developments can consider a parallel-arranged system of open thin-walled beams, as well as open-section profiles having local closures at specific locations, like those of present in some tall building structures.

1. INTRODUCTION

Buckling and structural stability is a fundamental topic for civil, mechanical and aerospace engineering practitioners. The phenomenon of buckling is especially important for thin-walled and open-section members that are extensively used in engineering applications due to their high strength-to-weight ratio and structural efficiency. Indeed, thin-walled and open-section members form the backbone of many lightweight structural work modules (i.e. frames, bridges, aerospace components) in engineering applications. However, owing to their geometry they are also more prone to buckling phenomena (local, distortion, global, etc.). Furthermore, the complex behaviors of these members under load do require robust and extensive analysis, which takes into consideration the geometry and the boundary and loading conditions.

The primary aim of this thesis is to investigate the buckling behavior of thin-walled open-section rods, particularly the mechanisms of buckling and what factors affect their capacity under load. This investigative work is carried out using a combination of theoretical analysis, numerical simulations, and structural analysis using computational software.

The discussion proceeds on the basis of the fundamentals of buckling and the main theories of elastic buckling then proceeds to an analysis of the geometric and mechanical properties of the thin-walled open sections. At the end of this discussion, numerical analyses of results and concluding comments are documented, for the express purpose to know and understand the phenomenon and what its implications are for design.

The thesis is divided into eight main chapters, each developing a specific component of the problem being investigated. The first chapter introduces the notion of structural stability and provides an overview of the main types of buckling phenomena as bifurcation instability, limit point instability and snap-through instability.

The relationship between the global stability of the structure as a whole, and the local stability of each individual section, is also examined, at this point.

Following that, there is a detailed exploration of the Vlasov postulate that is key to open-section, thin-walled elements. The exploration how the internal stress distribution - the axial and tangential stresses - will affect the buckling behavior of this form of structural element.

The focus is on elastic buckling of this type of thin-walled open section member and reference will reveal the elastic stiffness operator, geometric stiffness operator, the equilibrium equations and the elastic potential energy. The investigation will also include a specific case of uniformly compressed beams.

An important aspect of the investigation to ensure a full representation of the topic, and therefore, to clarify torsional behavior of thin-walled sections is the shear center methodology, which will include descriptions of the various methods of calculating shear center for a number of geometries including rectangles and C-sections.

The thesis will in addition include the consideration of the Finite Element Method (FEM) applied to modelling and investigation of behavior of thin-walled sections. It will also discuss polynomial elements, interpolation functions and the stiffness matrices. The thesis will also consider some real applications for beams subjected to different loading and boundary conditions.

The last part of the thesis will involve the application of stability concepts to tall buildings involving lateral (transverse) load distributions coming from wind or seismic action. It will also investigate local stability of structural elements, and the relationship between global instabilities with local instabilities, including some notes on implications for design.

In providing this context, and to represent effectively and interpretively the buckling phenomenon of open-wall thin sections, the thesis will adopt a mixed theoretical, analytical and application based methodology. The outcomes will provide effective, simple and quick tools for the elastic buckling analysis, including the possibility to be embedded into more general Matlab codes.

2. STABILITY

2.1 Preliminary Considerations about Stability and Equilibrium

Structural stability is the ability of a structure to maintain its shape and resist deformation or collapse under the action of external loading, e.g. earthquakes, wind, snow and environmental factors, among others. Structural stability is, mainly, known as a field of mechanics that studies the behavior of structures under compression [1].

A structure is referred to as stable if it can retain its equilibrium under the applied loads, and any small perturbation does not cause the structure to fail or collapse [1].

Analyzing this concept more in detail, it is possible to say that, considering a system, the concept of stability is linked to the idea that a small disturbing action does not change the state of equilibrium achieved, while the concept of equilibrium is connected to the permanence of the system in the state in which it finds itself, in the absence of disturbing actions and under the effect of the forces applied to it [2].

Taking into account an elastic body, like a beam, called *Ci* the generic equilibrium configuration under the action of the load F applied to it, if the external actions are suddenly made to vary by ΔF, that for hypothesis is very small, the body assumes a new configuration very close to the initial one [2].

If the perturbing cause of ΔF is removed, depending on the behavior assumed by the system, it will be said that the body, in configuration C_i, is in equilibrium:

- Stable: if it returns to the initial configuration;
- Unstable: if it takes on new configurations different from the previous ones;
- Indifferent or neutral: if it remains in the assumed configuration [2].

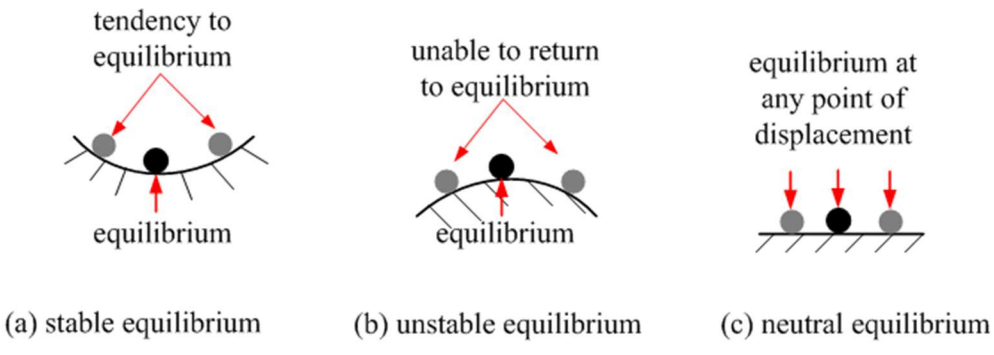

Figure 1: Stable (a), Unstable (b) and Indifferent (c) equilibrium configurations [29]

Depending on whether the loss of stability concerns more or less conspicuous parts of a structure, instability can be defined:

- Global: if it affects the entire structure (e.g. an arch or a vault):
- Partial: if it affects only a part of the structure (e.g. the compressed beam of a truss);
- Elementary: if it affects only one element of the structure (e.g. a frame member);
- Local: if it affects a part of an element (e.g. the outline of the core of a solid-walled beam).

Instability can only occur in structures that are either long and slender or relatively thin, meaning their thickness or one of their dimensions is significantly smaller compared to the others [2].

2.2 Stability of a Structure

As can be easily understood, the stability of a structure, in relation to the forces that are applied to it, represents a critical aspect of structural engineering.
In particular, structural stability refers to the ability of a built system or structure to maintain its equilibrium under the influence of external forces without experiencing failure or collapse, therefore the behavior of structures subjected to different loading conditions have to be analyzed [3].

When a structural stability analysis is performed, there are a lot of aspects that have to be taken into account, such as load-bearing capacity, material strength, geometric configuration, and the effects of dynamic forces like wind, seismic activity, and temperature variations [3].

Structural stability assessment need computer simulations and physical testing to assess the structural integrity and performance under different loading scenarios.
In particular, thanks to finite element analysis, structural dynamics analysis, as well as experimental tests, can be a valuable aid to predict structural behavior and which elements are most likely to collapse or failure [3].
To reduce the possibility of structural failures and increase the durability of structures, it is possible to follow the design guidelines that allow for comprehensive stability

assessments. This way, the structure is designed in a way that the structures can withstand forces such as wind, seismic activity and material fatigue, improving overall safety and longevity [3].

To improve structural stability, it is necessary to adopt appropriate design practices, choose suitable materials and use advanced calculation methods. It is also possible to use reinforcement techniques and retrofit solutions to increase stability and robustness [3].

As far as existing structures are concerned, regular monitoring, continuous maintenance and scheduled inspections are of paramount importance to detect potential stability, collapse and deformation problems at an early stage [3].

Thanks to technological innovations and design standards, analysis techniques to assess the stability and safety of structures are increasingly improving, which make it possible to promote more sustainable and resilient built environments [3].

2.3 Structural Instability

Taking into account the behavior of structures under a sufficiently high compressive force (or stress), that leads to losing its stiffness, experiencing a noticeable change in geometry, and becoming unstable, it is possible to notice that the structure loses its capacity to carry the applied loads and is incapable of maintaining a stable equilibrium configuration [4].

Examples of structural instability include:

- buckling of a column under a compressive axial force,
- lateral torsional buckling (LTB) of a beam under a transverse load,
- sideways buckling of an unbraced frame under a set of concentric column forces,
- etc... [4].

2.4 Types of Instability

Instability can generally be classified into: Bifurcation (branching) instability, limit point instability, finite disturbance instability, and snap-through instability [4].

2.5 Preliminary Information about Bifurcation

The phenomenon of bifurcation, which is a fundamental concept in the mechanics of materials and stability theory, is related to dynamic analysis and occurs when a system, subjected to loads, passes through a critical point where its behavior characteristics change drastically. Bifurcation theory is the mathematical study of how the qualitative or topological structure of a set of curves or the solutions of differential equations changes. In particular, the phenomenon of bifurcation occurs when, due to a small gradual change in the parameters of a System, a sudden change in the behavior of the structure is generated. Bifurcations can occur in both continuous and discrete systems, leading to significant changes in system dynamics [10].

2.5.1 Mathematical definition of bifurcation

Mathematically, a bifurcation occurs when the stability of an equilibrium points of a differential equation or a dynamical system change as a parameter varies. Consider a system described by:

$$\frac{dx}{dt} = f(x, \mu) \tag{2.1}$$

where: x represents the state variable, μ is a control parameter and $f(x, \mu)$ is a smooth function describing the system.

A bifurcation point occurs at $\mu = \mu_c$ when the qualitative nature of the solutions $x(t)$ changes, such as losing stability or branching into new equilibrium states [10].

2.5.2 Types of bifurcation

It is useful to divide bifurcations into two principal classes, local and global bifurcations:

Local Bifurcations: these are analyzed by examining changes in the local stability of equilibria, periodic orbits, or other invariant sets as parameters cross critical thresholds. Examples include:

- Saddle-Node Bifurcation: two fixed points (one stable, one unstable) collide and annihilate each other.
- Pitchfork Bifurcation: a single stable equilibrium splits into multiple equilibria, which can be stable or unstable depending on whether the bifurcation is subcritical or supercritical.
- Hopf Bifurcation: a stable equilibrium loses stability and generates a periodic orbit, which can be stable (supercritical) or unstable (subcritical).
- Trans-critical Bifurcation: two fixed points exchange stability as parameters are varied.

Global Bifurcations: these occur when larger invariant sets "collide" with each other or with system equilibria. They are often more difficult to analyze and typically involve complex topological changes [10].

2.5.3 Considerations

By understanding the phenomenon of bifurcation, it is possible through structural engineering, to predict and prevent undesirable behavior of structures, making sure that they remain in a state of stable equilibrium during their use, thus preventing failures or instabilities [10].

Bifurcation can happen in multiple instances:

1. Buckling of beams and columns represent a structural element that compresses to a point that exceeds a critical load that generates stability and instability, i.e., two equilibria.

2. In fluid dynamics, the transition from laminar flow to turbulent flow can be represented with a bifurcation diagram.
3. When predator-prey dynamics have bifurcation effects when the rates of change of population either increase or decrease.
4. In economics, the initial changes of markets occurring from crashes or shocks can be analyzed using bifurcation theory [10].

2.6 Buckling and Post-buckling of Conservative Systems

Conservative mechanical systems, particularly elastic structures subjected to potential loads (primarily dead loads), constitute a significant topic of interest in the study of bifurcation phenomena. Numerous academic works are dedicated exclusively to this subject.

The pertinent theoretical framework, commonly referred to as Buckling and Post-Buckling Theory, is predominantly formulated within a static context. This is because dynamic effects are generally considered irrelevant to the stability of such systems [11].

In the analysis of static systems, the initial step involves determining the fundamental equilibrium path, which represents the succession of equilibrium states traversed by the system as a control parameter is progressively increased from zero.

This evaluation can be conducted either numerically, via continuation methods, or analytically (or semi-analytically) using perturbation or asymptotic methods. While continuation methods offer a high degree of accuracy, their application requires repeating the analysis for every new set of parameters, such as varying imperfections [11].

Conversely, perturbation methods, although approximate, provide explicit analytical expressions that facilitate parametric studies.

Once the fundamental equilibrium path is established, the occurrence of bifurcations along this path must be thoroughly examined.

The bifurcation analysis involves the resolution of the following points:

a) an eigenvalue problem associated with the bifurcation parameter,

b) a sequence of linear equations, all governed by the same singular operator.

Bifurcations can occur at branch points, which represent many different paths are intersecting, or at bend points, which represent the existence of limit loads [11].

The perturbation method has advantages:

a) It is possible to make asymptotic expressions for the branched equilibrium paths,

b) It is possible to learn about the impact of imperfections, which usually diminish the maximum load we can sustain,

c) It is possible to make non-trivial fundamental paths, by extrapolating from the equilibrium points we have, we can estimate the limit loads [11].

2.6.1 Static analysis of conservative systems

The nonlinear equilibrium equation of an undamped elastic system with n degrees of freedom (DOF), subjected to positional conservative forces influenced by a single parameter μ, can be derived from the stationary condition of the Total Potential Energy (TPE) [11].

$$\Pi(\mathbf{q}) \coloneqq U(\mathbf{q}) + \mu V(\mathbf{q}) \tag{2.2}$$

Here, *U(q)* represents the elastic potential energy of the system, which is assumed to be positive definite. *V(q)* denotes the potential energy of the applied loads, while q is the vector of Lagrangian parameters describing the system's configuration.

The stationary condition of the Total Potential Energy, Π, is expressed as:

$$\delta\Pi(\mathbf{q}) = \left(\left[\frac{\partial U}{\partial \mathbf{q}}\right]^T + \mu\left[\frac{\partial V}{\partial \mathbf{q}}\right]^T\right)\delta\mathbf{q} = 0, \qquad \forall\delta\mathbf{q} \tag{2.3}$$

which implies:

$$\frac{\partial U}{\partial \mathbf{q}} + \mu\frac{\partial V}{\partial \mathbf{q}} = 0 \tag{2.4}$$

This expression represents the nonlinear equilibrium equation of the system.

By definition, the internal elastic force is given by:

$$\mathbf{f}^{el}(\mathbf{q}) \coloneqq -\frac{\partial U}{\partial \mathbf{q}} \tag{2.5}$$

and the positional external force is defined as:

$$\mathbf{f}^{ext}(\mathbf{q}) \coloneqq -\frac{\partial V}{\partial \mathbf{q}} \tag{2.6}$$

Therefore, Equation 4.3 can be equivalently rewritten as:

$$\mathbf{f}^{el}(\mathbf{q}) + \mu \mathbf{f}^{ext}(\mathbf{q}) = 0 \tag{2.7}$$

Alternatively, this can be written via a direct equilibrium approach, i.e., particularizing the cardinal equation of dynamics [11]:

$$\mathbf{M}\ddot{\mathbf{q}} = \mathbf{f}^{int}(\mathbf{q}, \dot{\mathbf{q}}) + \mu \mathbf{f}^{ext}(\mathbf{q}, \dot{\mathbf{q}}) \tag{2.8}$$

2.6.2 Equilibrium paths and bifurcation

The (generally multiple) solutions of the nonlinear Equation to define $\mathbf{f}^{el}$ characterize the equilibrium paths of the system, typically represented in a parametric form such as $\mathbf{q} = \mathbf{q}(s)$ and $\mu = \mu(s)$, where s denotes a control parameter.

The primary objective of static bifurcation analysis is to thoroughly describe the neighborhoods surrounding the singularity points that occur along these equilibrium paths.

Achieving this objective requires two main tasks:

a. identifying and characterizing the singularity points, and
b. in the case of branching points, constructing the paths that emerge from these points.

Regarding the construction of equilibrium paths, two approaches are commonly employed: numerical and analytical methods [11].

2.7 Observation about Elasto-Plastic Buckling of Planar Beam Systems

Analyzing elasto-plastic buckling of planar beam systems is invariably complicated when considering buckling behavior beyond the elastic limit, both from an algorithmic and conceptual standpoint [11].

Algorithmically, it is not possible to derive equilibrium equations using the familiar stationary condition from total potential energy, as there is no potential for a non-conservative system, and we will need to use a different route, such as the direct method or the principle of virtual work. Further, the piecewise nature of the constitutive law to describe the mechanical behavior of the system through its stages of plasticization, makes the task of evaluating the response of the entire system incrementally [11].

Conceptually, even though static analyses based on energy criteria are readily applicable to elastic systems, it is not possible to easily hold the same assumption for elasto-plastic systems due to the obvious elastic unloadings. However, under monotonic increasing stresses, the system will tend to act as a nonlinearly elastic structure, somewhat allowing for the more classical analytical techniques [11].

2.8 Bifurcation Instability

Bifurcation instability happens when deformation that occurs in one direction suddenly changes to another direction. An example is that of a perfectly straight column subject to a concentric compressive load. When the load is first applied, the column shortens or experiences axial deformation in the direction of the applied force [4].

When the applied load gradually increases, there comes a point when the mode of deformation suddenly switches from one of axial to one of lateral in which the column buckles in a direction perpendicular to the direction of the applied force. The load at which this occurs is referred to as the bifurcation, or critical, load. Bifurcation instability can be symmetric or asymmetric [4].

As shown in *Fig. 2*, for symmetric bifurcation the secondary equilibrium path, that is the equilibrium path that corresponds to the buckled configuration of the structure, is symmetric about the primary equilibrium path (the equilibrium path that corresponds to the pre-buckled configuration of the structure) [4].

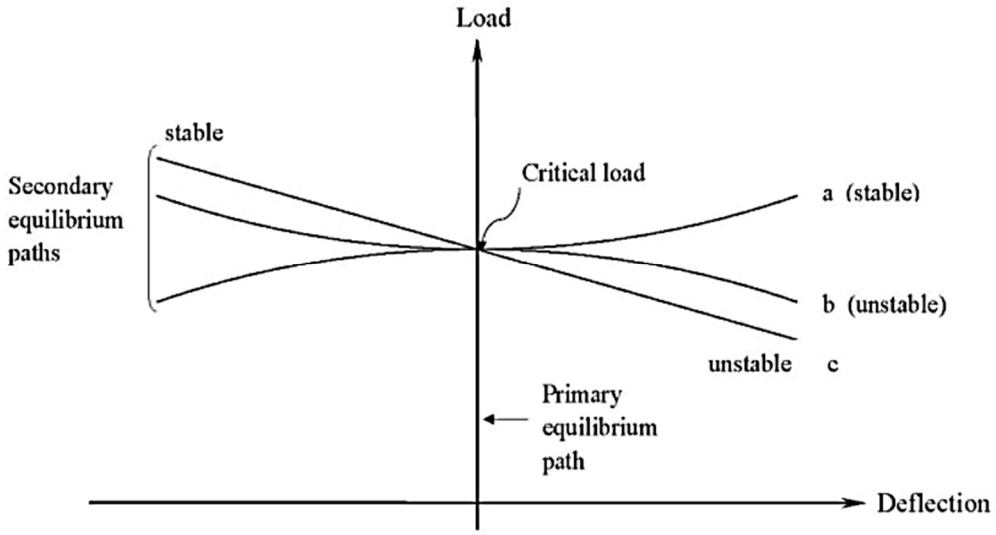

Figure 2: Bifurcation Instability [4]

Symmetric bifurcation is considered stable when the secondary equilibrium path rises above the critical load (as shown in *Curve a*), while it becomes unstable if the path drops below the critical load (as in *Curve b*).

A classic example of stable symmetric bifurcation is the elastic buckling of a perfectly straight, slender column under a centrally applied compressive load.

On the other hand, an example of unstable symmetric bifurcation is the elastic buckling of a guyed tower in asymmetric bifurcation, the secondary equilibrium path does not mirror the primary path (illustrated by Curve c). For instance, in a geometrically perfect L-shaped frame subjected to a concentric axial load on the column, the secondary equilibrium path may either drop below or rise above the critical load. This depends on whether the buckling direction causes the beam's shear force to act downward or upward on the column, respectively [4].

2.9 Limit Point Instability

Limit point instability refers to the scenario when a single deformation mode exists throughout the load history. The deformation increases when the load increases from start of loading to final failure. The load-deflection behavior of a structure that experiences limit point instability is shown in *Fig. 3*.

The maximum load that the structure can carry before failure is referred to as the limit load. Examples of structures that exhibit limit point instability are geometrically imperfect (crooked) columns subject to concentric compressive forces [4].

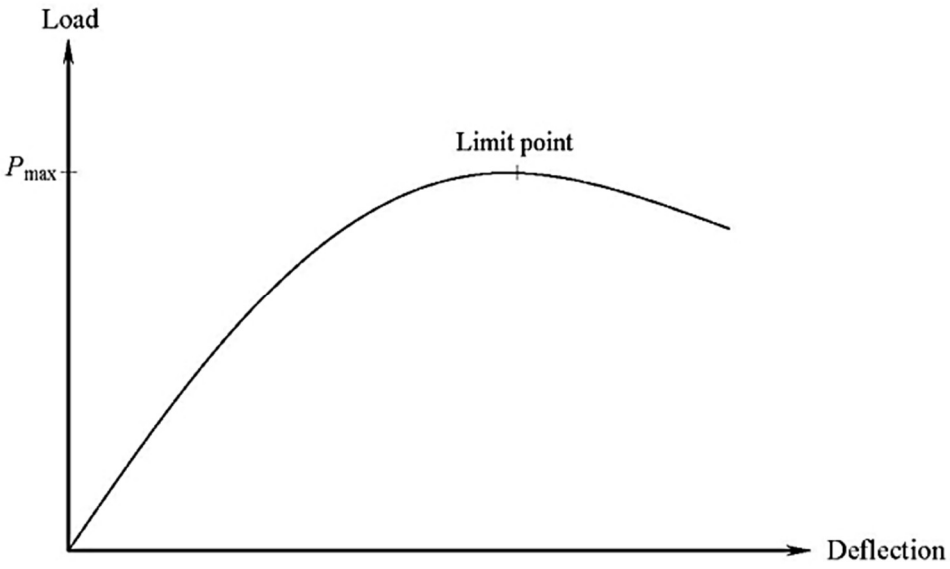

Figure 3: Limit Point Instability [4]

2.10 Finite Disturbance Instability

Finite disturbance instability occurs when a compressive force is applied along the longitudinal or axial direction of a thin-walled cylinder shell [4].

As depicted schematically in *Fig. 4*, the load-deflection curve rises to the (theoretical) critical load N_{cr}, then drops suddenly to a lower value in order for the structure to maintain equilibrium. The value of N_{cr} has been shown by Donnell and Wan to be very sensitive to the initial geometrical imperfections present in the shell. The slightest imperfections drastically reduce N_{cr} [4].

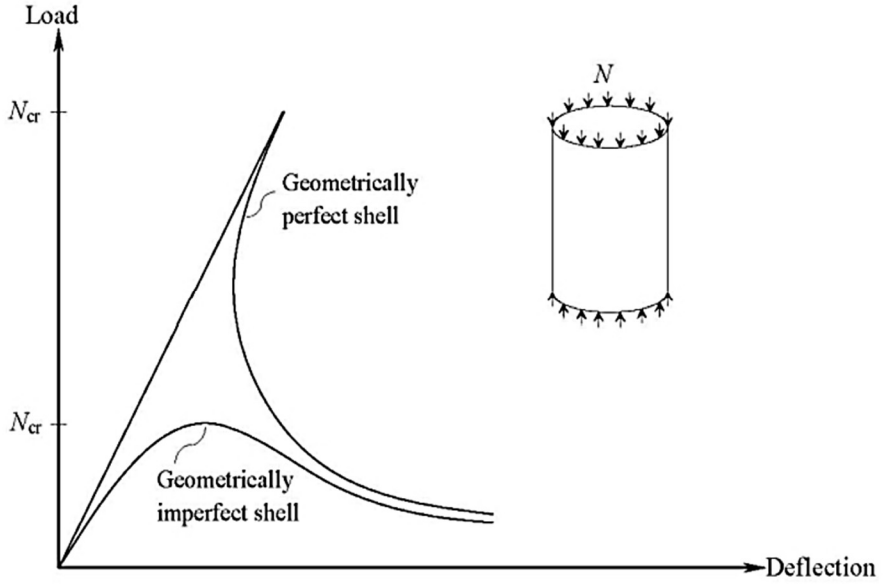

Figure 4: Finite Disturbance Instability [4]

Finite disturbance buckling is of particular interest for thin cylindrical shells because, unlike perfect elastic buckling, it accounts for the unavoidable geometric imperfections encountered during production. These geometric imperfections introduce loss of stability and reduce critical N_{cr} load considerably.

The N_{cr} values experimentally established are usually less than the theoretical N_{cr} values exactly because of these initial imperfections, emphasizing the importance of considering these imperfections in numerical models and design procedures.

2.11 Snap-Through Instability (limit-point instability)

Snap-through instability occurs when there is a sudden, large deformation under a constant load [4].

For certain systems, such as the in-plane buckling of a shallow truss or arch subjected to a transverse load, or the buckling of a shallow spherical cap under a radial load, equilibrium can only be maintained when the load reaches a critical point (*point A* in *Fig. 5*) [4].

At this stage, the displacement abruptly shifts from *point A* to *point B*, as indicated by the solid horizontal line. The dotted curved line represents an unstable equilibrium state, which can only be observed under ideal displacement-controlled conditions [4].

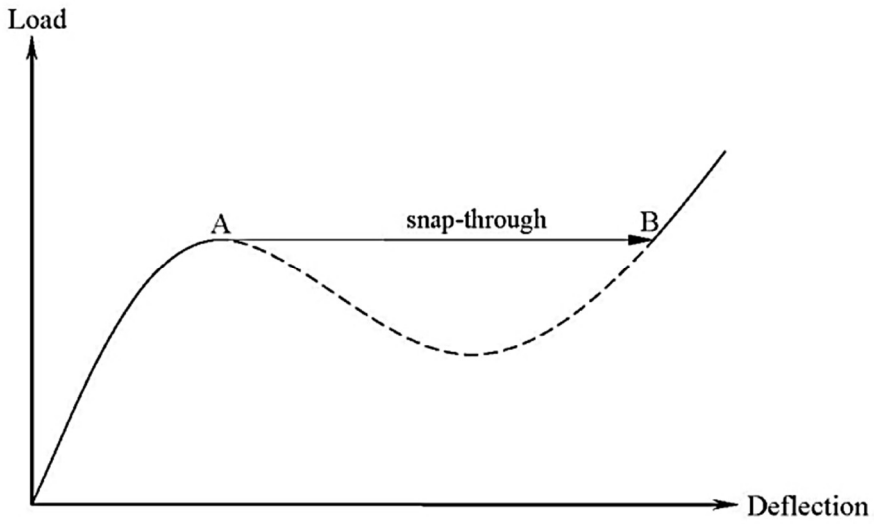

Figure 5: Snap-Through Instability [4]

Therefore, it is possible to say that Snap-Through Instability is a form of nonlinear geometric instability characterized by a sudden and non-gradual change in structural equilibrium, often modelled by force-displacement diagrams with bifurcations and multiple equilibrium paths.

This phenomenon is relevant for thin and light structures, such as arches, shells, trusses, deployable structures, MEMS systems, and shape memory materials. It is analyzed using methods such as finite element analysis (FEM) and bifurcation and post-buckling theories.

2.12 Stability in NTC 2018

When designing a structure, there are several effects that need to be taken into consideration. A building has to be able to transfer loads to the ground, this includes both vertical forces from the structural system and interior, and also lateral loads (Gardner, 2014).

In the Italian technical standard NTC 2018 (Technical Standards for Construction), there are references and definitions relating to the stability of structures [6].

The NTC 2018 states that structures must be designed and constructed in such a way as to ensure their stability under all expected load conditions. This includes resistance to phenomena such as buckling and global stability [6].

The standard specifies that the load-bearing capacity of the structures must be such as to guarantee stability, avoiding subsidence or collapse. The stability check must take into account all permanent, variable and accidental loads [6].

In addition, designers are required to perform specific analyses to evaluate the behavior of structures subjected to compressive or torsional loads. In particular, reference is made to buckling analysis for columns and beams [6].

Regarding the stability conditions, NTCs provide guidance on stability verification methods, including analytical and numerical methods. The constraint conditions and interactions between the different parts of the structure must also be considered [6].

The standard also defines the use of safety coefficients to take into account uncertainties related to materials, load conditions and construction methods [6].

Therefore, in summary, it is possible to say that the evaluation of the stability of a structure requires a careful analysis of both the individual sections and the overall stability, as the stability of the individual sections directly affects the overall stability, so it is essential to perform integrated analyses to ensure the safety and reliability of the structure as a whole [6].

2.13 Global Stability Analysis

Talking about Global stability, it is necessary to consider the entire structure and its capacity to maintain integrity if subjected to external loads and is influenced by the geometry of the structure, the materials used, and the restraint conditions [7].

Therefore, a global analysis considers the interactions between the different parts of the structure and their distribution of loads, and in particular it has the aim to identify buckling modes that can compromise overall stability [7].

2.14 Stability of Individual Sections

In addition to the overall stability, the stability of the individual sections must also be evaluated, so for each section the resistance to compression, bending, and torsional loads.

In particular, the stability of a section is determined by its load capacity, which must be sufficient to support the forces acting on it without experiencing excessive deformation or failure [7].

2.15 Global System Buckling

An entire building can buckle as a whole due to lacking stiffness created by the vertical members on each level of the building. The vertical elements need to ensure stability on each level of the building (Gardner, 2014).

It is useful to have a fairly constant utilization of the resistance on each story, so, it is generally beneficial to maintain a fairly consistent utilization of the resistance on each story, because a failure could develop on any level [7].

From a Rules point of view, in the Eurocode, the global buckling issue is taken into account by examining the elastic buckling load or conducting second-order analysis. Alternatively, the deflection can be measured to indicate a possible deficiency in the global stability of the structure [7].

2.15.1 Deflection

The deflection limits are defined in order to guarantee adequate comfort criteria for the occupants of the building and maintaining the safety and durability of the structure, so in general the guidelines for each floor collectively establish an overall deflection standard [7].

The deflection is an indicator of the effects of lateral actions, such as global buckling. A deflection can also lead to additional effects. One of these effects is when vertical loads act on these displacements (Hoenderkamp, 2002).
The eccentricities of the vertical loads can cause additional bending moments on the structure, which can cause global failure [7].

2.15.2 Member buckling

The instability can also occur in individual members of the system, when large deformations can develop and there is a redistribution of loads, due to the fact that the member will no longer be able to carry a load, this can cause other members to fail, due to the increase in load, until the entire structure becomes unstable [7].

As indicated in the Eurocode, the possible types of buckling instability that can occur in members, as already said before, are:

- flexural buckling (caused by compressive stresses), can lead members to deflect perpendicularly to loading in the weak axis, this type of instability is closely related to the *Euler critical load*, which defines the theoretical limit at which a perfectly straight and ideal member under compression becomes unstable and buckles;
- torsional buckling arises due to a lack of torsional stiffness;
- lateral torsional buckling (caused by bending stresses), can result in a deflection of flanges due to compression;
- plate buckling (caused by compressive stresses in either the webs or the flanges) that can occur in steel members where plates have been welded together to form a cross-section [7].

Euler buckling

As pointed-out before, the Euler buckling phenomenon is a specific case of flexural buckling, which occurs when a slender member under axial compression reaches its critical load and becomes unstable [26].

Let's consider a homogeneous, isotropic and perfectly straight beam, and assume that the (compressive) load is perfectly axial, that the stress state of the beam is purely elastic and that the deflection occurs on a single plane.

Given these assumptions, it is possible to derive a mathematical expression capable of describing this type of subsidence [26].

Now consider the boundary condition for which P is just above the critical load P_{cr}. Under these conditions, even a very small radial force F (imbalance) immediately leads to a deformation of the beam, which cannot be recovered even by eliminating the stress.

To describe this evidence mathematically it is possible to rely on the elastic line equation. For a beam supported by two supports (carriage hinge) and axially loaded, this second-order differential equation admits a solution for the displacement v which, considering that at the hinges this displacement must be zero, turns out to be:

$$v = C_1 \cdot sin\left(n \cdot \frac{\pi x}{L}\right) \tag{2.9}$$

In which L is the length of the beam while n is an integer called the number of half-waves. The constant C_1 represents the maximum deflection of the beam [26].

The minimum value of P, called the *Eulerian Critical Load*, is obtained with $n = 1$.

$$P_{cr} = \frac{\pi^2 EJ}{L^2} \tag{2.10}$$

This is the minimum load for which the member can be subjected to buckling.

"n =1" means that the deformation will simply be a single sine half-wave passing through the two points [26].

Conversely, with "n = 2", the value of the critical load quadruples but deformations can occur with a double wave (complete sine wave).

Analyzing the formula, it is possible to say that the value of the critical load does not depend on the strength characteristics of the material with which the beam is made but only on the length L, the inertial properties *J* and modulus of elasticity E. From Euler's formula it is also easy to guess how the instability of will occur in the plane with minimal inertial properties. From here it is immediate to understand why the columns often have a circular section (balanced moments of inertia) [26].

In the same way as for a member with double support, it is possible, starting from the equation of the elastic line, to determine the solution in terms of deflection *v* for a member with double interlocking which will result:

$$v = \frac{M_0}{P} \cdot \left[1 - cos\left(2\frac{\pi x}{L}\right)\right] \tag{2.11}$$

where M_0 is the constraining relation given by the interlocking. In this case, the critical load, considering $L_L = 0.5L$, is:

$$P_{cr} = \frac{\pi^2 EJ}{{L_L}^2} \tag{2.12}$$

L_L is called the free length of inflection, and represents the distance between two points where the bending moment is zero, its values are shown in the table below:

Pinned - Pinned	Fixed - Free	Fixed - Pinned	Fixed - Fixed
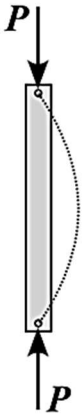	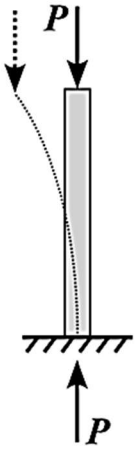	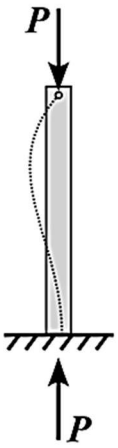	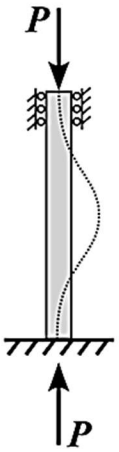
$k = 1$	$k = 2$	$k = 0.7$	$k = 0.5$
$L_L = L$	$L_L = 2L$	$L_L = 0.7L$	$L_L = 0.5L$
$P_{cr} = \frac{\pi^2 EJ}{L^2} = \frac{\pi^2 EJ}{L_L^2}$	$P_{cr} = \frac{\pi^2 EJ}{4L^2} = \frac{\pi^2 EJ}{L_L^2}$	$P_{cr} \approx \frac{2 \cdot \pi^2 EJ}{L^2} = \frac{\pi^2 EJ}{L_L^2}$	$P_{cr} = \frac{4 \cdot \pi^2 EJ}{L^2} = \frac{\pi^2 EJ}{L_L^2}$

Table 1: Euler free deflection lengths L_L and Critical Load P_{cr} for beams with different constrains, modified by [27], [28]

2.15.3 Additional stability effects

There are further effects in buildings that can cause lacking stability, such as thermal action, creep and moisture. Thermal expansion and contraction can either cause deformations or stresses dependent on the degree members are restrained. These additional effects can cause the structure to become unstable. The main components that affect the distribution of temperature are solar radiation, humidity, wind speed and changes in air temperature in shade (Radovanović et al, 2015).

There are a lot of factors that can influence the effects of the external forces acting on a structure, such as its orientation, climate, structural mass, geometry, and the materials used. Consequently, an important factor to take into account is the thermal effects. A possible solution is to implement suitable expansion joints that can help manage controlled expansion and contraction [7].

In addition, in concrete structures, moisture can cause shrinkage, leading to additional stresses in the system. Moreover, creep in these structures can reduce stiffness, increasing their susceptibility to instability issues [7].

2.16 Link between Section Stability and Global Stability

The stability of a single section is closely linked to the stability of the entire structure, that is because, of course, if a section exhibits unstable behavior this can negatively affect overall stability.

In particular, in composite structures, the behavior of one section can affect the load distributed over other sections.

This leads to the facts that stability checks of individual sections must be integrated with global analyses to ensure that even if each section is stable individually, the entire structure remains stable as a whole [8].

2.17 Methods of Analysis

Several analysis methods can be applied to analyze a structure:

- Linear Analysis: uses simplified models to define internal forces and deformations. Linear models may not be enough for complex structures or structures subject to different loads.
- Nonlinear Analysis: looks at how structures behave in real-life loading conditions, addressing that structures can sustain plasticity or buckling.
- Numerical Models: structural analysis programs, like Finite Element Method (FEM), can be used to analyze the behavior of complex structures and provide in-depth simulations [8].

The linear analysis is used when the relationships between the variables are easy and direct, and this means that the relation between the input and output is a straight line. Linear equations are used, therefore, they are the primary tool for this type of analysis. The non-linear analysis is used when the relationships between the variables are hard and indirect, because this means that the relation between the variables is not direct. More complex mathematical functions are needed; thus, they are used to model the relationships between the variables [8].

2.17.1 Linear analysis

Linear analysis is a branch of mathematics that deals with the study of linear relationships and systems. It involves analyzing and understanding linear equations, functions, and transformations using the principle of linearity such that the operations of addition and scalar multiplication preserve the properties of linearity.
Solving systems of linear equations, eigenvalues and eigenvectors, and behavior of linear transformations can be determined [8].

The features of linear analysis are:

- Linearity: the principle of superposition applies, so the total response to multiple inputs is simply the sum of the responses to each individual input.

- Proportionality: Linear analysis focuses on understanding proportional relationships, where the output varies directly with changes in the input.
- Additivity: Linearity in analysis entails that adding two solutions or inputs together results in the sum of their individual solutions or outputs.
- Homogeneity: if the input is scaled by a constant factor, also the output is scaled by the same factor.
- Linear Transformations: linear transformations are mappings between vector spaces that preserve linearity properties.
- Systematic Solution: Linear analysis provides systematic techniques for solving systems of linear equations.
- Eigenvalues and Eigenvectors: Linear analysis involves determining eigenvalues and eigenvectors of linear transformations.
- Generalization: Linear analysis serves as a foundation for more advanced mathematical concepts, allowing for generalizations to more complex systems [8].

2.17.2 Non-linear analysis

Non-linear analysis focuses on the study of complex mathematical functions, equations, and transformations that display non-linear behavior, which does not follow the principles of proportionality, superposition, or linearity [8].

The features of nonlinear analysis are:

- Non-linearity: Nonlinear analysis focuses on the study of relationships and systems that do not follow linear patterns or exhibit linear behaviors.
- Complexity: Nonlinear analysis and discourse engage with mathematically complicated functions and systems that often involve exponential growth, curves, and non-unique solutions.
- Sensitivity to Initial Conditions: Non-linear systems are sensitive to minor variations in the initial conditions, which also contributes to the butterfly effect and increased difficulties in making long-term prediction.

- Nonlinear Differential Equations: Nonlinear analysis deals with nonlinear differential equations, which model many different phenomena, and require special methods to analyze.
- Bifurcation Analysis: Non-linear analysis deals with changes to the qualitative behavior of a system as some parameter varies, referred to as bifurcation analysis.
- Numerical Methods: Non-linear analysis often employs numerical methods and computation, as closed form solutions are often not available.
- Nonlinear Optimization: it is concerned with optimization of non-linear objective functions subject to non-linear constraints requiring different optimization algorithms.
- Mathematical Modeling: Non-linear analysis is necessary for modelling and understanding complex real-world phenomena that exist in non-linear environments [8].

2.17.3 Numerical models

When dealing with a complex structure, to evaluate the stability, a good solution is the use of structural analysis software [9].

Finite Element Method (FEM) is a computational technique widely used in structural analysis to model and evaluate complex structures, because allows the simulation of how structures will respond to different loading conditions, including stress, strain, and displacement.

The approach, which is a numerical one, consists in subdividing a complex structure into smaller and simpler parts called finite elements, and then to study them by applying a set of equations that governs these elements based on physical laws [9].

FEM is a powerful instrument because is capable to handle complex geometries, materials, and boundary conditions, so it a versatile tool for a wide range of engineering applications.

In additions, since FEM works by creating a finite element mesh, it helps to simulate and analyze local effects and their impact on the overall structure [9].

3. VLASOV'S THEORY

Vlasov's theory is applied in the study of the torsion of open thin sections and is a generalization of Saint-Venant's classical theory of torsion, with the addition of the introduction of the concept of non-uniform torsion, which takes into account the deformation of the cross-section along the axis of the beam [18].

Vlasov's theory is the most widely used method to study the behavior of open thin sections subject to torsion, because it takes into account the phenomenon of warping, which cannot be neglected in these structures.

Therefore, it is applied when De Saint Venant's theory, which provides uniform torsion, is insufficiency [18].

This is the case, for example, for open sections (such as L, C, I, T, Z profiles), where the uniform torsion is not sufficient to describe the real behavior, since the thin walls deform along the longitudinal axis (warping), so that, when an open section is subjected to torsion, the cross-section does not simply rotate around its axis. but deforms out of the plane.

This leads to additional normal stresses (in addition to the classic tangential stresses of the Saint-Venant torsion). Vlasov's theory allows us to calculate the real torsional stiffness [18].

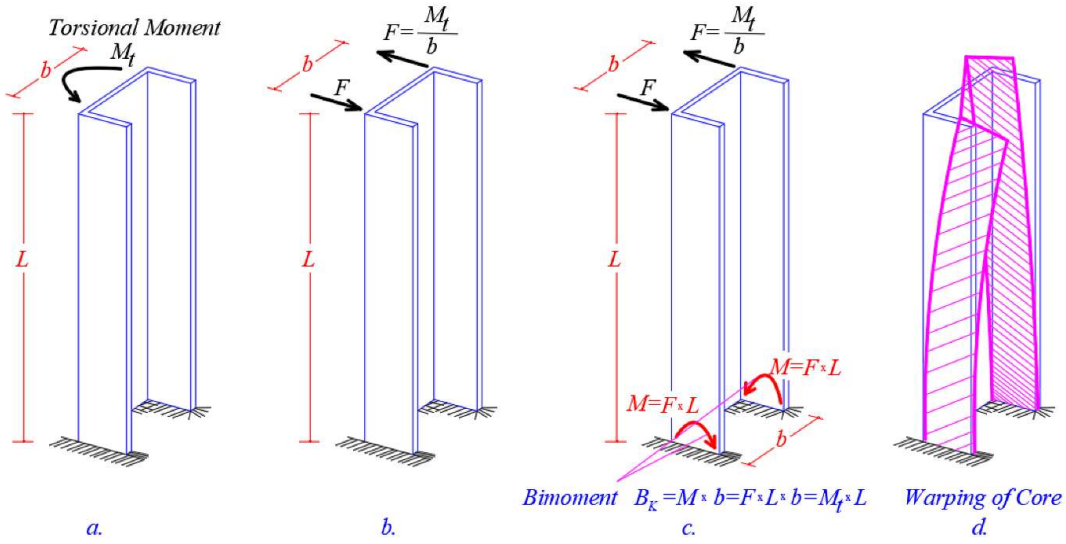

Figure 6: Bi-moment in a cantilever with thin-walled open cross-section and the torsion-warping phenomenon. (a) cantilever with a torsional moment at the top, (b) forces that produce the torsional moment, (c) bending moment and bimoment, (d) warping [18]

3.1 Introduction to Vlasov's Theory

A torsional load applied to a thin-walled open core generates a warping of the section, which would be prevented if the floors were infinitely rigid.

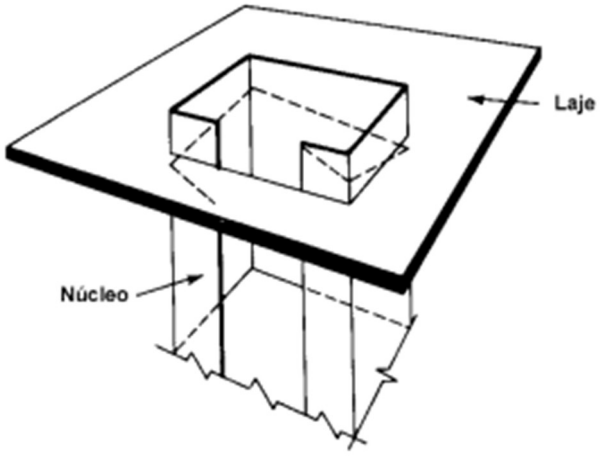

Figure 7: Structural core (Nucleo) and Floor slab (Laje) [5]

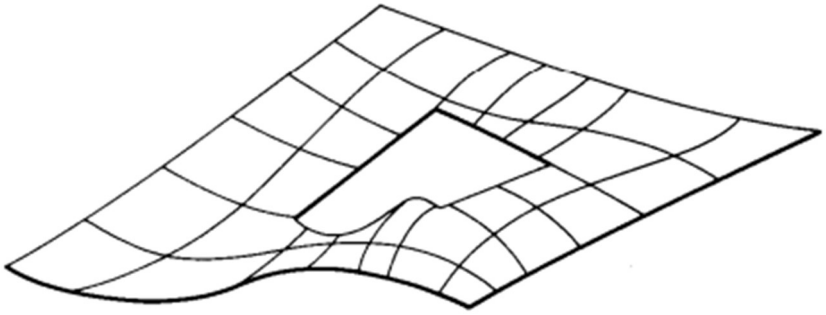

Figure 8: Warping Deformation of Floor Slab [5]

Warping is totally prevented in the built-in at the base of the core, whereas it is only partial in correspondence of the floors.

$$w = -v'y - \theta'\omega \tag{3.1}$$

$$w' = -v''y - \theta''\omega \tag{3.2}$$

Kinematics → warping

Statics → additional axial stress [12].

3.2 Vlasov's Theory

The hypothesis of transversal indeformability:

$$u = \xi(z) - \theta(z)y \tag{3.3}$$

$$v = \eta(z) - \theta(z)x \tag{3.4}$$

ξ and η are the transversal displacements in the X and Y directions and θ is the rotation angle about the Z axis.

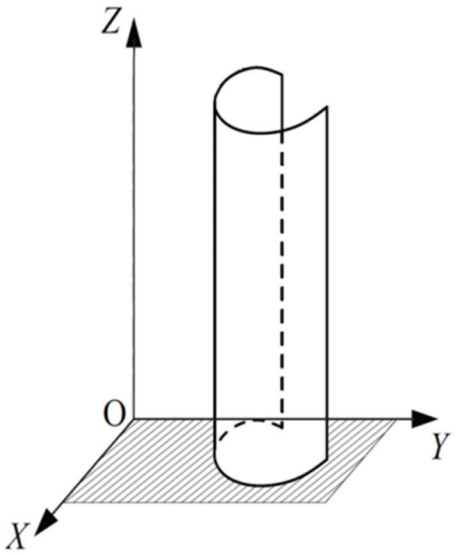

Figure 9: Open-section surface in a 3D coordinate system [12]

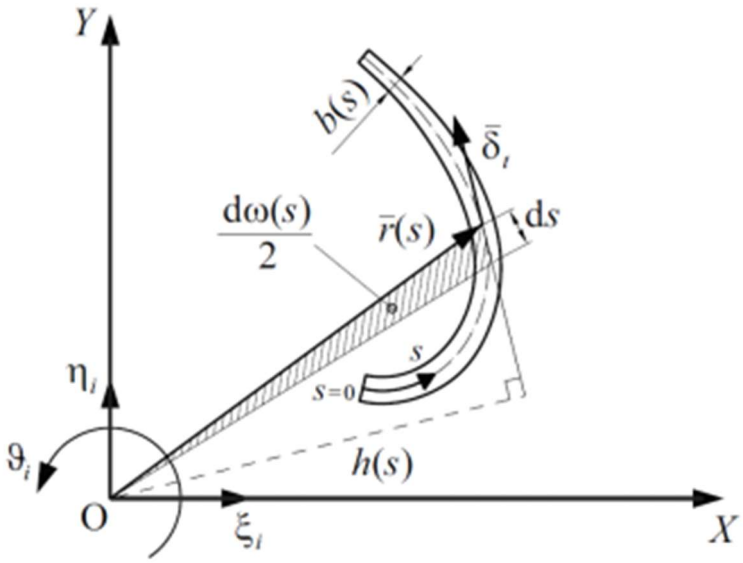

Figure 10: Thin-walled open beam section element, showing arc length s, the sectorial coordinate ω(s), the vector δt representing the transverse displacement, the width b(s), and the warping function h(s) in a 2D coordinate system [12]

The tangential displacement of the generic point of the thin-walled section is δ_t:

$$\delta_t = \{\delta\}^T\{u_t\} = u\frac{dx}{ds} + v\frac{dy}{ds} \tag{3.5}$$

and, according to Eqs. (3.3) and (3.4), we have:

$$\delta_t = \xi\frac{dx}{ds} + \eta\frac{dy}{ds} + \theta h(s) \tag{3.6}$$

h(s) represents the distance between the origin *O* of the reference system and the tangent line to the section midline:

$$h(s) = \{r\}^T\{u_n\} = x\frac{dy}{ds} - y\frac{dx}{ds} \tag{3.7}$$

Considering that:

$$\bar{u}_t = \frac{dx}{ds}\bar{\imath} + \frac{dy}{ds}\bar{\jmath} \tag{3.8}$$

$$\bar{u}_n = \frac{dy}{ds}\bar{\imath} + \frac{dx}{ds}\bar{\jmath} \tag{3.9}$$

The axial displacement component *w* can be obtained by Vlasov's second hypothesis, according to which the shearing strains γ_{zs} on the midline are considered negligible:

$$\gamma_{zs} = \frac{\partial w}{\partial s} + \frac{\partial \delta_t}{\partial s} \tag{3.10}$$

Deriving Eq.(3.6) and substituting into Eq.(3.10), we have:

$$\gamma_{zs} = \frac{\partial w}{\partial s} + \xi'\frac{dx}{ds} + \eta'\frac{dy}{ds} + \theta' h(s) \tag{3.11}$$

and then, equating to zero and integrating in the variable *s*, we have:

$$w = \zeta(z) + \xi' x - \eta' y + \theta'\omega \tag{3.12}$$

where *ζ(z)* is an arbitrary constant of integration, which represents the axial displacement due to the axial force, and ω is the sectorial area:

$$d\omega = h(s)ds \tag{3.13}$$

The warping function ω is twice the sectorial area generated by the radial vector r, that is, the area of the infinitesimal triangle which has base ds and height $h(s)$ [12].

$$\omega(s) = \int_0^s h(s)ds \tag{3.14}$$

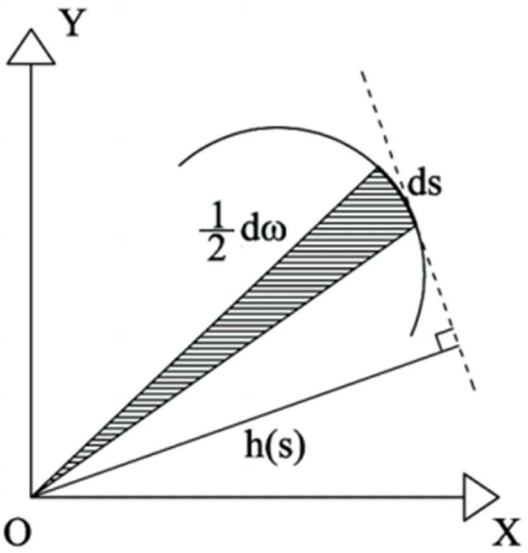

Figure 11: Geometric representation of a curved beam element in Vlasov's theory, illustrating the sectorial coordinate dω/2, the arc length ds, and the warping function h(s) in a 2D coordinate system [12]

Eqs.(3.3), (3.4), (3.12) show the four fundamental unknowns, which are functions of z:

$$\zeta = \zeta(z)\,, \qquad \xi = \xi(z)\,, \qquad \eta = \eta(z)\,, \qquad \theta = \theta(z) \tag{3.15a,b,c,d}$$

Deriving Eq. (3.12), the axial deformation ε_z is obtained:

$$\varepsilon_z = \frac{\partial w}{\partial z} = \zeta' - \xi'' x - \eta'' y - \theta'' \omega \tag{3.16}$$

The normal axial stress $\sigma_z = E\varepsilon_z$ can be written as:

$$\sigma_z = E(\zeta' + \xi'' x - \eta'' y + \theta'' \omega) \tag{3.17}$$

$$\sigma_z = {\sigma_z}^{SV} + {\sigma_z}^{VL} \tag{3.18}$$

Where:

$${\sigma_z}^{VL} = -E\theta'' \omega \tag{3.19}$$

3.3 Internal Actions Producing Axial Stress σ_z

The static moments are defined as follows, where a is the cross-sectional area of the beam:

$$S_y = \int_A x dA \ , \qquad S_x = \int_A y dA \ , \qquad S_\omega = \int_A \omega dA \tag{3.20a,b,c}$$

On the other hand, the moments of inertia are defined as:

$$I_{yy} = \int_A x^2 dA \ , \qquad I_{xx} = \int_A y^2 dA \ , \qquad I_{\omega\omega} = \int_A \omega^2 dA \tag{3.21a,b,c}$$

$$I_{yx} = I_{xy} = \int_A xy dA \, , I_{x\omega} = I_{\omega x} = \int_A \omega y dA \, , I_{y\omega} = I_{\omega y} = \int_A \omega x dA \tag{3.22a,b,c}$$

Eq. (3.18) allows the definition by integration of the internal actions related to the extensional and flexural behavior of the beam (static equivalence) [12]:

$$N = \int_A \sigma_z dA = E(A\zeta' - S_y\xi'' - S_x\eta'' - S_\omega\theta'') \tag{3.23}$$

$$M_y = \int_A \sigma_z x dA = E(S_y\zeta' - I_{yy}\xi'' - I_{yx}\eta'' - I_{y\omega}\theta'') \tag{3.24}$$

$$M_x = \int_A \sigma_z y dA = E(S_x\zeta' - I_{xy}\xi'' - I_{xx}\eta'' - I_{x\omega}\theta'') \tag{3.25}$$

$$B = \int_A \sigma_z \omega dA = E(S_\omega\zeta' - I_{\omega y}\xi'' - I_{\omega x}\eta'' - I_{\omega\omega}\theta'') \tag{3.26}$$

Remarks:

In the barycentric coordinate system:

$$S_x = S_y = 0 \tag{3.27}$$

With respect to sectorial barycenter:

$$S_\omega = 0 \tag{3.28}$$

With respect to principal axes:

$$I_{xy} = I_{yx} = 0 \tag{3.29}$$

If the origin of the reference system coincides with the shear center:

$$I_{x\omega} = I_{\omega x} = I_{y\omega} = I_{\omega y} = 0 \tag{3.30}$$

and, therefore:

$$\theta'' = -\frac{B}{EI_{\omega\omega}} \quad , \quad \sigma_z^{VL} = \frac{B\omega}{I_{\omega\omega}} \tag{3.31a,b}$$

3.4 Internal Actions Producing Tangential Stress τ_{zs}

Eqs. (3.23), (3.24), (3.25) highlight the axial and bending moment internal actions. On the other hand, Eq. (3.26) defines the internal action of bimoment, as a further action that produces axial stress σ_z [12].

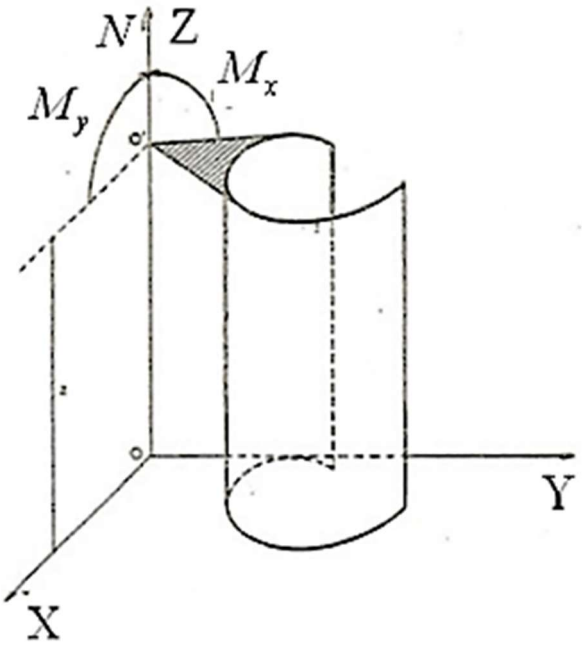

Figure 12: Diagram illustrating the internal actions producing tangential stress τ_{zs}, including axial force N, bending moments M_x and M_y [12]

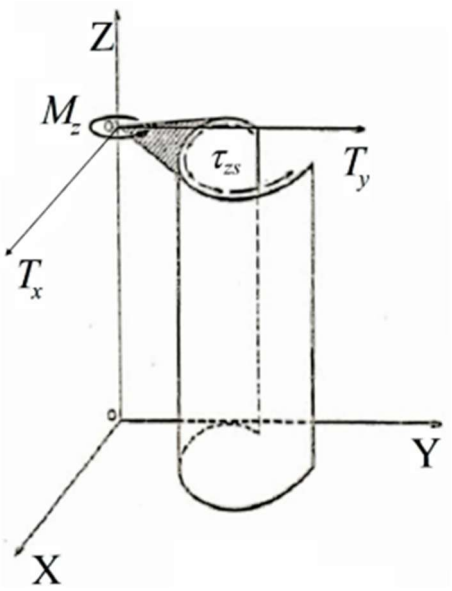

Figure 13: Tangential stresses τ_{zs} under general loading conditions, including torsional moment Mz and shear forces T_x and T_y. [12]

In the more general load conditions, the tangential stresses τ_{zs} are also present and are assumed to be uniform through the thickness *b* of the beam wall [12].

The three internal actions producing tangential stresses are:

$$T_x = \int_A \tau_{zs} \frac{dx}{ds} dA \tag{3.32}$$

$$T_y = \int_A \tau_{zs} \frac{dy}{ds} dA \tag{3.33}$$

$$M_z^{VL} = \int_A \tau_{zs} h dA \tag{3.34}$$

Where h is the oriented distance expressed by Eq. (3.7), and m_z^{vl} is the secondary torsional moment according to Vlasov [12].

Expressing *h(s)* by Eq. (3.13) and setting: $dA = bds$.

Simple integration by parts provides the following three relations:

$$T_x = \int_A \tau_{zs} \frac{dx}{ds} dA = -\int_C \frac{\partial(\tau_{zs} b)}{\partial s} x ds \tag{3.35}$$

$$T_y = \int_A \tau_{zs} \frac{dy}{ds} dA = -\int_C \frac{\partial(\tau_{zs} b)}{\partial s} y ds \tag{3.36}$$

$$M_z^{VL} = \int_A \tau_{zs} h dA = -\int_C \frac{\partial(\tau_{zs} b)}{\partial s} \omega ds \tag{3.37}$$

Eqs. (3.35), (3.36), (3.37) do not contain the finite terms as a consequence of the tangential stresses τ_{zs} vanishing at the extreme points of the section (principle of reciprocity) [12].

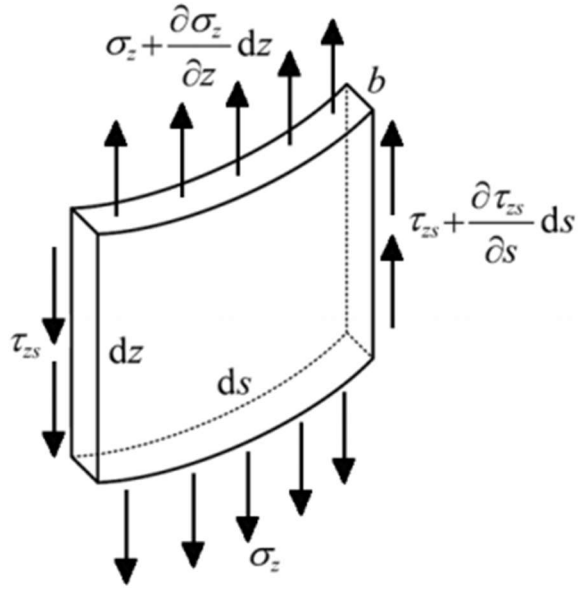

Figure 14: Diagram illustrating the distribution of axial stresses σ_z and tangential stresses τ_{zs} in a beam element [12]

Furthermore, the equilibrium to the axial translation requires:

$$\left(\frac{\partial \tau_{zs}}{\partial s} ds\right) b dz + \left(\frac{\partial \sigma_z}{\partial z} ds\right) b ds = 0 \tag{3.38}$$

Or:

$$\frac{\partial(\tau_{zs} b)}{\partial s} + \frac{\partial(\sigma_z b)}{\partial z} = 0 \tag{3.39}$$

Eqs. (3.35), (3.36), (3.37) can be expressed in the following form:

$$T_x = -\int_C \frac{\partial(\tau_{zs} b)}{\partial s} x ds = \int_C \frac{\partial(\sigma_z b)}{\partial z} x ds = \frac{d}{dz}\int_A \sigma_z x dA \tag{3.40}$$

$$T_y = -\int_C \frac{\partial(\tau_{zs} b)}{\partial s} y ds = \int_C \frac{\partial(\sigma_z b)}{\partial z} y ds = \frac{d}{dz}\int_A \sigma_z y dA \tag{3.41}$$

$$M_z^{VL} = -\int_C \frac{\partial(\tau_{zs} b)}{\partial s} \omega ds = \int_C \frac{\partial(\sigma_z b)}{\partial z} \omega ds = \frac{d}{dz}\int_A \sigma_z \omega dA \tag{3.42}$$

The previous relations, considering Eqs. (3.24), (3.25), (3.26) become:

$$T_x = \frac{dM_y}{dz} = E(S_y \zeta'' - I_{yy}\xi''' - I_{yx}\eta''' - I_{y\omega}\theta''') \tag{3.43}$$

$$T_y = \frac{dM_x}{dz} = E(S_x \zeta'' - I_{xy}\xi''' - I_{xx}\eta''' - I_{x\omega}\theta''') \tag{3.44}$$

$$M_z^{VL} = \frac{dB}{dz} = E(S_\omega \zeta'' - I_{\omega y}\xi''' - I_{\omega x}\eta''' - I_{\omega\omega}\theta''') \tag{3.45}$$

If the origin of the reference system coincides with the shear center, we have:

$$\theta''' = -\frac{M_z^{VL}}{EI_{\omega\omega}} \tag{3.46}$$

Applying the indefinite equations of equilibrium, we obtain the generalized equations of the elastic line or Vlasov equations:

$$p_x = -\frac{dT_x}{dz} = E(-S_y \zeta''' + I_{yy}\xi^{IV} + I_{yx}\eta^{IV} + I_{y\omega}\theta^{IV}) \tag{3.47}$$

$$p_y = -\frac{dT_y}{dz} = E(-S_y \zeta''' + I_{xy}\xi^{IV} + I_{xx}\eta^{IV} + I_{x\omega}\theta^{IV}) \tag{3.48}$$

$$m_z^{VL} = -\frac{M_z^{VL}}{dz} = E(-S_\omega \zeta''' + I_{\omega y}\xi^{IV} + I_{\omega x}\eta^{IV} + I_{\omega\omega}\theta^{IV}) \tag{3.49}$$

If the origin of the reference system coincides with the shear center, we have:

$$\theta^{IV} = \frac{m_z^{VL}}{EI_{\omega\omega}} \tag{3.50}$$

In each cross-section of the beam, the torsional moment is the sum of the two contributions:

$$M_z = M_z^{SV} + M_z^{VL} \tag{3.51}$$

$$M_z = GI_t\theta' - EI_{\omega\omega}\theta''' \tag{3.52}$$

The indefinite equation of equilibrium related to the torsional moment is:

$$m_z = -\frac{dM_z}{dz} \tag{3.53}$$

By replacing the previous expression of m_z in the indefinite equation of equilibrium, we obtain the non-uniform torsion equation (thin-walled open-section beams):

$$EI\theta^{IV} - GI_t\theta'' = m_z \tag{3.54}$$

Which is analogous to the equation of the elastic line with second-order effects and a tensile axial force:

$$EIv^{IV} - Nv'' = q(z) \tag{3.55}$$

Both stiffening and stabilizing contributions [12].

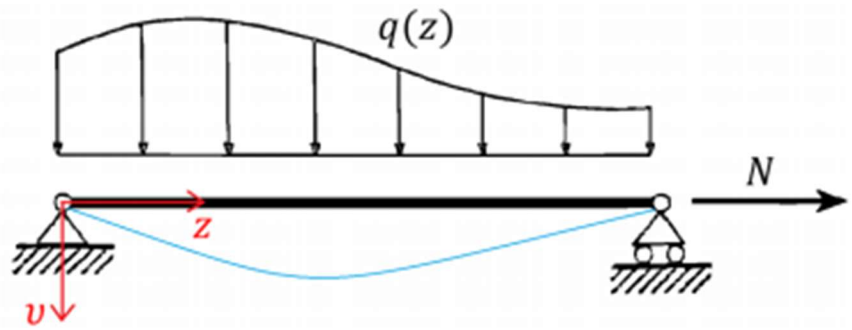

Figure 15: Beam under a distributed load q(z) and an axial tensile force N. The figure shows the deflection v along the beam's length z, representing the deformation due to second-order effects [12]

4. BUCKLING OF TWB

4.1 Introduction to Buckling of TWB

In this chapter, an alternative theory will be discussed, still for the study of the behavior of thin-walled open sections, from source [11].

The form of buckling manifested, due to the low torsional stiffness, is the flexural-torsional buckling and lateral buckling, in which the beam bends into one or both the principal inertia planes, and, at the same time, twists.
The flexural-torsional coupling also occurs in beams solicited by forces transversal to the axis, contained in one of the two principal planes.
Upon reaching the critical load, the beam buckles into the plane orthogonal to that of solicitation and simultaneously twists. [11].

The same behavior happens both if the beam is simply bent or eccentrically compressed in a plane: this form of buckling is called lateral instability [11].

The beam model used is based on Vlasov's theory of non-uniform torsion, which considers the warping by curvature, because describes the torsional behavior of the TWB, with respect to its elastic and geometric stiffness.
This theory says that the cross-section of the beam maintains its natural shape in its own plane, but undergoes warping out of this plane. [11].

Because of the non-uniformity of the torsion and the fact that the warping is generally variable along the beam axis, complementary normal and tangential stresses arise and are not negligible compared to those predicted by the de Saint-Venant (DSV) model of uniform torsion. [11].

Another important aspect to consider is the determination of the centre of torsion.
The centre of torsion is a geometric property of the cross-section, generally different from the centroid because the rotation of the cross-section takes place around it.
It is found to be coincident with the shear centre of the Jourawsky theory of non-uniform bending. [11].

Because of all this, in the case of TWB, it is useful to describe the displacement field with reference not only to the centroid, as usually done for compact beams. [11].

It has to be described also with reference to the centre of torsion, as regards the in-plane displacements, and to the centroid, as regards the out-of-plane displacements. [11].
So, one of the distinctive characteristics of TWB, is that they have two different axes.

4.2 Elastic Stiffness Operator

To define the elastic stiffness operator, reference is made to a 1D model of a beam, with TWB section. Initially, the elastic problem is formulated in the context of the linear theory to identify the elastic stiffness operator. Afterwards, the analysis of the effects of the prestress is performed. [11].

4.2.1 Kinematics

A straight beam is considered, with centroidal axis z, and an open and thin cross-section that has central inertia axes x and y, originating by the centroid G (*Fig. 16a*).
It can be also introduced a basis of orthonormal vectors ($\mathbf{a}_x$, $\mathbf{a}_y$, $\mathbf{a}_z$), aligned with the homonym axes. [11].
Γ is the midline of the cross-section, and along it, a curvilinear abscissa s of origin O is taken.
The thickness of the cross-section can be variable and is denoted by $b(s)$.
In our analysis, it is assumed that all the quantities of interest are constant on the thickness, in this way the displacement is $\mathbf{u} = \mathbf{u}(s, z)$. [11].

As hypothesis, is it possible to assume that the cross-section is undeformable in its own plan π, but not out of this plane, orthogonally to which it undergoes a warping $\omega(s, z)$.
The TWB is assumed to be shear undeformable on its middle surface S, that means on the surface of trace Γ on the cross-section: this means that in bending and extension, the beam has the same behavior of an Euler-Bernoulli beam and that warping depends only on twist.
However, the shear strains are nonzero beyond the middle surface, where they are defined according to the DSV torsion model. [11].

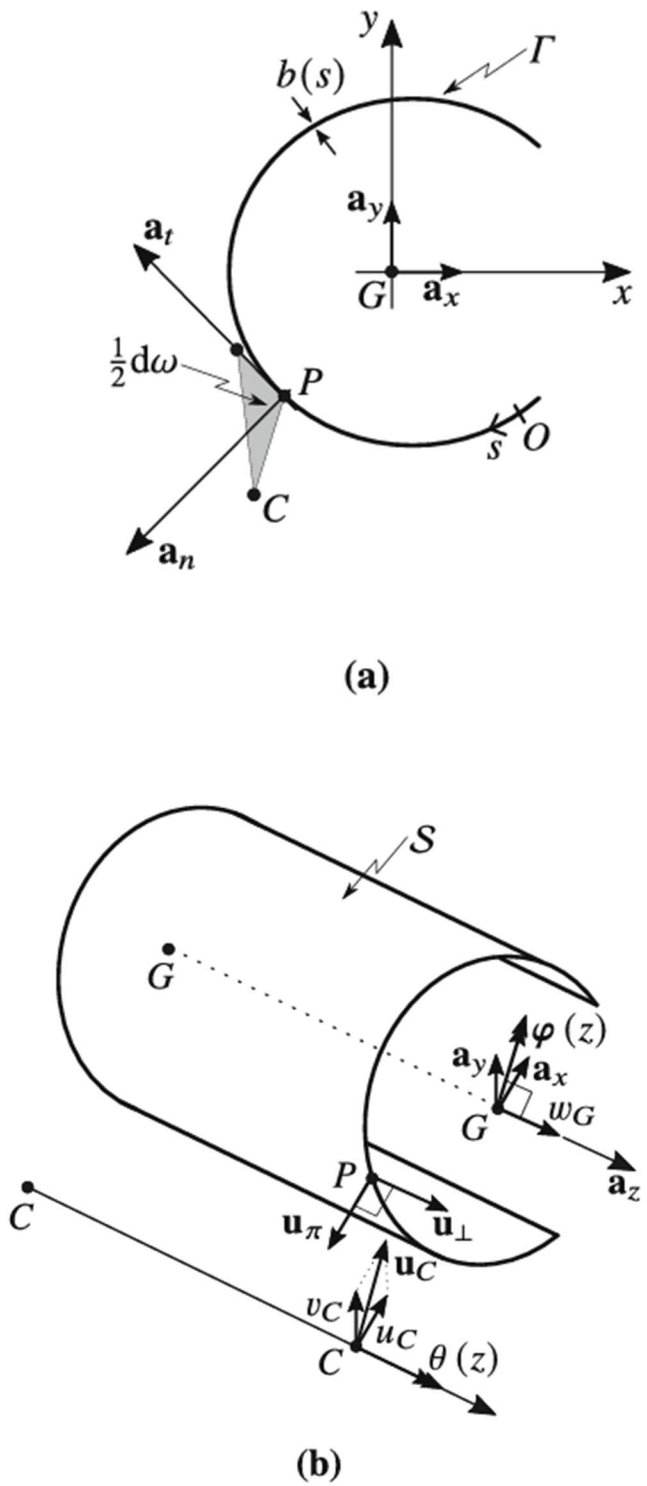

Figure 16: Open thin-walled beam: (a) cross-section and sectorial area, (b) displacements [11]

4.3 In Plane Displacements

Following the theory of non-uniform torsion, the cross-section rotates within its own plane around a point *C* (centre of torsion which coincides with the shear centre), whose coordinates are x_C and y_C. [11].

Consequently, it is practical to describe the rigid in-plane displacement relative to this point. Let $\mathbf{u}_C(z) = u_C(z)\ \mathbf{a}_x + v_C(z)\ \mathbf{a}_y$ represents the in-plane translation of the centre *C*, and $\theta(z)$ the angle of twist. [11].

The in-plane (infinitesimal) displacement $\mathbf{u}_\pi := u(s,z)\ \mathbf{a}_x + v(s,z)\ \mathbf{a}_y$ of a point *P(s)*, with coordinates *x(s)*, *y(s)*, is expressed as (*Fig. 16b*) [11]:

$$\boldsymbol{u_\pi} = u_C(z) + \theta(z)\ \boldsymbol{a}_z \times \boldsymbol{CP}(s) \tag{4.1}$$

The projection of this relationship onto the axes gives that [11]:

$$u = u_C(z) - \theta(z)\ (y(s) - y_C) \tag{4.2}$$

$$v = v_C(z) - \theta(z)\ (x(s) - x_C) \tag{4.3}$$

4.4 Out-of-Plane Displacements

Regarding the Out-of-Plane Displacements, the displacement $\mathbf{u}_\perp := \omega(s,z)\ \mathbf{a}_z$, that is the one orthogonal to the cross-section plane, is related to the superposition of three effects [11]:

- a translation along *z*,
- a rotation $\varphi(z) := \varphi_x(z)\ \mathbf{a}_x + \varphi_y(z)\ \mathbf{a}_y$ around an axis lying in the plane π,
- a warping proportional to pure torsion, $\kappa_t = \theta'(z)$.

Considering the rotation around an axis, which passes through the barycenter *G* of the cross-section, and taking into account the results obtained through Vlasov's theory, we have that (*Fig. 16b*) [11]:

$$\omega = \omega_G(z) + \boldsymbol{\varphi}(z) \times GP(z)\boldsymbol{a}_z - \theta'(z)\ \omega(s) \tag{4.4}$$

Where $\omega_G(z)$ is the axial displacement of the centroid, and $\omega(s)$ represents the warping function (which corresponds to twice the sectorial area, as illustrated in *Fig. 16a*).

To determine the rotation ***φ(z)***, the shear undeformability condition is applied when the beam undergoes no torsion (*Fig. 17*). [11].

The internal constraint dictates that the cross-section (which remains planar during this motion) remains perpendicular to all longitudinal fibers, which rotate by the same angle ***φ(z)***.

Given that the transverse displacement of each longitudinal fiber is $\mathbf{u}_C(z)$, the relative displacement between two points *P* and *Q*, separated by a distance d*z* along the same fiber, is $d\mathbf{u}_C = \boldsymbol{\varphi}(z) \times dz\, \mathbf{a}_z$ [11].

Hence, $\mathbf{u}'_C(z) = \boldsymbol{\varphi}(z) \times \mathbf{a}_z = \varphi_y\, \mathbf{a}_x - \varphi_x\, \mathbf{a}_y$ (as shown in *Fig. 17*). [11].

Taking into account that $\mathbf{u}'_C(z) = u'_C(z)\, \mathbf{a}_x + v'_C(z)\, \mathbf{a}_y$, so $\varphi_x = -v'_C(z)$ and $\varphi_y = u'_C(z)$, thus:

$$\omega = \omega_G - v'_C(z)\, y(s) - u'_C(z)\, x(s) - \theta'(z)\, \omega(s) \qquad (4.5)$$

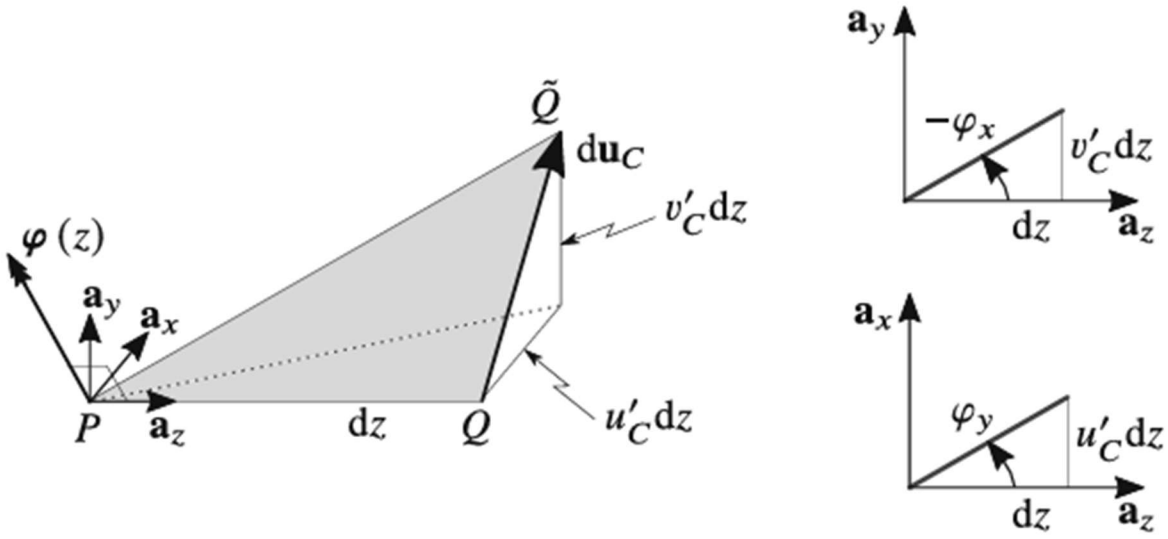

Figure 17: Unshearability condition [11]

4.5 Strains

Taking into account that the central surface of the TWB is non-deformable under shear and that the cross-section retains its shape in the π plane, the axial unit extension remains the only non-zero deformation on this surface, $\varepsilon_Z = \frac{\partial w}{\partial z}$; by using Eq. 4.5, it reads:

$$\varepsilon_Z = \omega'_G(z) - u''_C(z)x(s) - v''_C(z)y(s) - \theta''(z)\omega(s) \tag{4.6}$$

In the previous expressions, it is possible to identify two effects:

- an axial extension, two Euler-Bernoulli bending modes,
- the Vlasov warping.

To incorporate the axial extension in Eq. (4.6), the shear strain beyond the mid-surface SS must also be taken into account, as outlined in the de Saint-Venant (DSV) torsion theory [11].

The strains determined, obviously produces a normal stress: $\sigma_z = E\varepsilon_Z$.

The following are relationships that apply to both Euler-Bernoulli and Vlasov beams:

$$\omega'_G = \frac{N}{EA} \quad , \quad u''_C = \frac{M_y}{EI_y} \quad , \quad v''_C = -\frac{M_x}{EI_x} \quad , \quad \theta'' = \frac{B}{EI_\omega} \tag{4.7a,b,c}$$

where B is the bimoment and I_ω the sectorial inertia of the cross-section [11].

4.5.1 Equilibrium equations

To obtain the equilibrium equations of the TWB, the stationary of the total potential energy (TPE) has been enforced:

$$\Pi = U + V \tag{4.8}$$

Where the two contributes are the elastic potential energy, U, and of the potential energy of the external forces, V [11].

4.6 Elastic Potential Energy

The elastic potential energy of the beam, computed as:

$$U := U_\varepsilon + U_\gamma \tag{4.9}$$

has two components:

- U_ε, related to the axial extensions,
- U_γ, related to the shear strains.

The expression for the first contribution is given by:

$$\begin{aligned} U_\varepsilon &= \frac{1}{2}\int_0^l dz \int_\Gamma E\varepsilon_z^2(s,z)b(s)ds \\ &= \frac{E}{2}\int_0^l dz \int_\Gamma (\omega_G' - u_C''x - v_C''y - \theta''\omega)^2 b ds = \\ &= \frac{1}{2}\int_0^l \left(EA{\omega_G'}^2 - EI_y{u_C''}^2 - EI_x{v_C''}^2 - EI_\omega{\theta''}^2\right)dz \end{aligned} \tag{4.10}$$

The orthogonality properties of the functions *x(s)*, *y(s)*, and *ω(s)* have been utilized.

As usual, A represents the cross-sectional area, I_x and I_y denote the moments of inertia about the principal axes, and I_ω corresponds to the sectorial moment of inertia. The second contribution to the potential energy is related to the shear strains, as described by the De Saint-Venant (DSV) theory [11].

Considering the one-dimensional model, it can be expressed as follows:

$$U_\gamma = \frac{1}{2}\int_0^l GJ{\theta'}^2 dz \tag{4.11}$$

where GJ is the De Saint-Venant torsional stiffness [11].

Considering these two contributions it is possible to define the strain energy is obtained, whose first variation reads [11]:

$$\delta U = \int_0^l \left(EA\omega_G'\delta\omega_G' - EI_y u_C''u\delta_C'' - EI_x v_C''\delta v_C'' - EI_\omega\theta''\delta\theta'' + GJ\theta'\delta\theta'\right)dz \tag{4.12}$$

4.7 Load Potential Energy

To define the Load potential energy, the forces that are considered to act on the thin-walled beam (TWB) are the following ones [11].:

- transverse loads with a linear density of $\mathbf{p} = p_x(z)\ \mathbf{a}_x + p_y(z)\ \mathbf{a}_y$ applied along the center of the torsion axis,
- twisting couples with a linear density of $c_z(z)$.

Considering the one-dimensional model and the loads, the potential energy can be expressed as:

$$V = -\int_0^l \left(p_x u_C + p_y v_C + c_z \theta\right) dz \tag{4.13}$$

Whose first variation is:

$$\delta V = -\int_0^l \left(p_x \delta u_C + p_y \delta v_C + c_z \delta\theta\right) dz \tag{4.14}$$

As an alternative, p_x, p_y, and c_z, (generalized forces) could also be derived from a 3D model, but that won't be covered in this analysis.

The derivation shows that when distributed longitudinal forces are also considered, they not only generate bending moments but also introduce a new generalized force, known as the distributed bicouple; this force is the dual of the twist gradient [11].

4.8 Equilibrium Equations

Taking into account the previous equations, the first variation of the TPE, equated to zero, can be written as [11].:

$$\delta\Pi = \int_0^l \left(EA\omega_G'\delta\omega_G' - EI_y u_C''\delta u_C'' - EI_x v_C''\delta v_C'' - EI_\omega\theta''\delta\theta'' + GJ\theta'\delta\theta'\right)dz + \\ - \int_0^l \left(p_x\delta u_C + p_y\delta v_C + c_z\delta\theta\right)dz = 0\,,\ \ \forall(\delta\omega_G, \delta u_C, \delta v_C, \delta\theta) \tag{4.15}$$

Performing an integration by parts, it is possible to obtain the following field equations:

$$-EA\omega_G'' = 0 \tag{4.16}$$

$$EI_y u_C'''' = p_x \tag{4.17}$$

$$EI_X v_C'''' = p_y \tag{4.18}$$

$$EI_\omega\theta'''' - GJ\theta'' = c_z \tag{4.19}$$

with the relative geometric or mechanical boundary conditions, alternately:

$$[EA\omega_G'\delta\omega_G']_0^l = 0 \tag{4.20}$$

$$\left[EI_y u_C''\delta u_C'\right]_0^l = 0 \tag{4.21}$$

$$\left[-EI_y u_C'''\delta u_C\right]_0^l = 0 \tag{4.22}$$

$$[EI_x v_C''\delta v_C']_0^l = 0 \tag{4.23}$$

$$[-EI_x v_C'''\delta v_C]_0^l = 0 \tag{4.24}$$

$$[(GJ\theta' - EI_\omega\theta''')\delta\theta]_0^l = 0 \tag{4.25}$$

$$[EI_\omega\theta''\delta\theta']_0^l = 0 \tag{4.26}$$

This equations, as said before, comes from source [11].

The field equations, Eqs. (4.16), (4.17), (4.18), (4.19), which will be referred to as the elastic line equations of the open TWB, can be expressed in the operational form:

$$\mathfrak{K}_e \mathrm{u}(z) = \mathrm{p}(z) \tag{4.27}$$

where $\mathrm{u}(z) := (\omega_G(z),\ u_C(z), v_C(z), \theta(z))^T$ is the vector of unknown displacement components, and $\mathrm{p}(z) := (0, p_x(z),\ p_y(z), c(z))^T$ is the vector of applied loads [11].

It is also possible to define the diagonal elastic stiffness operator, in which $\partial z := \frac{d}{dz}$:

$$\mathfrak{K}_e := \begin{bmatrix} -EA\partial_z^2 & 0 & 0 & 0 \\ 0 & EI_y\partial_z^4 & 0 & 0 \\ 0 & 0 & EI_x\partial_z^4 & 0 \\ 0 & 0 & 0 & EI_\omega\partial_z^4 - GJ\partial_z^2 \end{bmatrix} \tag{4.28}$$

It is convenient to partition the displacements as:

$$\mathrm{u}(z) \coloneqq (\mathrm{u}_\perp(z), \mathrm{u}_\pi(z)) \tag{4.29}$$

Where:

- $\mathrm{u}_\perp(z) \coloneqq (\omega_G(z))$ is the out-of-plane component,
- $\mathrm{u}_\pi(z) \coloneqq (u_C(z), v_C(z), \theta(z))^T$ is the generalized displacements in the cross section plane [11].

Consequently:

$$\mathfrak{K}_e := \begin{bmatrix} {K_e}^\perp & 0 \\ 0 & {K_e}^\pi \end{bmatrix} \tag{4.30}$$

where:

$$\mathfrak{K}_e{}^\perp := [-EA\partial_z^2] \tag{4.31}$$

$$\mathfrak{K}_e{}^\pi := \begin{bmatrix} EI_y\partial_z^4 & 0 & 0 \\ 0 & EI_x\partial_z^4 & 0 \\ 0 & 0 & EI_\omega\partial_z^4 - GJ\partial_z^2 \end{bmatrix} \tag{4.32}$$

4.9 Geometric Stiffness Operator

To perform the linearized stability analysis of a TWB it is necessary to construct the geometric stiffness operator [11].

This arises from the variation of the quadratic part of the prestressing energy:

$$U^0 = \int_0^l dz \int_\Gamma \left(\sigma_z^0 \varepsilon_z^{(2)} + \tau_{zs}^0 \gamma_{zs}^{(2)}\right) b ds \tag{4.33}$$

This expresses the work of normal prestresses $\sigma_z^0(s, z)$ and tangential stresses $\tau_{zs}^0(s, z)$, on the second-order components of the unknown incremental strains $\varepsilon_z^{(2)}(s,z)$, $\gamma_{zs}^{(2)}(s, z)$, all evaluated on the middle surface S [11].

Considering that the deformations depend on the displacements of the point $P(s)$ at the abscissa z and that this can be expressed in terms of displacements of the two central lines of the TWB, which depend only on z, it is possible to transform the three-dimensional model into a one-dimensional model [11].

4.10 Prestresses

By limiting the attention to beams under extension and bending (but not torsion) and resorting to results of DSV and Jourawsky theories, the prestresses are evaluated as:

$$\sigma_z^0 = \frac{N^0(z)}{A} + \frac{M_x^0(z)}{I_x} y(s) - \frac{M_y^0(z)}{I_y} x(s) \tag{4.34}$$

$$\tau_{zs}^0 = -\frac{T_x^0(z) S_y^*(s)}{I_y b(s)} - \frac{T_y^0(z) S_x^*(s)}{I_x b(s)} \tag{4.35}$$

where N_0, M_{0x}, M_{0y}, T_{0x}, and T_{0y} are, respectively, the axial force, the bending moments, and the shear forces acting in the prestressed configuration [11].

Here, the geometric characteristics of the cross-sections assume the usual meaning.

4.11 Quadratic Strains

From the quadratic component of the Green-Lagrange strain tensor it is possible to deduce the nonlinear part of the incremental strains:

$$\varepsilon_z^{(2)} = \frac{1}{2}\left(u_{,z}^2 + v_{,z}^2 + \cancel{\omega_{,z}^2}\right) \tag{4.36}$$

$$\gamma_{zs}^{(2)} = u_{,z}u_{,s} + v_{,z}v_{,s} + \cancel{\omega_{,z}\omega_{,s}} \tag{4.37}$$

where the barred terms are neglected, to take into account the fact that out-of-plane displacements are smaller than in-plane displacements [11].

Since the calculation of the geometric stiffness operator in the general case is very complex, it was decided to follow an approach that derives the operator in successive steps, starting from simple loads. Taking into account the linearity of the problem, the general case will be constructed by superposition [11].

4.12 Uniformly Compressed Thin-Walled Beams

In the following section, the analysis of the bifurcation of uniformly compressed TWB is performed. This problem extends Euler's planar beam problem to a TWB situated in 3D space.

First of all, the equilibrium equations are formulated and then, simple solutions are illustrated, to discuss important phenomenological aspects [11].

Considering a TWB, uniformly compressed by an axial force *P*, it is possible to write the state of prestress as:

$$\sigma_z^0 = -\frac{P}{A} \tag{4.38}$$

The relevant prestress energy, by Eq. (4.33), is written as:

$$U^0 = \int_0^l dz \int_\Gamma \sigma_z^0 \varepsilon_z^{(2)} b ds = -\frac{1}{2}\frac{P}{A}\int_0^l dz \int_\Gamma \left(u_{,z}^2 + v_{,z}^2\right) b ds \tag{4.39}$$

where use has been made of Eq. (4.36). By substituting Eqs. (4.2), (4.3), *u(s, z)*, *v(s, z)* are expressed in function of the generalized displacements $u_C(z)$, $v_C(z)$, $\theta(z)$ of the torsion center line; consequently:

$$\begin{aligned} U^0[\mathbf{u}_\pi] &= -\frac{P}{2A}\int_0^l dz \int_\Gamma \{[u_C' - \theta'(y - y_C)]^2 + [v_C' - \theta'(x - x_C)]^2\} b ds = \\ &= -\frac{P}{2}\int_0^l [u_C'^2 + v_C'^2 + r_C^2\theta'^2 + 2y_c u_C'\theta' - 2x_c v_C'\theta']dz \end{aligned} \tag{4.40}$$

Here, it has been considered that the static moments of the cross-section are zero [11].

r_C^2 is the square of the polar moment of inertia relative to the centre of torsion, also has been introduced, and it is possible to define it as:

$$r_C^2 \coloneqq \frac{1}{A}\int_\Gamma [(x - x_C)^2 + (y - y_C)^2] b ds =: \frac{I_C}{A} \tag{4.41}$$

It is noted that due to the approximation presented in Eq. (4.36), the functional U^0 relies solely on the in-plane displacements $\mathrm{u}_\pi(z) \coloneqq (u_C, v_C, \theta)^T$ and is independent of the axial displacement ω_G [11].

4.13 Geometric Stiffness Operator

If the first variation of the energy and integration by parts are performed, it is possible to write:

$$\delta U^0 = -P\int_0^l [u_C'\delta u_C' + v_C'\delta v_C' + r_C^2\theta'\delta\theta' + y_c(u_C'\delta\theta' + \theta'\delta u_C')]\,dz$$

$$-P\int_0^l [-x_c(v_C'\delta\theta' + \theta'\delta v_C')]\,dz =$$

$$= P\int_0^l [(u_C'' + y_c\theta'')\delta u_C + (v_C'' + x_c\theta'')\delta v_C]\,dz + \tag{4.42}$$

$$+P\int_0^l [(r_C^2\theta'' + y_c u_C'' - x_c v_C'')\delta\theta]\,dz + [-P(u_C' + y_c\theta')\delta u_C]_0^l$$

$$+[-P(v_C' - x_c\theta')\delta v_C - P(r_C^2\theta' + y_c u_C' - x_c v_C')\delta\theta]_0^l$$

By letting $\delta U^0 = \int_0^l \delta \mathrm{u}_\pi^T \mathrm{K}_{g,c} \mathrm{u}_\pi dz + [\dots]_0^l$, the geometric stiffness operator of the compressed TWB is recognized:

$$\mathrm{K}_{g,c} := P\begin{bmatrix} 1 & 0 & y_C \\ 0 & 1 & -x_C \\ y_C & -x_C & r_c^2 \end{bmatrix}\partial_z^2 \tag{4.43}$$

It is non-diagonal, which results in coupling between the transverse displacement components u_C, v_C, and the twist θ [11].

4.14 Equilibrium Equations

By combining the elastic and geometric contributions, it is possible to derive the general equilibrium equations:

$$\mathrm{K}_e{}^{\perp}\mathrm{u}_{\perp} = 0 \tag{4.44}$$

$$(\mathrm{K}_e{}^{\pi} + \mathrm{K}_{g,c})\mathrm{u}_{\pi} = \mathbf{0} \tag{4.33}$$

that, in extended form, can be also written as:

$$-EA\omega_G'' = 0 \tag{4.34}$$

$$EI_y u_C''' + P(u_C'' + y_C\theta'') = 0 \tag{4.35}$$

$$EI_x v_C''' + P(v_C'' + x_C\theta'') = 0 \tag{4.36}$$

$$EI_\omega\theta'''' - GJ\theta'' + P(r_C^2\theta'' + y_C u_C'' - x_C v_C'') = 0 \tag{4.37}$$

Operating in the same way, the boundary conditions are found:

$$[EA\omega_G'\delta\omega_G']_0^l = 0 \tag{4.38}$$

$$\left[EI_y u_C''\delta u_C'\right]_0^l = 0 \tag{4.39}$$

$$\left[(-EI_y u_C''' - P(u_C' + y_C\theta'))\delta u_C\right]_0^l = 0 \tag{4.40}$$

$$[EI_x v_C''\delta v_C']_0^l = 0 \tag{4.41}$$

$$[(-EI_x v_C''' - P(v_C' + x_C\theta'))\delta v_C]_0^l = 0 \tag{4.42}$$

$$[(GJ\theta' - EI_\omega\theta''' - P(r_C^2\theta' + y_C u_C' - x_C v_C'))\delta\theta]_0^l = 0 \tag{4.43}$$

$$[EI_\omega\theta''\delta\theta']_0^l = 0 \tag{4.44}$$

The field equations, together with their boundary conditions, show that the axial displacement ω_G is independent of the other displacements [11].

Since the operator $-EA\partial_z^2$ is non-singular and the boundary conditions are homogeneous, Eqs. (4.16) and (4.20) only allow the trivial solution $\omega_G = 0$ [11].

This allows us to say that the first-order mode of instability is inextensible, similar to that found for the Euler bundle [11].

The remaining equations involving u_C, v_C, θ create a twelfth-order differential problem, which makes finding analytical solutions difficult [11].

Subsequently, in Chapter 6, the general problem will be addressed using numerical methods [11].

5. SHEAR CENTER

5.1 What is Shear Center?

The shear centre is the point through which if the resultant shear force acts then member is subjected to simple bending without twisting. It means a load acting on a beam through shear centre will produce bending without torsion or twisting. Shear centre is also called centre of flexure [15].

5.2 Location of Shear Center

- Shear centre always lies on the axis of symmetry if exists [15].
- Shear centre generally does not coincide with the centroid of section, but if there are two or more than two axes of symmetry, then shear centre will coincide with the point of intersection of the axes of symmetry. In this case, the shear centre of the area will be the same as the centroid of the area [15].
- If a section is made of two narrow rectangles, then shear centre lies on the junction of both rectangles [15].

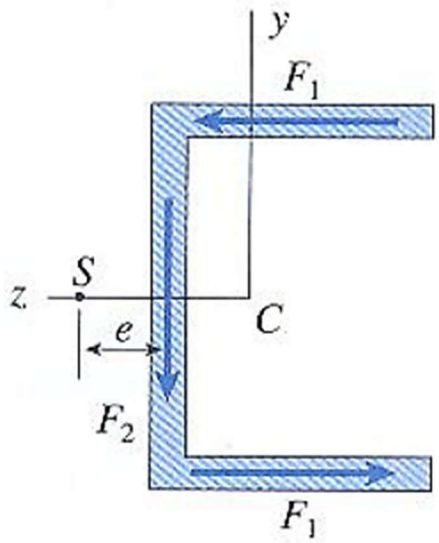

Figure 18: Diagram of an C-shaped section with shear centre and centroid marked [19]

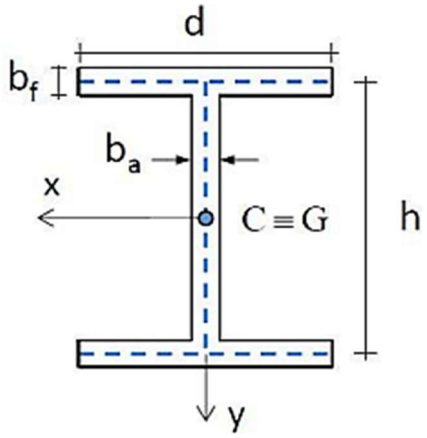

Figure 19: Diagram of an I-section and a plus-section with shear centre = centroid (S = CG) [16]

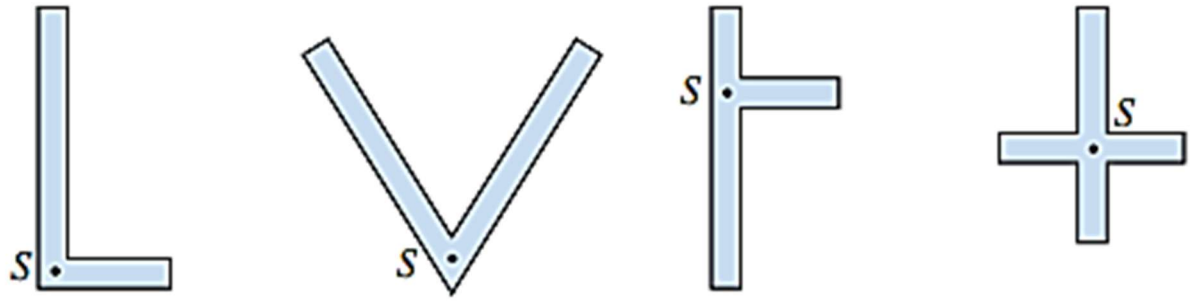

Figure 20: Set of diagrams showing different sections with shear centre (S) and centroid (CG) marked, including L-shape, T-shape, cross-shape, and angled sections [19]

5.3 Steps to Compute the Shear Center

- Define the geometry: specify the coordinates of the cross-section and its thickness.
- Calculate the centroid: compute the centroid of the section, as it is needed for further calculations.
- Determine the moment of Inertia: calculate the second moments of area (I_x, I_y, and I_{xy}) about the centroidal axes.
- Shear flow distribution: find the shear flow along the section using equilibrium equations.
- Locate the shear center: find the point at which the resultant moment due to shear flow is zero.

5.4 Shear Center of Rectangular Cross-Sections with $b \ll h$

Considering a thin rectangle section, symmetric about the vertical axis with:

- Height h
- Base b (very small, $b \ll h$)
- Thickness t (assumed constant along the perimeter).

It is possible to say that the centroid of the section lies at the geometric centre: $C_x = b/2$, $C_y = h/2$, because of symmetry. Any applied shear force along the vertical axis will not cause twisting.

5.5 Shear Center of Narrow Circular Cross-Section

For a hollow circular section, the shear centre coincides with the geometric centre (or centroid) of the section. This is because of the symmetry of the section: any applied shear force will not cause twisting, as the shear flow is symmetric around the centre.

The shear flow is constant along the circular wall for a thin-walled hollow section.

So, for a thin-walled hollow circular section, the centroid is at *(0,0)* and the shear centre is also at *(0,0)*, i.e., it coincides with the centroid.

5.6 Shear Center of a C-Section

The cross-section *C* in *Fig. 21* has a horizontal axis of symmetry; therefore, the principal inertia axes are the axis of symmetry and the orthogonal axis to it. If the applied load is vertical, as shown in *Fig. 21*, the neutral bending axis coincides with the horizontal principal inertia axis [20].

Since the section walls are thin, the moment of inertia of the section with respect to the neutral axis can be calculated in a simplified manner, without significant errors, by considering the section's midline.

$$J = \frac{h \cdot c^3}{12} + 2 \cdot (a \cdot h) \cdot \left(\frac{c}{2}\right)^2 \tag{5.1}$$

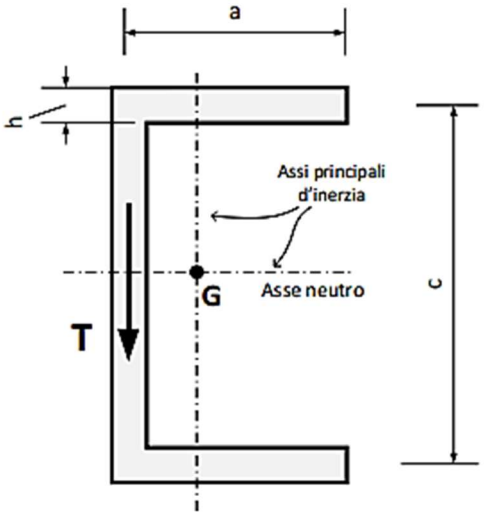

Figure 21: C-section subjected to a vertical shear action [20]

Shear stresses in the flanges

If we cut the section (*Fig. 22*) along a generic chord in a flange (chord 1-1), we can calculate the average shear stress along the chord using Jourawski's formula:

$$\tau = \frac{T \cdot S}{b \cdot J} = \frac{T \cdot (\eta h) \cdot \frac{c}{2}}{h \cdot J} \tag{5.2}$$

The shear stress τ is directed parallel to the axis line of the flange. Eq. (5.2) shows that the stress τ varies linearly with respect to the coordinate η.

The stress τ is zero at the extreme of the wing and is valid at the intersection of the wing with the soul $\tau = \frac{T \cdot \frac{ac}{2}}{J}$ [20].

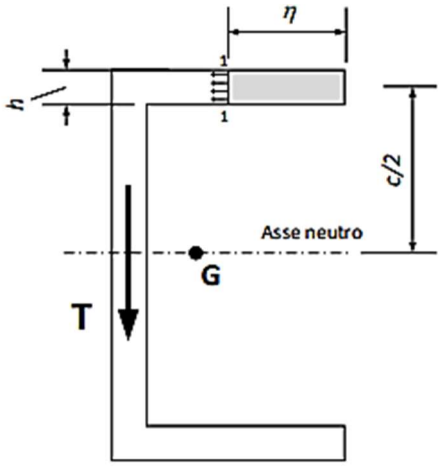

Figure 22: Calculating Tangential Forces in a Wing in a C-Section [20]

Shear stresses in the web

If we consider (*Fig. 23*) the generic chord in the web (chord 2-2), we can calculate the average shear stress along chord 2-2 as:

$$\tau = \frac{T \cdot S}{b \cdot J} = \frac{T \cdot \left[(ah) \cdot \frac{c}{2} + (\eta h) \cdot \left(\frac{c}{2} - \frac{\eta}{2}\right)\right]}{h \cdot J} \tag{5.3}$$

The shear stress τ is directed parallel to the midline of the web. Eq. (5.3) indicates that the stress τ varies according to a parabolic law with respect to the coordinate η.

The stress τ is worth: $\tau = \frac{T \cdot \frac{ac}{2}}{J}$ at the upper end of the core and reaches its maximum value at the neutral axis $\tau = \frac{T \cdot \left[\frac{ac}{2} + \frac{c^2}{8}\right]}{J}$ [20].

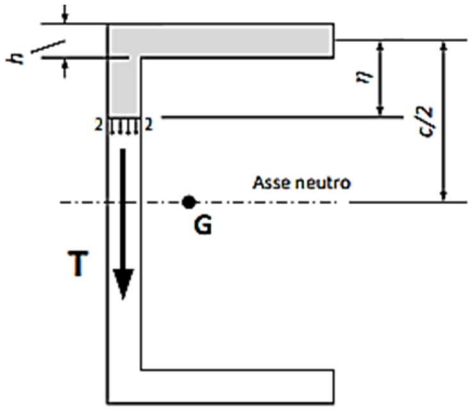

Figure 23: Calculating Tangential Forces in a Wing in a C-Section [20]

The distribution of shear stresses τ in the section is illustrated in *Fig. 24*.

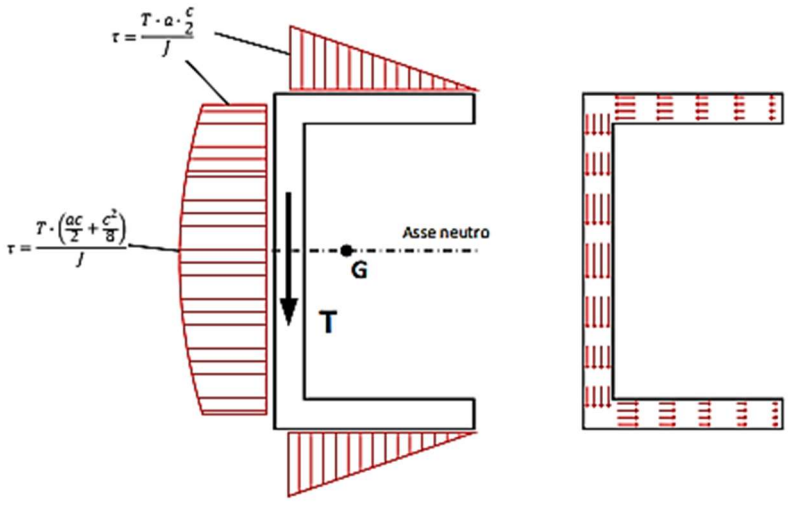

Figure 24: Trend of tangential forces in a C-section [20]

Let's now calculate the resulting forces F_1 and F_2 of the stresses acting on the flanges and the web, respectively (*Fig. 25*) [20].

$$F_1 = \int_0^a \tau(\eta) \cdot h \cdot d\eta = \int_0^a \frac{T\eta c}{2J} \cdot h \cdot d\eta = \frac{Tc}{4J} \cdot h \cdot a^2 \tag{5.4}$$

$$F_2 = 2\int_0^{\frac{c}{2}} \tau(\eta) \cdot h \cdot d\eta = \int_0^a \frac{T}{J}\left[a\frac{c}{2} + \eta \cdot \left(\frac{c}{2} - \frac{\eta}{2}\right)\right] \cdot h \cdot d\eta = \cdots = T \tag{5.5}$$

As illustrated in *Fig. 25*, it can be observed that the forces F_1 and F_2 acting on the flanges and the web (*Fig. 25a*) are statically equivalent to a system composed of a vertical force T and a torsional moment of value F_1c (*Fig. 25b*). This system is, in turn, statically equivalent to a single force T (*Fig. 25c*) acting at a specific point C, known as the shear center.

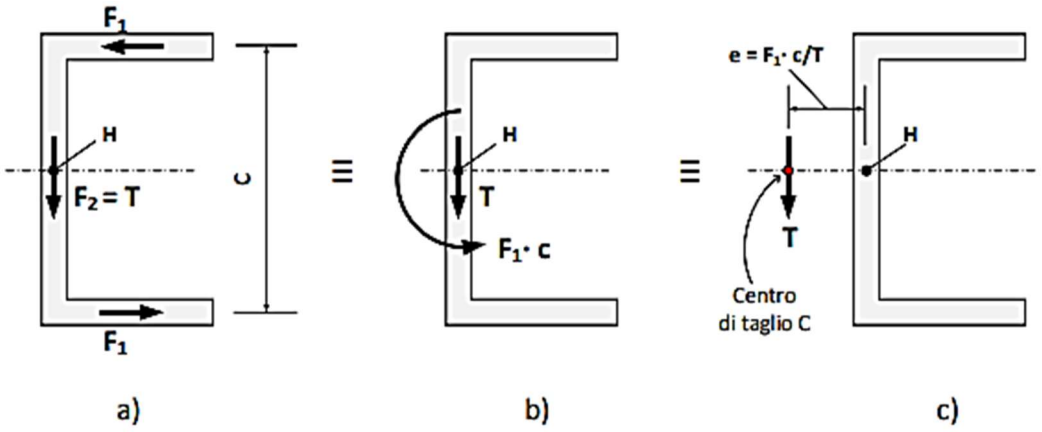

Figure 25: Equivalent systems of forces and shear center [20]

The shear center is, therefore, the specific point of the section such that if the applied load passes through this point, no spurious torsional moment is generated, and the beam bends without twisting.

Conversely, if the load does not pass through the shear center, the shear stresses generated by the shear force produce a spurious torsional moment, causing the beam to undergo both twisting and bending [20].

To calculate the position of the shear centre, we can impose that the equivalent systems (i.e., the system consisting of force F_1 plus the force couple F_2, and the system consisting of the single force T) have the same moment with respect to a freely chosen point.

In this specific case, we can, for example, choose point *H* and equate the moments of the two systems with respect to that point.

$$F_1 \cdot c = T \cdot e \tag{5.6}$$

So:

$$e = \frac{F_1 \cdot c}{T} \tag{5.7}$$

The shear center is therefore located on the horizontal axis of symmetry at a distance ee from point *H*. The position of the torsion center for thin-walled sections with different shapes can be determined by following a similar approach [20].

6. FINITE ELEMENT METHOD

6.1 What is FEM?

The Finite Element Method (FEM) is a numerical procedure used to obtain approximations to the solution of boundary value problems. These problems typically involve sets of ordinary or partial differential equations, where the solution is subject to specific boundary conditions. FEM works by discretizing the domain into smaller, simpler parts (elements), and then solving the resulting system of equations that governs the behavior of the entire structure or system under the given conditions [21].

The Finite Element Method (FEM) was developed to address complex problems of elastic and structural analysis, particularly in the fields of civil and aerospace engineering. Its origins can be traced back to the years 1930-1935, with the work of A. R. Collar and W. J. Duncan, who introduced a primitive concept of structural elements to solve aeroelasticity problems.

Later, between 1940 and 1941, Alexander Hrennikoff and Richard Courant, although using different approaches, shared the idea of breaking down a complex problem into simpler subdomains, known as finite elements [22].

The real rise of FEM happened in the late 1950s, as a result of a series of 1970 key works by M. J. Turner of Boeing, who first created and improved upon the so-called Direct Stiffness Method, the first FEM method to be applied to continuous systems. In civil engineering, Turner's work was replicated and disseminated by John Argyris (University of Stuttgart) and Ray W. Clough (University of Berkeley). Clough, who was first to use the name "FEM," teamed with Turner for a book that is deemed the starting point of modern FEM.

Significant developments were made by B. M. Irons, who invented or developed isoparametric elements, shape functions, the patch test, and the frontal solver for linear algebraic systems, and R. J. Melosh, classified FEM as a Rayleigh-Ritz method and specified its variational format, which was elaborated further by Strang and Fix in 1973 [22].

Additionally, E. L. Wilson developed the first open-source FEM software known as SAP, which became a reference model for many similar programs.

In 1967, Zienkiewicz published the first book dedicated to finite elements. From the 1970s onwards, FEM rapidly became a popular numerical modelling technique in various engineering fields, such as electromagnetism, fluid dynamics, geotechnics, and structural analysis. This period also marked the emergence of major commercial FEM software packages, including NASTRAN, ADINA, ANSYS, ABAQUS, SAMCEF, and MESHPARTS [22].

Although FEM competes with other numerical strategies in specific areas (such as the finite difference method, finite volume method, boundary element method, cell method, and spectral method), it retains a dominant position in the landscape of numerical approximation techniques.

FEM serves as the core of most commercially available automatic analysis codes, particularly in structural and thermo-structural applications. However, its use in Computational Fluid Dynamics (CFD) is more limited due to the instability of solvers at relatively high Reynolds numbers [22].

The general idea is to formulate a deformation of a solid or fluid as a matrix equation of the following form:

$$Ku = f \tag{6.1}$$

Here K is a symmetric, positive definite stiffness matrix, u is a vector of nodal displacements and f is a vector of external forces.

The goal of FEM is to solve for u [21].

6.2 Characteristics of the Elements

Each finite element is characterized by:

- Dimension: elements can be 1-dimensional (1D), 2-dimensional (2D), or 3-dimensional (3D), depending on the complexity of the problem and the detail required for the analysis.
- Nodes: nodes are discrete points used to define the geometry of the element. The degree of every field or field gradient of interest is provided at each node, and these values describe the response of the entire structure. In mechanical elements, proposed reaction forces and displacements are normally expressed for each node in the form of a field.
- Degrees of Freedom (DOF): the possible values of the fields or field gradients at each node. All adjacent nodes have the same values for their corresponding DOF. In structural analysis, they are typically expected displacements and rotations.
- Nodal Forces: external forces applied to the nodes or the effect of reaction forces. A fundamental principle of FEM is the duality between forces and displacements. Given f as the external force vector at a node and u as the vector of DOF, the relationship is assumed to be linear and expressed by Eq. (6.1). The relationship highlights the duality between external forces and displacements, where the scalar product fu corresponds to the work done by external forces. The terms "force", "reaction force", and "stiffness matrix" are broadly applicable beyond mechanical structures, where FEM was initially developed.
- Constitutive Properties: these define the material properties and behavior of the element. For instance, an isotropic material with linear elastic behavior is characterized by Young’s modulus and Poisson’s ratio.
- Solution of a System of Equations: the overall problem is solved by numerically handling a potentially nonlinear system of equations. In linear systems, like the one under consideration, the numerical error introduced by the solution process is typically negligible [22].

The Finite Element Method (FEM) has originated and has been used in academia and the industry entirely because it can be used as a versatile and flexible analytical tool. Focusing on either finite or infinite physical and engineering problems, for example, approximate numerical solutions to complex equations, from a practical point of view it is useful, since a true analytical solution would be often difficult to find and not very useful at all [23].

Research on FEM began somewhat quietly back in the 1960s, but a development boom took place because of the computational tools available during that period had a broad use of the principles and practices of FEM. Its development has been spectacular because of its applicability in so many different fields [23].

FEM has proven itself as one of the best tools available when there is a system to be analyzed, especially when experimental investigation and laboratory testing would lead to huge relative costs and difficulties in measuring physics values [23].

While early automated approaches for solving differential equations governing physical phenomena primarily relied on finite difference methods, FEM expanded these capabilities by offering unparalleled flexibility.

The generality of the method, initially developed by engineers and later rigorously formalized by mathematicians, has enabled numerous studies and applications. This foundational work has paved the way for new research avenues addressing both theoretical and practical challenges of great interest [23].

The method involves discretizing the structure into finite elements, each of which is represented by a set of mathematical equations.

These equations describe the material behavior, geometric properties, and loading conditions applied to the individual elements. Once all the elements are mathematically defined, they are assembled into a comprehensive computational model of the structure [24].

The numerical solution method allows users to find the stress and deformation conditions within the structure at all points in the model.

This allows the FEM model to be a reliable tool for predicting structural behavior when subjected to an external load, and providing insights into areas of stress and deformation [24].

The FEM model is one of the most frequently used modelling methods across many engineering fields, including structural strength analysis, simulation of mechanical system behavior, product design, and performance optimization [24].

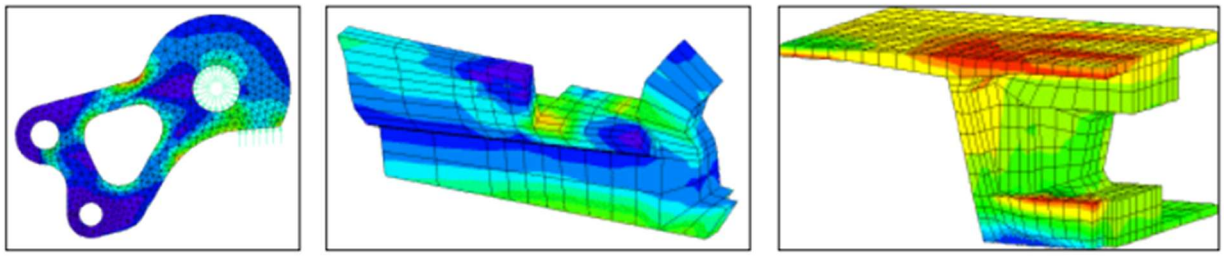

Figure 26: Example results of a FEM analysis [23]

6.3 FEM Analysis of Thin-Walled Beams

The buckling behavior analysis of thin-walled open section beams can be particularly challenging, especially when seeking for a solution in an exact form [11].

This complexity arises from several factors:

1. Constraint Conditions: The specific constraints imposed on the beam can significantly influence its buckling behavior, particularly in terms of warping.
2. Variable Coefficients: When the beam is subjected to transverse loads, the equilibrium equations involve variable coefficients, further complicating the analysis.
3. Load Application Point: The location of the applied transverse loads can also affect the buckling response.

For this study in the field of finite elements, it was decided to analyze a single, straight beam. Polynomial interpolation functions are only used, since the problem cannot be integrated in exact form, even in a subdomain [11].

To perform the analysis some hypothesis have been taken into account:

- The initial bending moment, which can vary arbitrarily along the beam's length, is simplified by approximating it as a piecewise linear function. This approximation is based on the nodal values of the bending moment.
- Additionally, the axial force is assumed to be constant within each element of the finite element model [11].

6.3.1 Polynomial Finite Element

As is usually the case in the application of the finite element methodology, the analysis was carried out on a single element of a beam with an open thin section; the individual elements were then combined to obtain the complete analysis of the beam [11].

6.3.2 Total potential energy

The analyzed element e of the open TWB section, has a length *l* and is pre-solicited by a constant axial force N_0 and bending moments $M_x^0(z)$ and $M_y^0(z)$, variables along z [11].

It is possible to define:

- the transverse nodal displacements u_{Ci}, v_{Ci}, θ_i with (i = 1,2) of the torsion center axis,
- the torsional curvatures $\kappa_{ti} \coloneqq \theta_i'$;
- the longitudinal nodal displacements ω_i, φ_{xi}, φ_{yi} with (i = 1,2) of the centroid axis.

The beam element therefore has 14 degrees of freedom:

$$\mathbf{q}^{(e)} \coloneqq \left(u_{C1}, v_{C1}, \omega_1, \varphi_{x1}, \varphi_{y1}, \theta_1, \kappa_{t1}; u_{C2}, v_{C2}, \omega_2, \varphi_{x2}, \varphi_{y2}, \theta_2, \kappa_{t2}\right)^T \quad (6.2)$$

The incremental nodal forces acting at the ends of the beam are:

$$\mathbf{f}^{(e)} \coloneqq \left(f_{x1}, f_{y1}, f_{z1}, m_{x1}, m_{y1}, m_{z1}, b_1; f_{x2}, f_{y2}, f_{z2}, m_{x2}, m_{y2}, m_{z2}, b_2\right)^T \quad (6.3)$$

Where f_{xi}, f_{yi}, f_{zi} are proper transverse and longitudinal forces; m_{xi}, m_{yi}, m_{zi} are flexural and torsional couples; b_i are bicouples, dual of the torsional curvature [11].

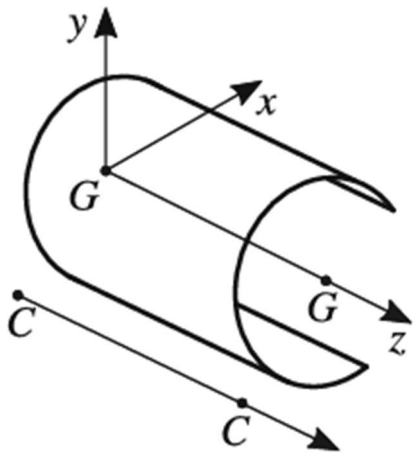

Figure 27: Finite element of open TWB: axes [11]

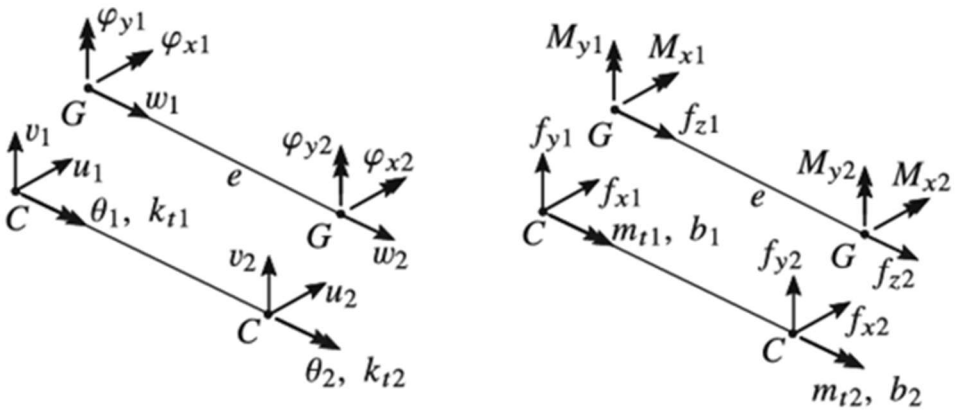

Figure 28: Finite element of open TWB: nodal displacements (on the left) and nodal forces (on the right) [11]

It is possible to compute the total potential energy of the prestressed system as:

$$\Pi = \widetilde{U} + U^0 + V \tag{6.4}$$

where $\widetilde{U}$ is the incremental elastic energy, U^0 is the prestress energy, and V is the load potential energy (of prestressing and incremental loads) [11].

These contributions can be calculated as:

$$\widetilde{U} = \frac{1}{2}\int_0^l \left(EA\omega_G'^2 + EI_y u_C''^2 + EI_x v_C''^2 + GJ\theta'^2 + EI_\omega \theta''^2\right)dz \tag{6.5}$$

$$\begin{aligned} U^0 = {} & \mu\frac{N_0}{2}\int_0^l [u_C'^2 + v_C'^2 + r_C^2\theta'^2 + 2y_C u_C'\theta' - 2x_C v_C'\theta']dz \\ & +\mu\int_0^l \left[-(M_x^0\theta)'(u_C' + y_H\theta') - \left(M_y^0\theta\right)'(v_C' + x_H\theta')\right]dz \end{aligned} \tag{6.6}$$

$$V = \mu\frac{e_Q}{2}\int_0^l p(z)\theta^2(z)dz - \mathbf{f}^{(e)T}\mathbf{q}^{(e)} \tag{6.7}$$

Where:

- x_C and y_C are the coordinates of the shear center *C*;
- e_Q is the distance between *C* and the point of application of force *Q*
- x_H and y_H coordinates of the axial center of force *H*, calculated as a correction with respect to the coordinates of the center of shear *C* according to the formulas:

$$x_H := x_C - \frac{1}{2I_y}\int_\Gamma x(x^2 + y^2)\,bds\,, y_H := y_C - \frac{1}{2I_x}\int_\Gamma y(x^2 + y^2)\,bds \tag{6.8a,b}$$

6.3.3 Interpolation functions

The displacement fields $u(z)$, $v(z)$, $\omega(z)$, and $\theta(z)$ are interpolated between the nodal values:

$$\omega(z) = \psi_1(z)\omega_1 + \psi_2(z)\omega_2 \tag{6.9}$$

$$u(z) = \psi_3(z)u_1 + \psi_4(z)\varphi_{y1} + \psi_5(z)u_5 + \psi_6(z)\varphi_{y2} \tag{6.10}$$

$$v(z) = \psi_3(z)v_1 - \psi_4(z)\varphi_{x1} + \psi_5(z)v_2 - \psi_6(z)\varphi_{x2} \tag{6.11}$$

$$\theta(z) = \psi_3(z)\theta_1 + \psi_4(z)\kappa_{t1} + \psi_5(z)\theta_2 + \psi_6(z)\kappa_{t2} \tag{6.12}$$

Where $\psi_i(z)$, $i = 1,\ldots,6$, are the following interpolation functions:

$$\psi_1(z) = 1 - \frac{z}{l} \quad , \quad \psi_2(z) = \frac{z}{l} \tag{6.13a,b}$$

$$\psi_3(z) = 1 - 3\left(\frac{z}{l}\right)^2 + 2\left(\frac{z}{l}\right)^3 \quad , \quad \psi_4(z) = z\left[1 - 2\frac{z}{l} + \left(\frac{z}{l}\right)^2\right] \tag{6.14a,b}$$

$$\psi_5(z) = 3\left(\frac{z}{l}\right)^2 - 2\left(\frac{z}{l}\right)^3 \quad , \quad \psi_6(z) = z\left[\left(\frac{z}{l}\right)^2 - \frac{z}{l}\right] \tag{6.15a,b}$$

The prestress bending moments are linearly interpolated between the nodal values M_{xi}^0, M_{yi}^0 $(i = 1, 2)$ as:

$$M_x^0(z) = \psi_1(z)M_{x1}^0 + \psi_2(z)M_{x2}^0 \tag{6.16}$$

$$M_y^0(z) = \psi_1(z)M_{y1}^0 + \psi_2(z)M_{y2}^0 \tag{6.17}$$

By substituting the equations of the displacement field and the prestress bending moments into the energy equations, integrating over z, and enforcing stationarity with respect to the Lagrangian parameters, the following element equilibrium equations are obtained:

$$\left(\mathbf{K}_e^{(e)} + \mu\mathbf{K}_g^{(e)}\right)\mathbf{q}^{(e)} = \mathbf{f}^{(e)} \tag{6.18}$$

Where $\mathbf{K}_e^{(e)}$ is the elastic matrix and $\mathbf{K}_g^{(e)}$ the geometric matrix [11].

In particular, the geometric matrix is the sum of three contributions:

$$\mathbf{K}_g^{(e)} =: \mathbf{K}_{g,N}^{(e)} + \mathbf{K}_{g,M}^{(e)} + \mathbf{K}_{g,p}^{(e)} \tag{6.19}$$

Which are the contributions, respectively, due to axial prestress, bending prestresses and eccentricity of the transverse loads [11].

6.3.4 Stiffness matrices of the TWB finite element

The stiffness matrices $\mathbf{K}_e^{(e)}$, $\mathbf{K}_{g,N}^{(e)}$, $\mathbf{K}_{g,M}^{(e)}$, $\mathbf{K}_{g,p}^{(e)}$ have the dimensions of DOF×DOF, so 14×14, and are partitioned into four sub-matrices of dimension 7×7 [11].

It is possible to write, in general:

$$\mathbf{K}_\alpha := \begin{bmatrix} \mathbf{K}_\alpha^{(1,1)} & \mathbf{K}_\alpha^{(1,2)} \\ \mathbf{K}_\alpha^{(2,1)} & \mathbf{K}_\alpha^{(2,2)} \end{bmatrix} \tag{6.20}$$

With $\mathbf{K}_\alpha^{(2,1)} = \left(\mathbf{K}_\alpha^{(1,2)}\right)^T$.

The following are the non-zero values of the elements of the four stiffness matrices [11].

• Elastic matrix [11]:

$\mathbf{K}_e^{(1,1)}$:

$$K_{e11}^{(1,1)} = \frac{EA}{l} \quad , K_{e22}^{(1,1)} = \frac{12EI_y}{l^3} \quad , \quad K_{e23}^{(1,1)} = \frac{6EI_y}{l^2} \quad , \quad K_{e33}^{(1,1)} = \frac{4EI_y}{l}$$

$$K_{e4}^{(1,1)} = \frac{12EI_x}{l^3} \quad , \quad K_{e45}^{(1,1)} = -\frac{6EI_x}{l^2} \quad , \quad K_{e5}^{(1,1)} = \frac{4EI_x}{l}$$

$$K_{e6}^{(1,1)} = \frac{12EI_\omega}{l^3} + \frac{6GJ}{5l} \quad , \quad K_{e67}^{(1,1)} = \frac{6EI_\omega}{l^2} + \frac{GJ}{10} \quad , \quad K_{e77}^{(1,1)} = \frac{4EI_\omega}{l} + \frac{2GJl}{15}$$

(6.21)

$\mathbf{K}_e^{(2,1)}$:

$$K_{e11}^{(2,1)} = -\frac{EA}{l} \quad , \quad K_{e22}^{(2,1)} = -\frac{12EI_y}{l^3} \quad , \quad K_{e23}^{(2,1)} = -K_{e3}^{(2,1)} = -\frac{6EI_y}{l^2}$$

$$K_{e33}^{(2,1)} = \frac{2EI_y}{l} \quad , \quad K_{e4}^{(2,1)} = -\frac{12EI_x}{l^3} \quad , \quad K_{e45}^{(2,1)} = -K_{e54}^{(2,1)} = \frac{6EI_x}{l^2}$$

$$K_{e55}^{(2,1)} = \frac{2EI_x}{l} \quad , \quad K_{e66}^{(2,1)} = -\frac{12EI_\omega}{l^3} - \frac{6GJ}{5l}$$

$$K_{e67}^{(2,1)} = -K_{e76}^{(2,1)} = -\frac{6EI_\omega}{l^2} - \frac{GJ}{10} \quad , \quad K_{e77}^{(2,1)} = \frac{2EI_\omega}{l} - \frac{GJl}{30}$$

(6.22)

$\mathbf{K}_e^{(2,2)}$:

$$K_{e1}^{(2,2)} = \frac{EA}{l} \quad , \quad K_{e22}^{(2,2)} = \frac{12EI_y}{l^3} \quad , \quad K_{e23}^{(2,2)} = -\frac{6EI_y}{l^2} \quad , \quad K_{e33}^{(2,2)} = \frac{4EI_y}{l}$$

$$K_{e44}^{(2,2)} = \frac{12EI_x}{l^3} \quad , \quad K_{e45}^{(2,2)} = \frac{6EI_x}{l^2} \quad , \quad K_{e55}^{(2,2)} = \frac{4EI_x}{l}$$

$$K_{e66}^{(2,2)} = \frac{12EI_\omega}{l^3} + \frac{6GJ}{5l} \quad , \quad K_{e67}^{(2,2)} = -\frac{6EI_\omega}{l^2} - \frac{GJ}{10} \quad , \quad K_{e77}^{(2,2)} = \frac{4EI_\omega}{l} + \frac{2GJl}{15}$$

(6.23)

• Geometric matrix, related to the axial force [11]:

$$\mathbf{K}_{g,N}^{(1,1)} := N_0 \begin{bmatrix} 0 & 0 & 0 & 0 & 0 & 0 & 0 \\ 0 & \frac{6l}{5} & \frac{1}{10} & 0 & 0 & \frac{6y_C}{5l} & \frac{y_C}{10} \\ 0 & \frac{1}{10} & \frac{2l}{15} & 0 & 0 & \frac{y_C}{10} & \frac{2ly_C}{15} \\ 0 & 0 & 0 & \frac{6l}{5} & -\frac{1}{10} & -\frac{6x_C}{5l} & -\frac{x_C}{10} \\ 0 & 0 & 0 & -\frac{1}{10} & \frac{2l}{15} & \frac{x_C}{10} & \frac{2lx_C}{15} \\ 0 & \frac{6y_C}{5l} & \frac{y_C}{10} & -\frac{6x_C}{5l} & \frac{x_C}{10} & \frac{6r_C^2}{5l} & \frac{r_C^2}{10} \\ 0 & \frac{y_C}{10} & \frac{2ly_C}{15} & -\frac{x_C}{10} & \frac{2lx_C}{15} & \frac{r_C^2}{10} & \frac{2lr_C^2}{15} \end{bmatrix}$$

$$\mathbf{K}_{g,N}^{(2,1)} := N_0 \begin{bmatrix} 0 & 0 & 0 & 0 & 0 & 0 & 0 \\ 0 & -\frac{6l}{5} & -\frac{1}{10} & 0 & 0 & -\frac{6y_C}{5l} & -\frac{y_C}{10} \\ 0 & \frac{1}{10} & -\frac{l}{30} & 0 & 0 & \frac{y_C}{10} & -\frac{ly_C}{30} \\ 0 & 0 & 0 & -\frac{6l}{5} & \frac{1}{10} & -\frac{6x_C}{5l} & -\frac{x_C}{10} \\ 0 & 0 & 0 & -\frac{1}{10} & -\frac{l}{30} & \frac{x_C}{10} & -\frac{lx_C}{30} \\ 0 & -\frac{6y_C}{5l} & -\frac{y_C}{10} & \frac{6x_C}{5l} & -\frac{x_C}{10} & -\frac{6r_C^2}{5l} & -\frac{r_C^2}{10} \\ 0 & \frac{y_C}{10} & -\frac{ly_C}{30} & -\frac{x_C}{10} & -\frac{lx_C}{30} & \frac{r_C^2}{10} & -\frac{lr_C^2}{30} \end{bmatrix} \tag{6.24}$$

$$\mathbf{K}_{g,N}^{(2,2)} := N_0 \begin{bmatrix} 0 & 0 & 0 & 0 & 0 & 0 & 0 \\ 0 & \frac{6l}{5} & -\frac{1}{10} & 0 & 0 & \frac{6y_C}{5l} & -\frac{y_C}{10} \\ 0 & -\frac{1}{10} & \frac{2l}{15} & 0 & 0 & -\frac{y_C}{10} & \frac{2ly_C}{15} \\ 0 & 0 & 0 & \frac{6l}{5} & \frac{1}{10} & -\frac{6x_C}{5l} & \frac{x_C}{10} \\ 0 & 0 & 0 & \frac{1}{10} & \frac{2l}{15} & -\frac{x_C}{10} & \frac{2lx_C}{15} \\ 0 & \frac{6y_C}{5l} & -\frac{y_C}{10} & -\frac{6x_C}{5l} & -\frac{x_C}{10} & \frac{6r_C^2}{5l} & -\frac{r_C^2}{10} \\ 0 & -\frac{y_C}{10} & \frac{2ly_C}{15} & \frac{x_C}{10} & \frac{2lx_C}{15} & -\frac{r_C^2}{10} & \frac{2lr_C^2}{15} \end{bmatrix}$$

• Geometric matrix, related to the bending moments [11]:

$\mathbf{K}_{g,M}^{(1,1)}$:

$$K_{g,M26}^{(1,1)} = -\frac{1}{10l}(11M_{x1}^0 + M_{x2}^0) \quad , \quad K_{g,M2}^{(1,1)} = -\frac{M_{x1}^0}{10}$$

$$K_{g,M36}^{(1,1)} = \frac{1}{10}(M_{x1}^0 - 2M_{x2}^0) \quad , \quad K_{g,M3}^{(1,1)} = -\frac{l}{10}(3M_{x1}^0 + M_{x2}^0)$$

$$K_{g,M4}^{(1,1)} = -\frac{1}{10l}\left(11M_{y1}^0 + M_{y2}^0\right) \quad , \quad K_{g,M4}^{(1,1)} = -\frac{M_{y1}^0}{10}$$

$$K_{g,M56}^{(1,1)} = \frac{1}{10}\left(2M_{y2}^0 - M_{y1}^0\right) \quad , \quad K_{g,M57}^{(1,1)} = \frac{l}{10}\left(3M_{y1}^0 + M_{y2}^0\right)$$

$$K_{g,M66}^{(1,1)} = \frac{1}{5l}\left[x_H\left(11M_{y1}^0 + M_{y2}^0\right) - y_H(11M_{x1}^0 + M_{x2}^0)\right]$$

$$K_{g,M67}^{(1,1)} = \frac{1}{5}\left(x_H M_{y2}^0 - y_H M_{x2}^0\right)$$

$$K_{g,M77}^{(1,1)} = \frac{l}{15}\left[x_H\left(3M_{y1}^0 + M_{y2}^0\right) - y_H(3M_{x1}^0 + M_{x2}^0)\right]$$

(6.25)

$\mathbf{K}_{g,M}^{(2,1)}$:

$$K_{g,M2}^{(2,1)} = \frac{1}{10l}(11M_{x1}^0 + M_{x2}^0) \quad , \quad K_{g,M2}^{(2,1)} = \frac{M_{x1}^0}{10}$$

$$K_{g,M3}^{(2,1)} = \frac{1}{10}(M_{x2}^0 - 2M_{x1}^0) \quad , \quad K_{g,M3}^{(2,1)} = \frac{lM_{x2}^0}{10}$$

$$K_{g,M46}^{(2,1)} = \frac{1}{10l}\left(11M_{y1}^0 + M_{y2}^0\right) \quad , \quad K_{g,M4}^{(2,1)} = \frac{M_{y1}^0}{10}$$

$$K_{g,M56}^{(2,1)} = \frac{1}{10}\left(2M_{y1}^0 - M_{y2}^0\right) \quad , \quad K_{g,M57}^{(2,1)} = -\frac{lM_{y2}^0}{30}$$

$$K_{g,M62}^{(2,1)} = \frac{1}{10l}(M_{x1}^0 + 11M_{x2}^0) \quad , \quad K_{g,M63}^{(2,1)} = \frac{1}{10}(2M_{x2}^0 - M_{x1}^0)$$

$$K_{g,M64}^{(2,1)} = \frac{1}{10l}\left(M_{y1}^{0} + 11M_{y2}^{0}\right) \quad , \quad K_{g,M65}^{(2,1)} = \frac{1}{10}\left(M_{y1}^{0} - 2M_{y2}^{0}\right)$$

$$K_{g,M67}^{(2,1)} = \frac{1}{5}\left(y_H M_{x2}^{0} - x_H M_{y2}^{0}\right) \quad , \quad K_{g,M72}^{(2,1)} = -\frac{M_{x2}^{0}}{10} \quad , \quad K_{g,M73}^{(2,1)} = \frac{lM_{x1}^{0}}{30}$$

$$K_{g,M74}^{(2,1)} = -\frac{M_{y2}^{0}}{10} \quad , \quad K_{g,M75}^{(2,1)} = -\frac{lM_{y1}^{0}}{30} \quad , \quad K_{g,M76}^{(2,1)} = \frac{1}{5}\left[x_H M_{y1}^{0} - y_H M_{x1}^{0}\right]$$

$$K_{g,M66}^{(2,1)} = -\frac{6}{5l}\left[x_H\left(M_{y1}^{0} + M_{y2}^{0}\right) - 6y_H\left(M_{x1}^{0} + M_{x2}^{0}\right)\right]$$

$$K_{g,M77}^{(2,1)} = -\frac{l}{30}\left[x_H\left(M_{y1}^{0} + M_{y2}^{0}\right) - y_H\left(M_{x1}^{0} + M_{x2}^{0}\right)\right]$$

(6.26)

$\mathbf{K}_{g,M}^{(2,2)}$:

$$K_{g,M26}^{(2,2)} = \frac{1}{10l}\left(M_{x1}^{0} + 11M_{x2}^{0}\right) \quad , \quad K_{g,M27}^{(2,2)} = \frac{M_{x2}^{0}}{10}$$

$$K_{g,M36}^{(2,2)} = \frac{1}{10}\left(2M_{x1}^{0} - M_{x2}^{0}\right) \quad , \quad K_{g,M37}^{(2,2)} = -\frac{l}{30}\left(M_{x1}^{0} + 3M_{x2}^{0}\right)$$

$$K_{g,M46}^{(2,2)} = -\frac{1}{10l}\left(M_{y1}^{0} + 11M_{y2}^{0}\right) \quad , \quad K_{g,M47}^{(2,2)} = \frac{M_{y2}^{0}}{10}$$

$$K_{g,M56}^{(2,2)} = \frac{1}{10}\left(M_{y2}^{0} - 2M_{y1}^{0}\right) \quad , \quad K_{g,M57}^{(2,2)} = \frac{l}{30}\left(M_{y1}^{0} + 3M_{y2}^{0}\right)$$

$$K_{g,M6}^{(2,2)} = \frac{1}{5l}\left[x_H\left(M_{y1}^{0} + 11M_{y2}^{0}\right) - y_H\left(M_{x1}^{0} + 11M_{x2}^{0}\right)\right]$$

$$K_{g,M6}^{(2,2)} = \frac{1}{5}\left(y_H M_{x1}^{0} - x_H M_{y1}^{0}\right)$$

$$K_{g,M77}^{(2,2)} = \frac{l}{15}\left[x_H\left(M_{y1}^{0} + 3M_{y2}^{0}\right) - y_H\left(M_{x1}^{0} + 3M_{x2}^{0}\right)\right]$$

(6.27)

• Geometric matrix, related to the eccentricity, with respect to the centre of torsion, of the application point of the transverse loads [11]:

$$\mathbf{K}_{g,p}^{(1,1)} = \begin{bmatrix} 0 & 0 & 0 & 0 & 0 & 0 & 0 \\ 0 & 0 & 0 & 0 & 0 & 0 & 0 \\ 0 & 0 & 0 & 0 & 0 & 0 & 0 \\ 0 & 0 & 0 & 0 & 0 & 0 & 0 \\ 0 & 0 & 0 & 0 & 0 & 0 & 0 \\ 0 & 0 & 0 & 0 & 0 & \frac{13}{35}e_Q pl & \frac{11}{210}e_Q pl^2 \\ 0 & 0 & 0 & 0 & 0 & \frac{11}{210}e_Q pl^2 & \frac{1}{105}e_Q pl^3 \end{bmatrix}$$

$$\mathbf{K}_{g,p}^{(2,1)} = \begin{bmatrix} 0 & 0 & 0 & 0 & 0 & 0 & 0 \\ 0 & 0 & 0 & 0 & 0 & 0 & 0 \\ 0 & 0 & 0 & 0 & 0 & 0 & 0 \\ 0 & 0 & 0 & 0 & 0 & 0 & 0 \\ 0 & 0 & 0 & 0 & 0 & 0 & 0 \\ 0 & 0 & 0 & 0 & 0 & \frac{9}{70}e_Q pl & \frac{13}{420}e_Q pl^2 \\ 0 & 0 & 0 & 0 & 0 & -\frac{13}{420}e_Q pl^2 & -\frac{1}{140}e_Q pl^3 \end{bmatrix} \tag{6.28}$$

$$\mathbf{K}_{g,p}^{(2,2)} = \begin{bmatrix} 0 & 0 & 0 & 0 & 0 & 0 & 0 \\ 0 & 0 & 0 & 0 & 0 & 0 & 0 \\ 0 & 0 & 0 & 0 & 0 & 0 & 0 \\ 0 & 0 & 0 & 0 & 0 & 0 & 0 \\ 0 & 0 & 0 & 0 & 0 & 0 & 0 \\ 0 & 0 & 0 & 0 & 0 & \frac{13}{35}e_Q pl & -\frac{11}{210}e_Q pl^2 \\ 0 & 0 & 0 & 0 & 0 & -\frac{11}{210}e_Q pl^2 & \frac{1}{105}e_Q pl^3 \end{bmatrix}$$

6.3.5 Matrix assembly

A straight TWB is considered, divided into finite elements labeled $e = 1,2,\ldots,m$.

Once the prestress state at the nodes is determined using the previous expressions, the stiffness matrices for each element are computed. These matrices are then assembled, and constraints are applied, following the standard linear elastic analysis approach. Specifically, when a torsional clamp is applied at node i, it holds that $\theta_i = 0$.

However, it is necessary to distinguish whether the constraint restricts or allows warping [11].

In the first scenario, the torsional curvature is set to zero $\kappa_{ti} = 0$, whereas in the second scenario κ_{ti} is left unrestricted (examples in Appendix C illustrate this concept) [11].

The procedure leads to the eigenvalue problem:

$$\left(\mathbf{K}_e + \mu \mathbf{K}_g\right)\mathbf{q} = 0 \tag{6.29}$$

where μ is the multiplier of the prestresses.

The smallest eigenvalue μ_c is the critical value sought for [11].

6.4 Implementation of the theory in a Matlab code: an overview of the code structure

Taking into account the analysis just proposed, a code was implemented using the "Matlab" software, to perform an elastic buckling analysis of thin-walled beams using the finite element method (FEM), with the aim of determining the critical buckling load and analyzing the behavior of the structure under load. The code has been structured as follows, specifically using Matlab functions to divide the problem into logical and independent modules, thus improving the readability and maintainability of the code, as each function has been designed to perform a specific task.

1. Definition of the Initial Parameters

Initially, the geometric parameters, material characteristics and numerical factors necessary for the analysis were defined:

- Degrees of Freedom (DOF): The total number of degrees of freedom per node and for the entire structure.
- Cross-sectional geometry: all parameters have been defined to characterise the section and the geometric properties of the section, such as area, moments of inertia and polar moment, have been calculated.
- Material properties: The modulus of elasticity E and the shear modulus G were defined to characterize the elastic behavior of the material.
- Discretization: the total length of the l_{tot} beam was defined, then divided into a number m of finite elements, each with a length le.

2. Applied loads

Subsequently, the loads acting on the structure were defined:

- Distributed load, p (it has been chosen to consider a uniform load along z-axes);
- Axial forces, N;
- Bending moments, $M_{y,first\_node}$, $M_{y,last\_node}$;
- Twisting moments, $M_{x,first\_node}$, $M_{x,last\_node}$.

3. Global Forces Vector

Subsequently, the vector of global forces was assembled considering the distribution of equivalent nodal loads along the degrees of freedom of the structure.

4. Definition of the Remaining Parameters Necessary for the Analysis

Other necessary parameters were calculated, such as: the coordinates of the shear center (x_C, y_C), the radius of the shear center (r_C), and the eccentricity of the load (e_Q).

These parameters are critical to consider the effects of torsional and flexural buckling.

5. Stiffness Matrices

The elastic stiffness matrices (K_e) and geometric (K_g) have been calculated for each finite element, taking into account:

- The axial, flexural and torsional stiffness,
- The geometric effects due to the applied loads.

The global stiffness matrices were then iteratively assembled for the entire structure.

6. Normalization of the Global Stiffness Matrix

To improve numerical stability, the global stiffness matrix K_{global}, has been normalized with respect to the maximum value of its elements.

7. Critical Load Analysis

To perform the critical load analysis, we solved a problem with eigenvalues and eigenvectors to determine the critical buckling load, considering:

- The identification of constrained degrees of freedom (*fixed_dof*);
- The modification of the stiffness matrices to include boundary conditions;
- The calculation of the global critical load (*Pc) and the related eigenvectors* (q_{Pc}).

8. Calculation of Critical Displacements

Finally, through the use of the interpolation functions reported above, the critical displacements of the beam under the critical load were calculated, including:

- Transverse displacements (w, v);
- Axial displacements (u);
- Rotations (θ);

The results have been normalized to take into account that a linear buckling analysis is being performed.

In the following section, a comparison between the results obtained through the code implemented on Matlab and the results obtained by the authors of the reported Theory, present in the source [11], has been reported.

To summarize the functioning of the code, a workflow was developed and is described in *Chapter 7*, prior to the presentation of the additional analyses conducted using it.

6.5 Simply Supported Beam with Circular Cross-Section Subjected to *P*

Parameters: $R = 40$ mm, $b = 4$ mm, $l = 4$ m, $E = 207{,}000$ N/mm^2 and $G = 79{,}300$ N/mm^2.

The analysis has been performed considering a mesh of $m = 50$.

Compressed TWB, simply supported, torsionally clamped with free warping:

Result from the book:

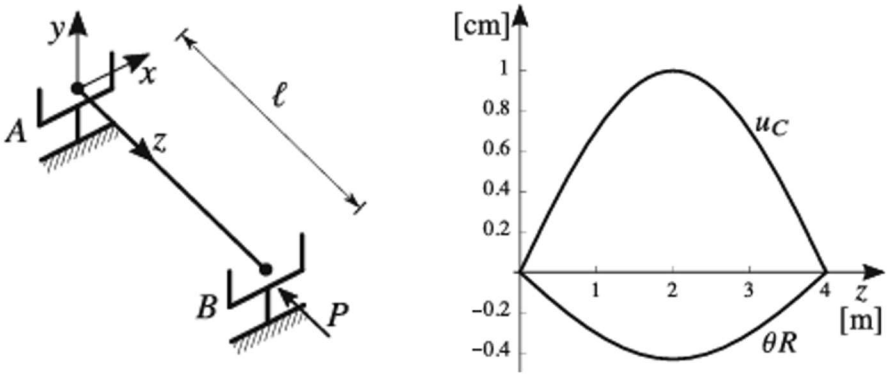

Figure 29: Model of the beam and applied load (on the left) and result of the analysis (on the right) [11]

$P_c = 55$ KN

Results from the Matlab code:

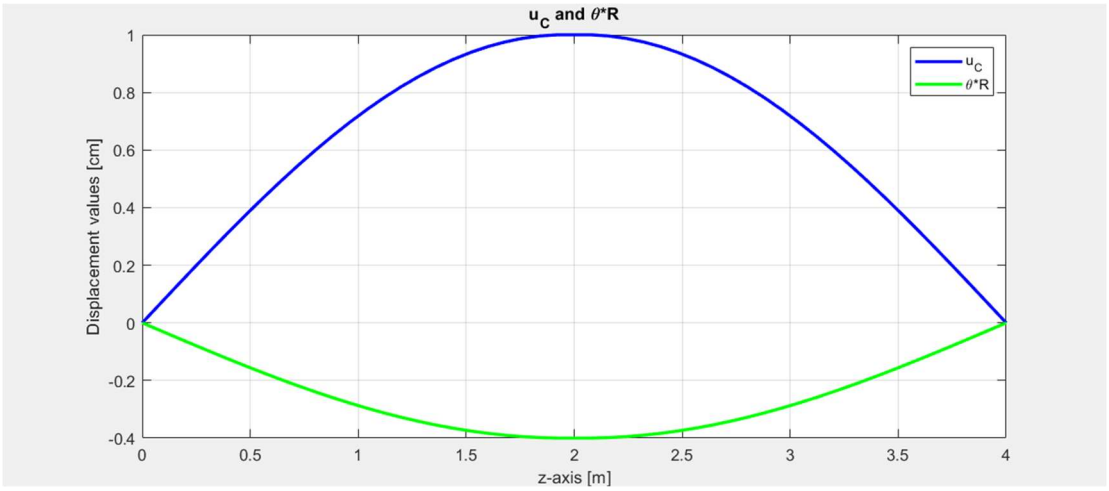

Figure 30: Result of the buckling analysis from Matlab code

The critical load calculated from the following analysis is: 5.1344 E+04 N

The percentage difference between the two values is: 6,64%

6.6 Simply Supported Beam Torsionally Constrained with Circular Cross-Section Subjected to *P*

Parameters: $R = 40$ mm, $b = 4$ mm, $l = 4$ m, $E = 207{,}000$ N/mm^2 and $G = 79{,}300$ N/mm^2.

The analysis has been performed considering a mesh of $m = 30$.

Simply supported compressed twin-walled beam, torsionally clamped with prevented warping:

Results from the book:

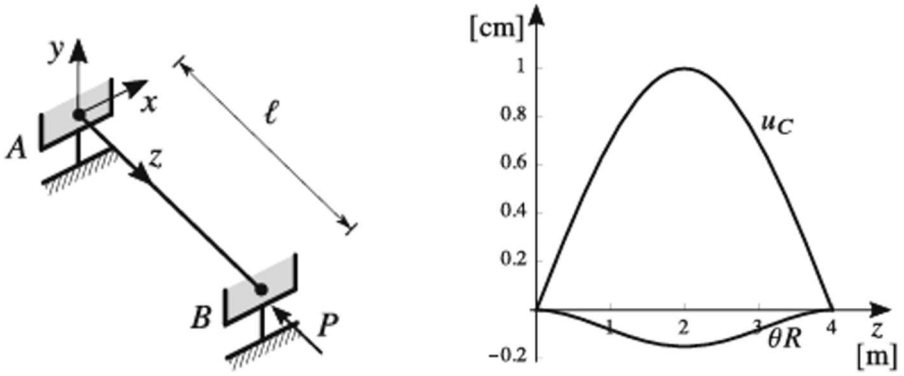

Figure 31: Model of the beam and applied load (on the left) and result of the analysis (on the right) [11]

$P_c = 81.04$ KN

Results from the Matlab code:

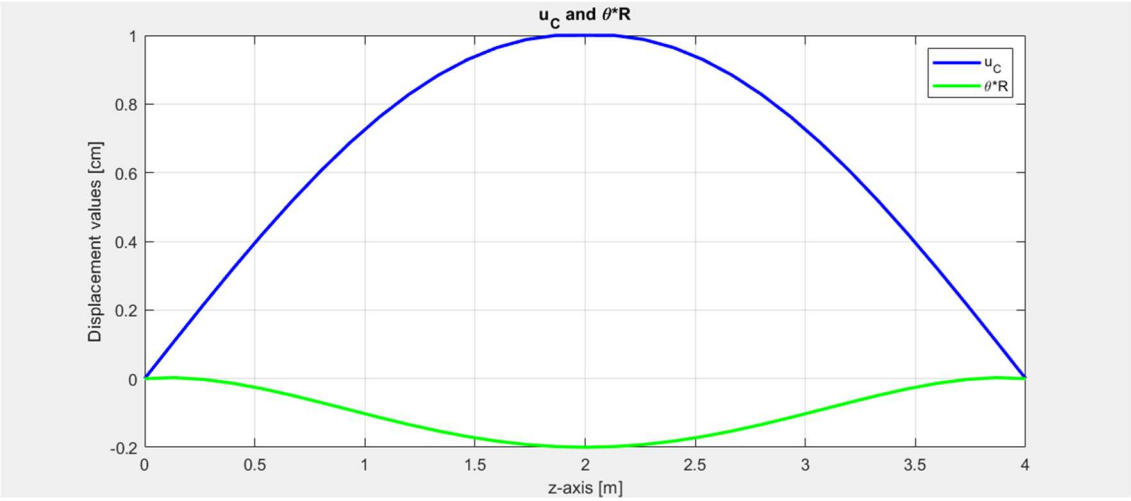

Figure 32: Result of the buckling analysis from Matlab code

The critical load calculated from the following analysis is: 8.2152 E+04 N

The percentage difference between the two values is: 1,37%

6.7 Simply Supported Beam with Circular Cross-Section Subjected to Couple *C*

Parameters: $R = 40$ mm, $b = 4$ mm, $l = 4$ m, $E = 207{,}000$ N/mm^2 and $G = 79{,}300$ N/mm^2.

The analysis has been performed considering a mesh of $m = 50$.

Uniformly bent thin-walled beam, simply supported, torsionally clamped with prevented warping:

Results from the book:

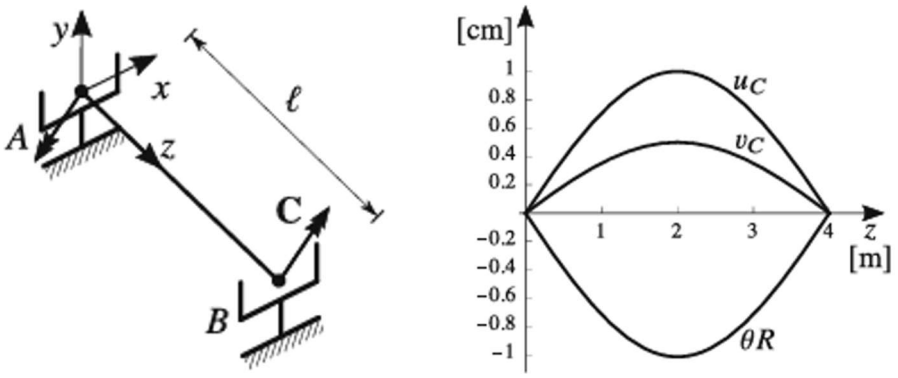

Figure 33: Model of the beam and applied load (on the left) and result of the analysis (on the right) [11]

C_c = - 4.06 KNm

Results from the Matlab code:

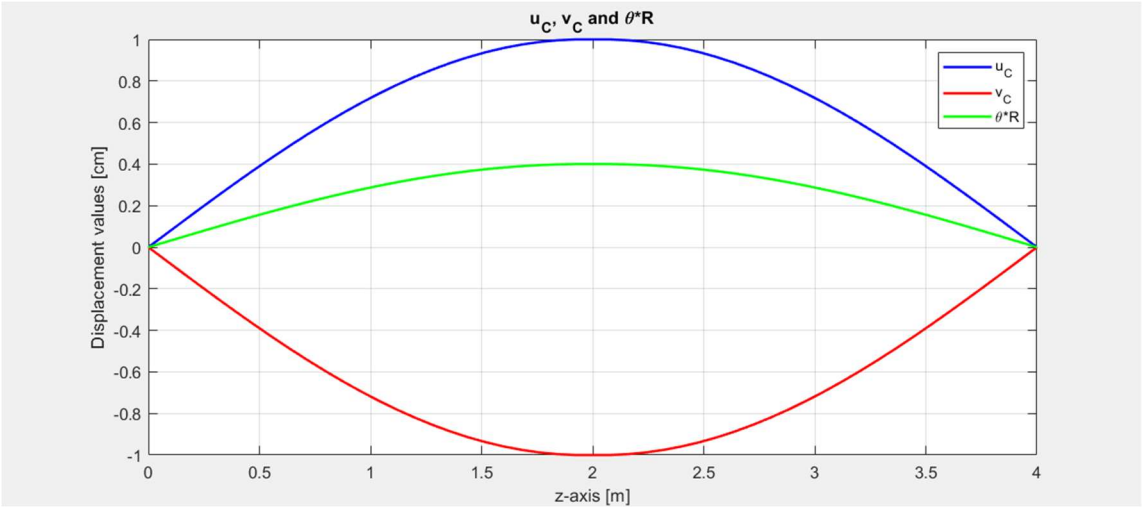

Figure 34: Result of the buckling analysis from Matlab code

The critical load calculated from the following analysis is: -3.81 Nm

The percentage difference between the two values is: 6,36%

6.8 Cantilever Beam with Narrow Rectangular Cross-Section Subjected to *F*

Parameters: $b = 2$ mm, $h = 100$ mm, $l = 1$ m, $E = 207{,}000$ N/mm^2 and $G = 79{,}300$ N/mm^2.

The analysis has been performed considering a mesh of $m = 500$.

Fixed-free TWB with thin rectangular cross-section, non-uniformly bent by a concentrated load:

Results from the book:

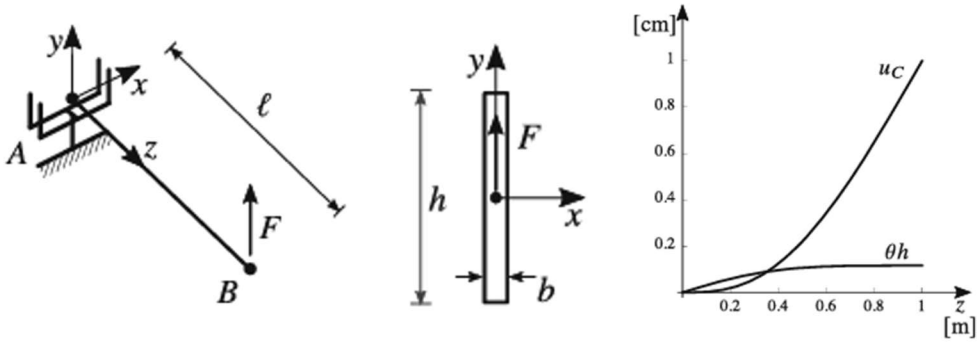

Figure 35: Model of the beam and applied load (on the left), geometric parameters of the section (in the center) and result of the analysis (on the right) [11]

$F_c = 68.9$ KN

Results from Matlab code:

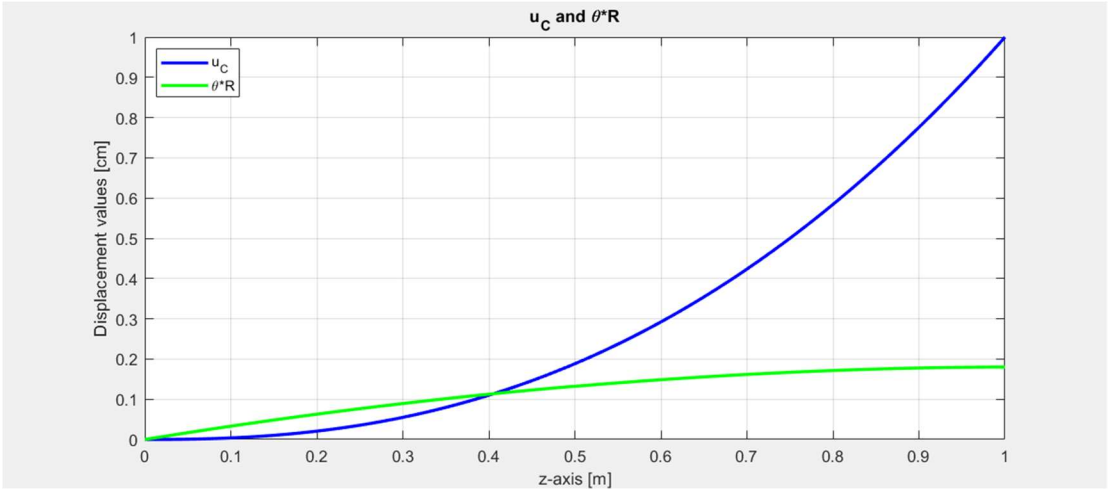

Figure 36: Result of the buckling analysis from Matlab code

The critical load calculated from the following analysis is: -7.1348 E+04 N

The percentage difference between the two values is: 4.35%

6.9 Simply Supported Beam with Narrow Rectangular Cross-Section Subjected to Distributed Load *p*

Parameters: $b = 2$ mm, $h = 100$ mm, $l = 1$ m, $E = 207{,}000$ N/mm^2 and $G = 79{,}300$ N/mm^2.

The analysis has been performed considering a mesh of $m = 50$.

Simply supported TWB with a thin rectangular cross-section with an applied distributed load:

Results from the book:

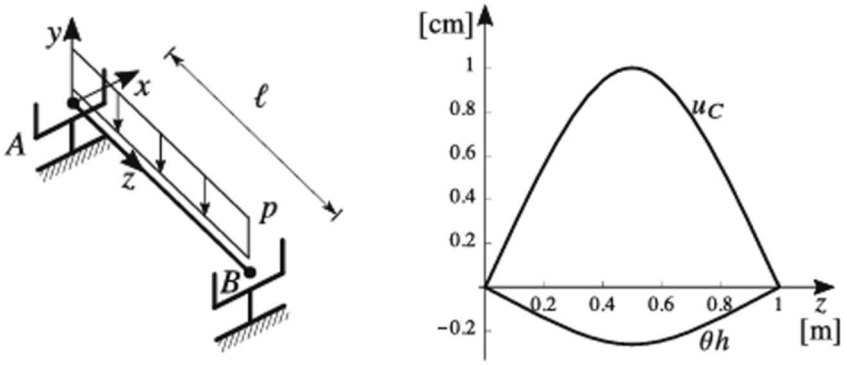

Figure 37: Model of the beam and applied load (on the left) and result of the analysis (on the right) [11]

$P_c \approx 500$ N/m

Results from Matlab code:

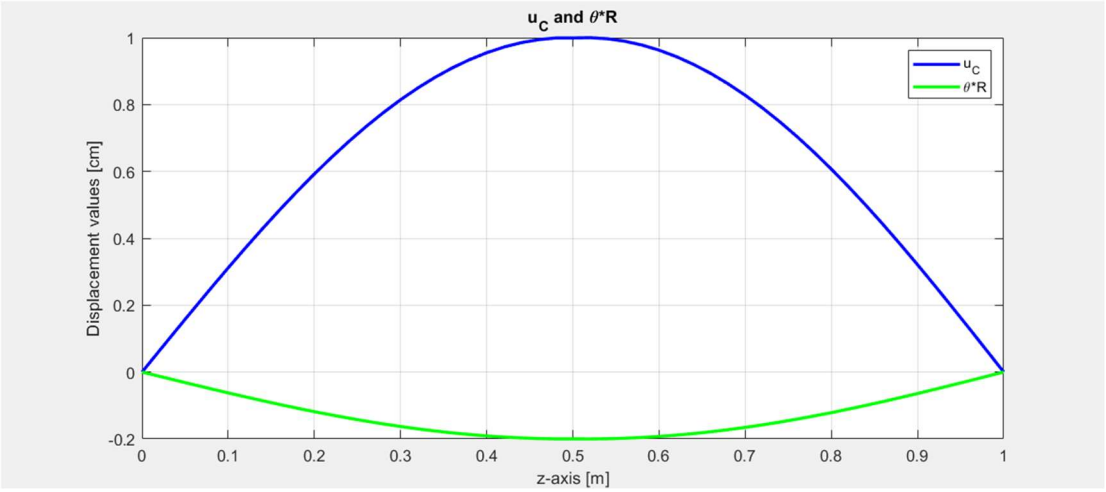

Figure 38: Result of the buckling analysis from Matlab code

The critical load calculated from the following analysis is: - 495.15 N/m

The percentage difference between the two values is: 0,80%

7. HIGH-RISE BUILDINGS

Emporis standards define a high-rise building as “A multi-storey structure between 35-100 meters tall, or a building of unknown height from 12-39 floors”. The International Conference on Fire Safety in high-rise buildings defined a high rise as “any structure where the height can have a serious impact on evacuation. Whereas, from a structural engineer’s perspective, a building is considered tall when, due to its height the lateral forces suffered by the structure play a significant role in the design [14].

7.1 Historical Aspects of High-Rise Buildings

In the last 200 years, there is been a demographic growth of the world population. Taking into account this, the classical development model, which relies on the infinite availability of land, water, and energy, cannot be sustainable anymore. Therefore, it became necessary to take advantage of tall buildings, an American invention from the late 19th century, after the fire that devastated Chicago in October 1871 [13].

This event presented a valuable opportunity to reassess the design and construction of the urban environment, evaluate the limitations of conventional materials, and explore the potential of innovative materials and structural systems [13].

The urgent need to rapidly rebuild structures while maximizing the use of expensive downtown space led to the emergence of a new architectural typology: the skyscraper [13].

With regard to the structural aspect, the buildings in wood and masonry could have a limited height, so to overcome this obstacle, masonry walls were replaced by steel beams and columns, forming a relatively thin metal skeleton that was identical on each floor. In this way, the facades, which had lost their load-bearing function, could be built by attaching closure panels to the structural frame, allowing for the construction of a large number of glass surfaces [13].

7.2 Evolutions and Structural Analysis

During that period, alongside technological advancements, significant progress was made in structural analysis methods. A key example is the work of Hardy Cross, a professor of structural engineering at the University of Illinois at Urbana-Champaign, who in 1930 published the article *"Analysis of Continuous Frames by Distributing Fixed-End Moments"*. This study introduced a method for determining stress distribution in indeterminate systems, addressing one of the most challenging problems in structural analysis at the time. After a pause due to World War II, the construction of steel skyscrapers resumed with a more essential and minimalist approach [13].

Further advancements took place in the 1970s with the arrival of the first supercomputers, such as the *Cray Computer*, which provided the computational power needed to model increasingly complex structures. Moreover, the development of new disciplines, including wind engineering and geotechnical engineering, contributed to the creation of ever more bold and innovative structural solutions [13].

7.3 Height Records

Below is a comparative diagram of the height of some of the world's tallest skyscrapers, with the height expressed in meters and the year of completion [13].

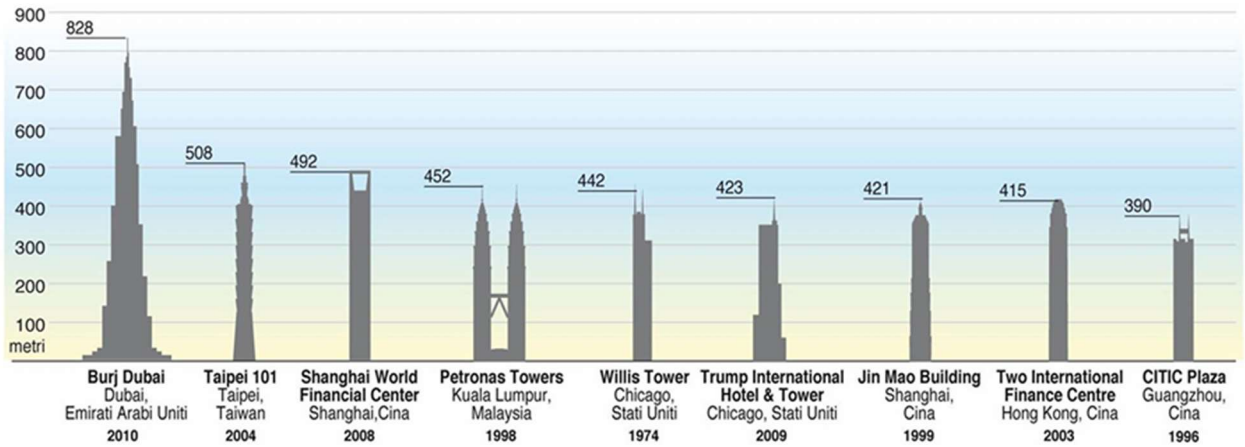

Figure 39: World's tallest skyscrapers heights [13]

7. HIGH-RISE BUILDINGS

Buildings represented (highest to lowest):

1. Burj Dubai (now Burj Khalifa) – 828 m, Dubai, United Arab Emirates, completed in 2010 (the highest in the world).
2. Taipei 101 – 508 m, Taipei, Taiwan, completed in 2004.
3. Shanghai World Financial Center – 492 m, Shanghai, China, completed in 2008.
4. Petronas Towers – 452 m, Kuala Lumpur, Malaysia, completed in 1998.
5. Willis Tower (formerly Sears Tower) – 442 m, Chicago, United States, completed in 1974.
6. Trump International Hotel & Tower – 423 m, Chicago, USA, completed in 2009.
7. Jin Mao Building – 421 m, Shanghai, China, completed in 1999.
8. Two International Finance Centre – 415 m, Hong Kong, China, completed in 2003.
9. CITIC Plaza – 390 m, Guangzhou, China, completed in 1996 [13].

The height of a skyscraper depends on:

- Material strength
- Site conditions
- Structural system
- Analytical modeling skills
- Understanding the structural behavior of the building
- Financial limitations
- Symbolic and representative requirements [13].

7.4 Functionality

Functionality is a fundamental requirement for effective design [13].

The most critical factor is the acceleration caused by wind-induced motion. How occupants perceive this movement depends on the building's intended use, as well as the stiffness, mass, and damping characteristics of the structural system [13].

Maximum displacement at the top

Currently, high-rise buildings are designed to have elastic displacements of h/500 due to wind with a 50-year return period. This specification outlines how stiff the structural system should be in terms of mass and damping properties of the entire building [13].

For high-rise buildings, a P-Δ effect caused by lateral displacement can produce many more deformations and consequently greater stresses in vertical gravity load elements. Damping will be a key aspect of developed design forces and the maximum wind-induced accelerations [13].

The P-Δ effect can be derived from the hysteresis cycles of several structural and non-structural materials, aeroelastic interactions, and/or by particular energy dissipation devices (supplemental damping). All so-called damping criteria help to mitigate acceleration and improve the comfort of the occupants [13].

7.4.1 Ratio of height to width (slenderness)

When the structural system is placed on the perimeter of a tall building, the optimal ratio between height and width ranges from 6 to 8. For higher ratios, it is advisable to use energy dissipation devices to reduce the amplitude of oscillations induced by the wind. For central stiffening cores (cores), the ratio can even reach 15 [13].

Building	Height	Aspect Ratio (height/width)	Material
Willis Tower (formerly Sears Tower)	445 m	6.4	Steel
Jin Mao Tower	421 m	7.0	Mixed
Amoco Building	346 m	6.0	Steel
John Hancock	344 m	6.6	Steel

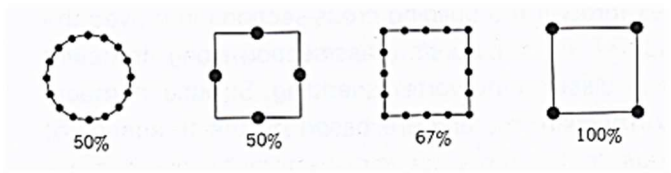

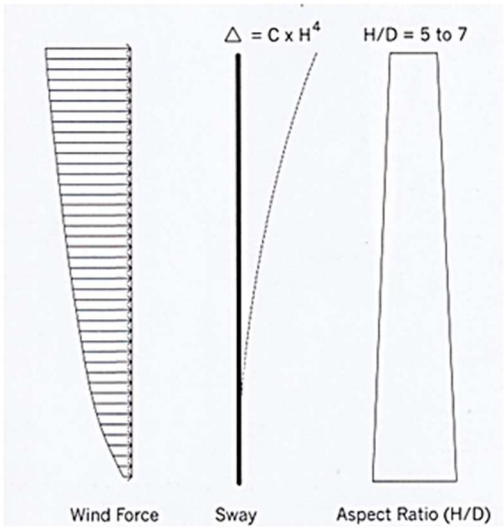

Figure 40: Comparison of skyscrapers based on height, aspect ratio, and materials, accompanied by diagrams illustrating mass distribution, the effect of wind forces, and structural behavior in relation to the height-to-width ratio (H/D) [13]

7.4.2 Lateral movements

The lateral displacement of a frame can be considered as the sum of two components, similar to those that occur in a prismatic cantilever beam. One component is due to bending deformation, while the other is due to shear deformation. Contrary to what happens with prismatic beams, in frames the shear deformation (70%) predominates over the bending deformation (30%), especially in the case of not-too-tall frames [13].

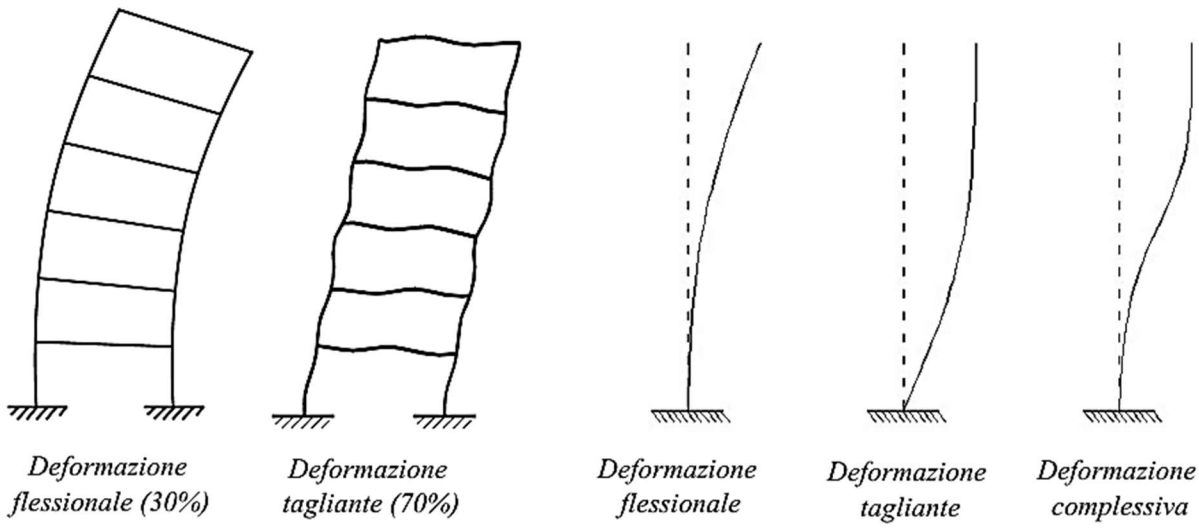

Figure 41: Illustration of structural deformations in buildings: flexural deformation (30%), shear deformation (70%), and their combined effect, highlighting the different contributions to overall structural behavior [13]

7.5 Remarks

It is possible to make some remarks:

- Bending deformation occurs through the change in length of the columns, caused by the axial force that balances the overturning moment of the horizontal forces. The upwind columns elongate, while the downwind ones shorten [13].
- Shear deformation is due to the bending of the columns and beams. The in-plane shear is distributed among all the columns in the plane, causing them to bend with double curvature and a flexure point around the midpoint. The moment at the joints is also transferred to the ends of the beams, which deform similarly to the columns [13].

Frame structures are generally not very efficient because horizontal forces are mainly balanced by the bending of structural elements, rather than by axial forces. This requires the use of significant amounts of material, especially in cases of considerable heights. In such cases, it is preferable to use other types of structures [13].

7.6 Central Core Systems

Central core systems are commonly employed in reinforced concrete buildings, where the core serves as the primary resistance against horizontal forces. To ensure stability, the core must be sufficiently rigid to limit horizontal displacements within acceptable thresholds. Floor systems in these structures can either be fully cantilevered or designed in modular arrangements, where perimeter columns transfer their loads to a specially reinforced lower floor [13].

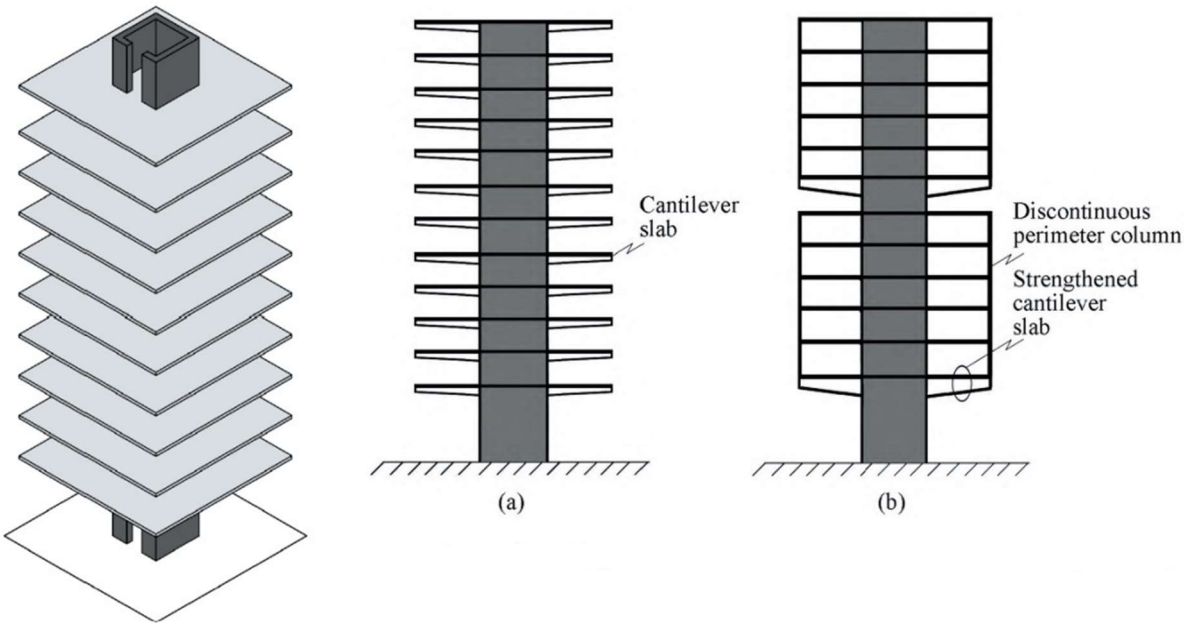

Figure 42: Slabss in core systems: cantilever slabs (a), strengthened cantilever slabs (b) [13]

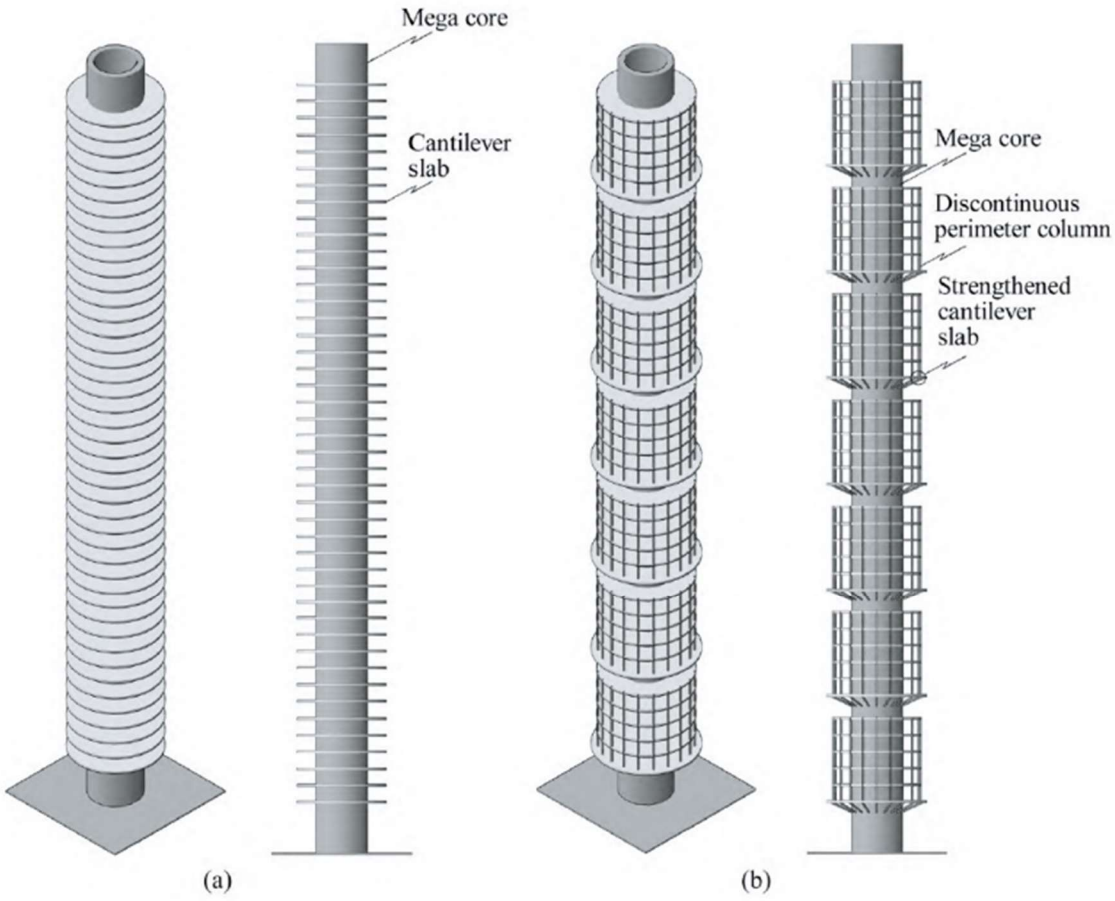

Figure 43: Slabs in the mega core system: cantilever slab (a), supported (b) [13]

The core consists of a number of rooms and functions that remain the same on all floors of the building. The core consists of emergency stairwells, elevators, staircases, restrooms, electrical panels, technical rooms for HVAC units, and utility shafts. There are three main cores: central, lateral, and multiple core, that can take from 15% to 30% of the floor area respectively [17].

Most commercial skyscrapers have a central core, providing the most flexible location of spatial arrangements in each floor. In addition, a central core enhances the location of distributed air ducts, since the floor can be configured from both sides of a core. A central core also has structural advantages due to the stiffness of the core that enhances resistance to wind loads [17].

In certain instances, a lateral core might be the best option, such as if the floors are shorter or an existing building is adjacent to the new building. The lateral core won't prevent winning from directly transporting the air supply from conditioning units for each level [17].

In cases of very large floor areas, multiple cores may be necessary to minimize the distance to the nearest restroom and the stairwells. The main concern with multiple cores is in terms of cost - each core needs an elevator and must have adequate service shafts for each stairwell [17].

7.7 Floor-to-Floor Height

The overall cost of a skyscraper is influenced by the internal height of each floor. Even a slight variation in height, when multiplied by the number of floors and considered across the entire floor area, can significantly increase the building's external surface area, thus raising the cost related to the building envelope [17].

The floor-to-floor height consists of four factors:

- The height of the raised floor, if present;
- The net height, which typically varies between 2.60 m and 3.00 m;
- The height of the suspended ceiling, which depends on lighting systems and air ducts;
- The thickness of the structural slab.

Overall, the floor-to-floor height generally ranges from 3.8 m to 4.1 m. However, there are specific areas, such as data centers (DCs), which require greater heights [17].

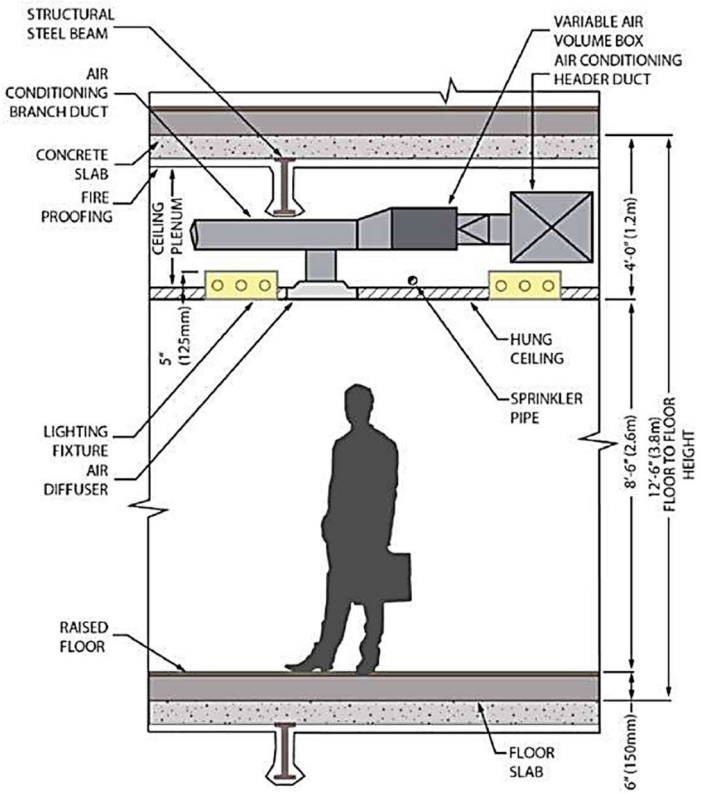

Figure 44: Interfloor height [17]

7.8 The Stability of High-Rise Buildings

The increasing demand for tall structures necessitates a thorough understanding of buckling phenomena that can occur in buildings. It is essential to have a solid grasp of reliable calculation methods for designing such structures and to be confident in applying them effectively.

Observations from past earthquakes have shown that buildings with discontinuities in stiffness and mass are prone to concentrations of forces and deformations at those points of discontinuity, potentially leading to member failure at junctions and overall structural collapse. The most economical approach to prevent soft-storey failure is by incorporating shear walls into tall buildings [14].

7.8.1 Wind effects on structures

Wind effects on structures can be classified as:

- Static: static wind effect primarily causes elastic bending and twisting of structure.
- Dynamic: for tall, long span and slender structures a “dynamic analysis” of the structure is essential. Wind gusts cause fluctuating forces on the structure which induce large dynamic motions, including oscillations [14].

The movement of air masses exerts pressure on the side of the building directly exposed to the wind, while creating a depression on the opposite side. On the surfaces parallel to the wind direction, a dragging action occurs. Additionally, the detachment of vortices generates variable transverse forces, which play a crucial role in the overall wind effects [14].

Wind actions are dynamic (changing over time) and induce vibrations in the entire structure, affecting the comfort conditions inside the building. A well-designed aerodynamic shape can significantly reduce wind forces [14].

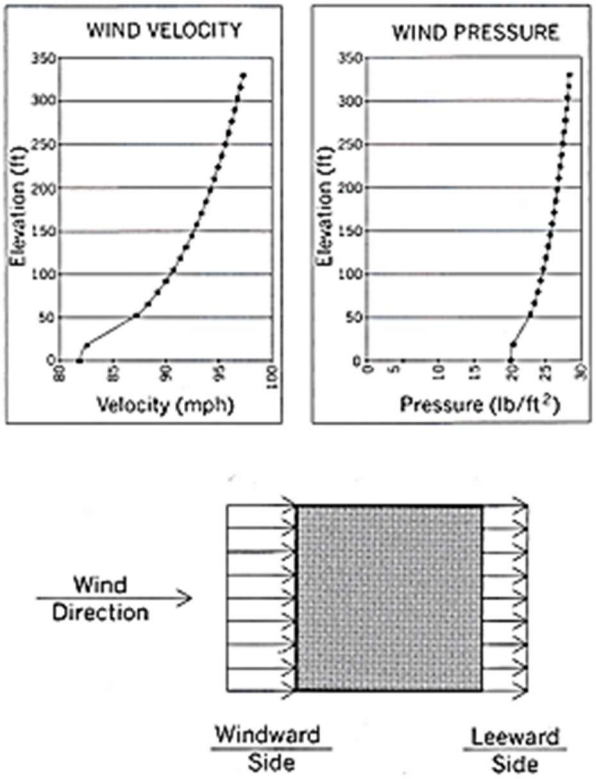

Figure 45: Graphs illustrating wind velocity and pressure variation with elevation, alongside a diagram showing wind direction and its impact on the windward and leeward sides of a building [14]

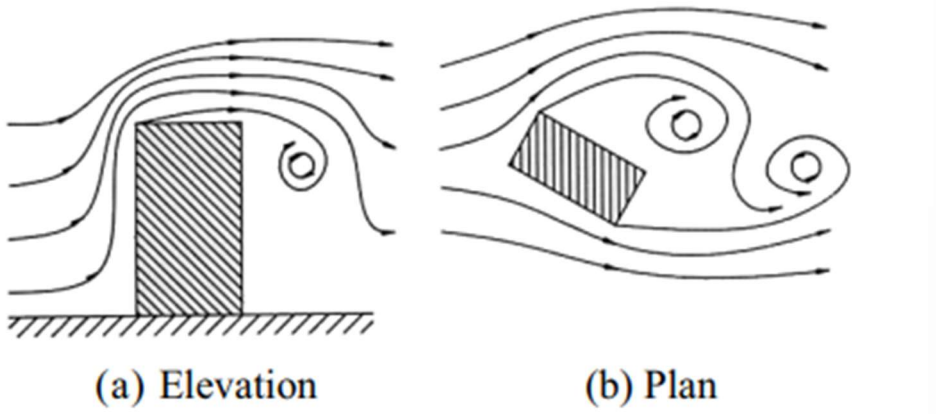

Figure 46: Generation of eddies In elevation (a) and in plan (b) [25]

The previous force was most often based on using some regulatory standards for determining the approximate wind forces. However, there is great advantage to wind tunnel testing, as especially navigating in the complex wind interactions created in urban assemblies of neighbouring tall buildings, [14].

More can be analyzed more deeply in terms of these concepts.

The structural design of tall buildings requires special consideration with respect to wind effects, as aerodynamic forces acting on these structures lead to substantial and complex loads. A quasi-static treatment of wind loads has been the traditional approach for low- and medium-rise buildings.

This pseudo-static approach neglects some critical aspects of the behavior of wind and the dynamic response of the structure itself. Hence, this treatment is not suitable for very tall buildings, as it may lead to grossly conservative estimates of the loads on the structure or dangerously underestimating them [25].

The limitations of this assumption are the neglect of proper dynamic response of the building, the effects of interference by adjacent buildings, directionality effects and crosswind response. All of these considerations must be evaluated in order to ensure the safety and functioning of a tall building.

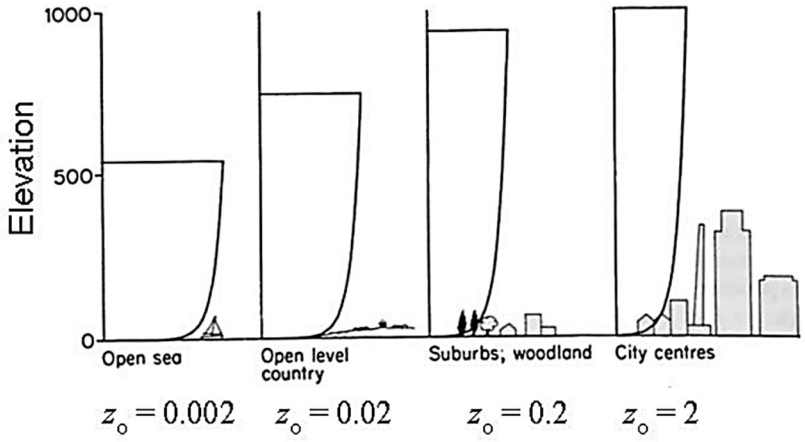

Figure 47: Mean wind profiles for different terrains [25]

The dynamic response of the structure is one of the most important aspects that the quasi-static consideration overlooks. As a result of their height and flexibility, tall buildings are particularly sensitive to resonance (the wind frequency matching the natural frequency of the structure) [25].

This can amplify the oscillations considerably and cause discomfort for the occupants as well as structural damage. In addition, acceleration, damping and stiffness of the structural system are critical to the dynamic response of buildings and must be considered in the design [25].

One further factor that is commonly overlooked is interference among structures.

In built up urban areas, structures that might exist together cannot just influence wind flows, they may create complex wind behaviors (e.g., turbulence, local accelerations, and changes in lateral loading) that cannot be estimated even from a simplified process, so the designer will require very advanced measures, such as wind tunnel testing, to repro- duce real world conditions, then study wind interaction with their structure, and to give them data with a better known measure to work from [25].

Wind directionality represents another critical factor. Wind does not always act uniformly or predictably but varies in intensity and direction over time. This can significantly influence the lateral and crosswind loads on tall buildings, requiring detailed analysis to ensure that the structure can withstand all possible loading conditions. Furthermore, the crosswind response to wind, which manifests as oscillations perpendicular to the primary wind direction, can cause discomfort to occupants and compromise the stability of the building if not adequately considered [25].

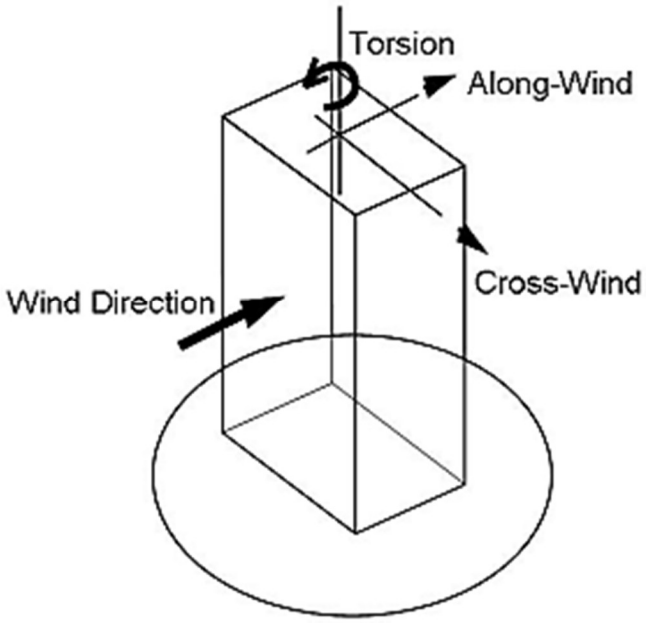

Figure 48: Wind response directions [25]

To take into account these complexities, it is necessary to adopt an advanced approach to wind load design, such as the one outlined in the Australian code.

This approach integrates dynamic analyses, numerical simulations, and wind tunnel testing to accurately assess the effects of wind on tall buildings. Wind tunnel tests, in particular, provide a level of detail and accuracy that cannot be achieved through traditional methods [25].

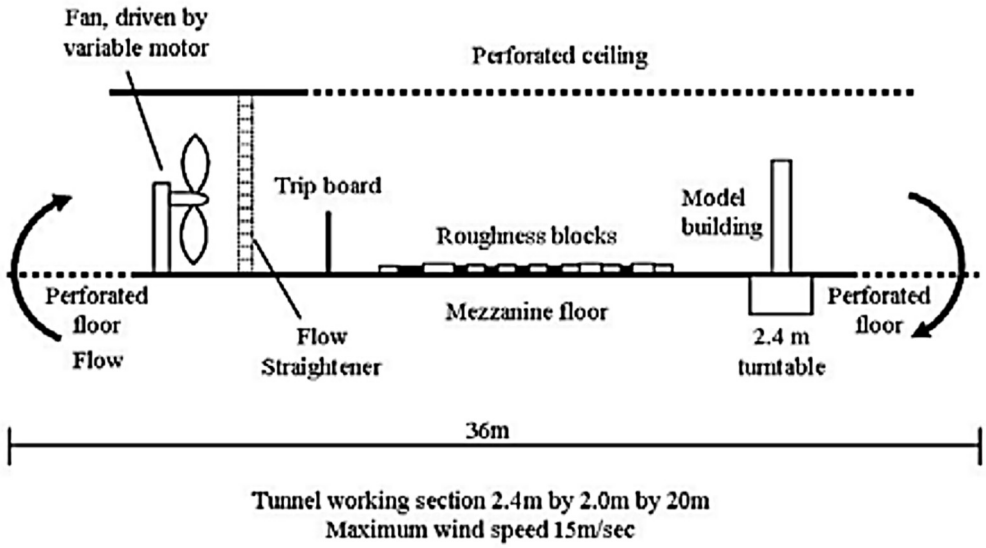

Figure 49: Schematic of a typical open-circuit wind tunnel [25]

They allow for wind behavior in real-world conditions, for turbulent conditions, interference of buildings and fluctuations of wind direction. The information from the results of the tests can contribute to better structural design, safety, stability, and provide a comfortable experience for the end user.

In summary, the design of tall buildings includes a process that is holistic with consideration of wind effects. This stage of the design process must use the most current techniques in order to guarantee tall buildings can resist the aerodynamic forces in a safe and efficient manner and improve quality of life in urban settings [25].

7.8.2 Seismic effects on high-rise buildings

When earthquakes occur, a building undergoes dynamic motion. This is because the building is subjected to inertia forces that act in the opposite direction to the acceleration of earthquake excitations. These inertia forces, called seismic loads, are usually dealt with by assuming forces external to the building. Time histories of earthquake motions are also used to analyze high-rise buildings, and their elements and contents for seismic design. The earthquake motions for dynamic design are called design earthquake motions [14].

In the previous recommendations, only the equivalent static seismic loads were considered to be seismic loads. In ISO/TC98 which deals with “bases for design of structures”, the term “action” is used instead of “load” and action includes not only load as external force but various influences that may cause deformations to the structures. In the future, “action” may take the place of “load” [14].

7.9 Final Observations about High-Rise Buildings

The most important factor in the designing of high-rise buildings, however, is the building’s need to withstand the lateral forces imposed by the winds and potential earthquakes. Most high-rises have frames made of steel or steel and concrete. Their frames are constructed of columns (vertical support members) and beams (horizontal support members). Cross-bracing or shear walls maybe used to provide a structural frame with greater rigidity in order to withstand wind stresses [14].

The shear force and bending moments are greater for ground-floor columns compared to the first-floor columns. In terms of storey drift, base shear, and roof displacement, square columns perform better than rectangular ones. Shear walls are employed to mitigate lateral loads and soft-storey effects. When placed centrally, shear walls have a minimal impact on the overall behavior of the structure. The inclusion of masonry infill in structures enhances the stiffness of the structural elements [14].

7.10 Stability in High Rise Buildings

In tall buildings, buckling problems can occur due to various structural phenomena related to bending, twisting and local buckling.

7.10.1. Global instability

This affects the entire structure and is often due to the action of horizontal loads such as wind and earthquakes.

a. Lateral load buckling (*P-Δ* effect)

   When a tall building flexes under wind or earthquake load, a secondary moment is generated due to the lateral displacement of vertical forces. This leads to an amplified effect of deformations, which can lead to progressive failure.

   Possible solutions to avoid this problems are: Increase stiffness with reinforced concrete cores, diagonal braces, or rigid frames and check the stability factor.

b. Global torsional buckling

   If the stiffness distribution is asymmetrical, a building can undergo rotation around its axis under lateral loading. This phenomenon is typical of buildings with off-center cores or asymmetry in the partitions and pillars.

   Possible solutions to avoid these problems are: design the center of gravity of the stiffness close to the center of gravity of the masses and use symmetrical diagonal bracing or strong core cores.

7.10.2. Local instability of structural elements

Even individual elements (pillars, walls, beams) can undergo local buckling phenomena, especially if they are slender or thin.

a. Buckling of the pillars (Very tall and thin pillars can lose stability under compressive load (Euler buckling)).

   Possible solutions to avoid this problem are: increase the stiffness of the section and reduce slenderness with cross-elements or rigid connections.

b. Thin wall buckling (hull)

   If the building has thin concrete or steel walls, these can deform locally under compression or shear. This problem is typical in very tall and thin reinforced concrete cores.

   Possible solutions to avoid these problems are: vertical and horizontal stiffeners (ribs or diaphragms) and thicker walls or with more resistant sections.

7.10.3. Aerodynamic instability

In very tall buildings, the effects of the wind can generate unstable oscillations.

a. Von Kármán vortex effect

   Wind can generate vortex trails that cause dangerous oscillations in the structure. If the frequency of the vortices is close to the building's own frequency, a resonance can be triggered.

   Possible solutions to avoid this problem is: modify the shape of the building to disturb the formation of vortices (rounded shapes or changes in section) and add dampers (e.g., TMD-tuned mass dampers used in high-rise buildings).

A good structural design must ensure a balance between stiffness, strength and damping, using braces, strong cores, stiffeners and optimal aerodynamic shapes.

7.11 Study of Tall Buildings

The study of tall buildings can be addressed, for example with the theory of open thin sections of Vlasov previously reported, particularly useful when the structure has a thin and open load-bearing core (e.g. “C”, “L”, “U” shape).

This theory allows us to analyze the combined effects of bending, torsion, and buckling with a more accurate formulation than the classical Saint-Venant torsion theory.

In particular, Vlasov's theory in tall buildings is applicable if a building has a thin, open core, and behaves like an open section subject to deformable torsion.

The torsional stiffness is very low, so the torsional deformation cannot be neglected.

Therefore, it is applicable to buildings with:

- Reinforced concrete core in the shape of “C”, “L”, “U”, “E”, where torsion can cause significant deformations.
- Tall towers with lightweight structures, where twisting and buckling effects are important.
- Steel structures with thin profiles, in which torsional behavior is dominant.

While not applicable if the section is completely closed, because in that case the torsional stiffness is very high and the behavior is closer to the Saint-Venant torsion.

The key effects of Vlasov's theory are that:

- Allows you to calculate the non-uniform torsion, considering the out-of-plane deformation of the section.
- Introduce a two-moment moment B to represent the distribution of tensions due to the war.
- Describe torsional deformation with a more complex differential equation that takes into account the stiffness at war.

7.12 Application of the Code to High-Rise Buildings

When it is needed to run a simplified study of the statics of tall buildings, a structure of great height is often assimilated to a corbel (or shelf embedded at the base) for several reasons related to structural behavior:

1. Base constraint: A tall building is generally anchored to the ground by a rigid foundation, which behaves in a similar way to a joint, preventing translation and rotation at the base.

2. Preponderant deformation: The main deformation of a tall building with respect to horizontal loads (wind or earthquake) is similar to those of a corbel, the structure tends to twist in which the maximum displacements occur at the tip with progressive deformation of curvature along the height.

3. Preponderant horizontal actions: In tall buildings, horizontal actions (wind, earthquake) become more important than vertical loads. The cantilever model allows the influence of these forces to be studied in a simplified manner in terms of flexural and shear resistance.

4. Bending moment distribution: As in a wedged shelf, tall buildings tend to have maximum bending moments at the base and minor bending moments at the top. This helps to design the stiffness and strength of the building efficiently.

5. Simplified engineering approach: Analogy with a shelf allows for quick estimates of stresses and strains without resorting to complex structural models, facilitating preliminary analysis of building behavior.

In summary, the cantilever model represents an effective schematization to understand the global behavior of a tall building under horizontal loads, while being a simplification with respect to the more complex structural reality. Taking this into consideration, and applying the theory previously described, the analysis of three models with cantilever schemes representing models of tall buildings was carried out.

The results were compared using finite element software, "LUSAS". In all the cases, a cantilevered beam of 100 m height was considered, representing a tall building and it has been considered a steel with Young Modulus equal to $210.0 \cdot 10^9$.

7.13 Flow-Chart

To summarize the functioning of the Matlab code, a flowchart is shown below:

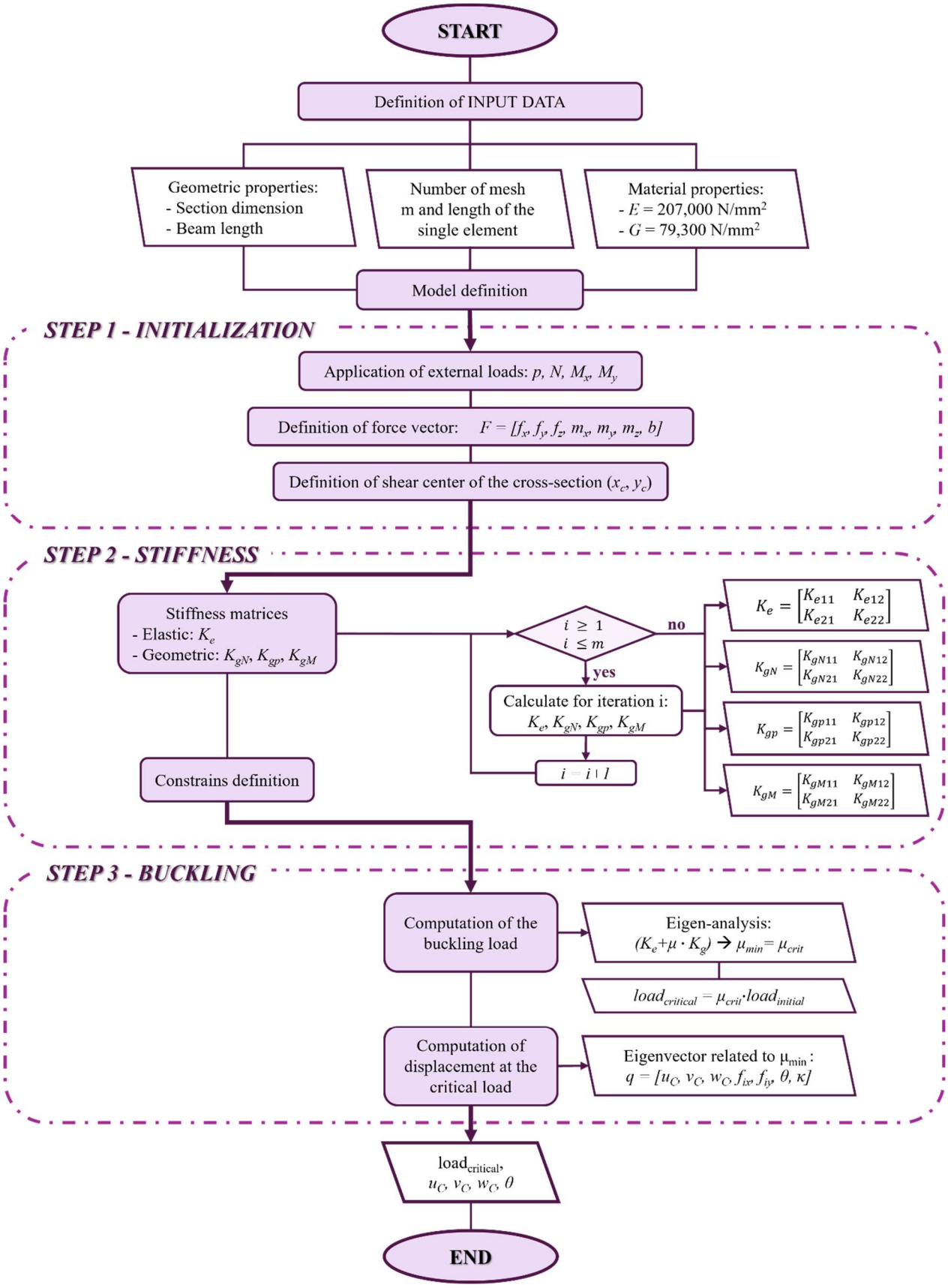

7.14 Example 1: Piecewise Constant Narrow Rectangular Section

Defined along the *z*-axis, divided in m = 100 (number of mesh), by narrow rectangular section, with same depth b = 4 m and height varying from 20 m at the base to 18 m at the top with successive Δ = 0.5 m.

The detailed characteristics of the sections have been here reported:

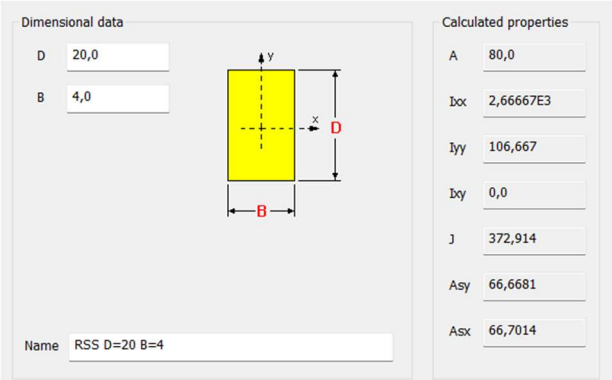

Figure 50: Characteristics of the section of the first fifth part of the model

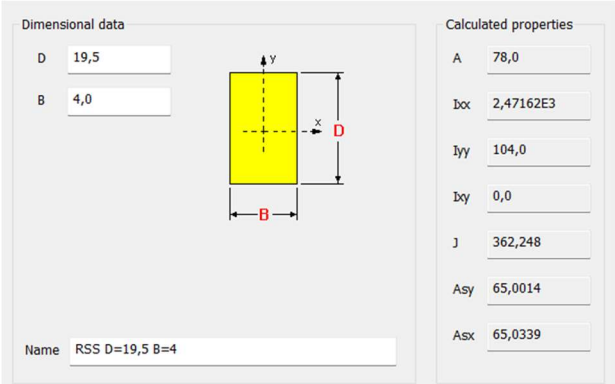

Figure 51: Characteristics of the section of the second fifth part of the model

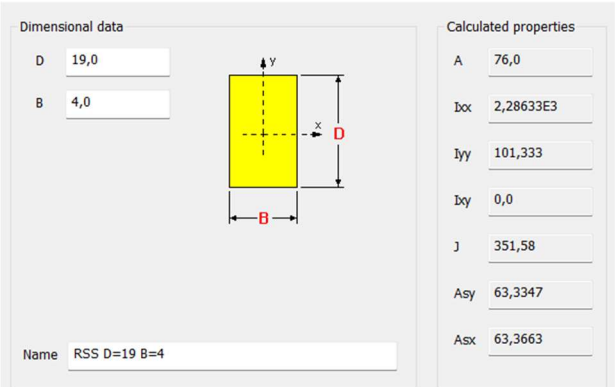

Figure 52: Characteristics of the section of the third fifth part of the model

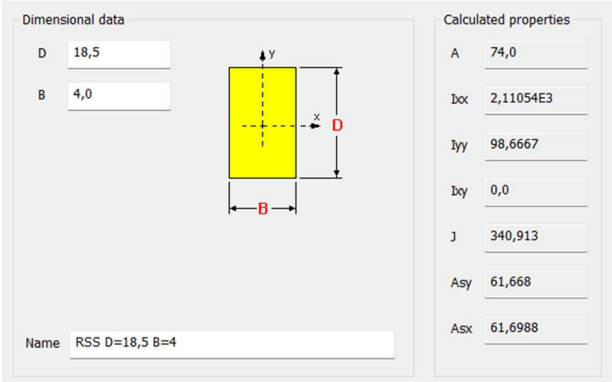

Figure 53: Characteristics of the section of the fourth fifth part of the model

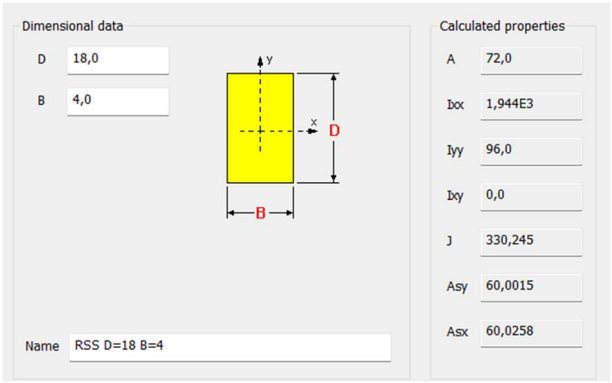

Figure 54: Characteristics of the section of the fifth fifth part of the model

A distributed load has been applied.

The model is the following one:

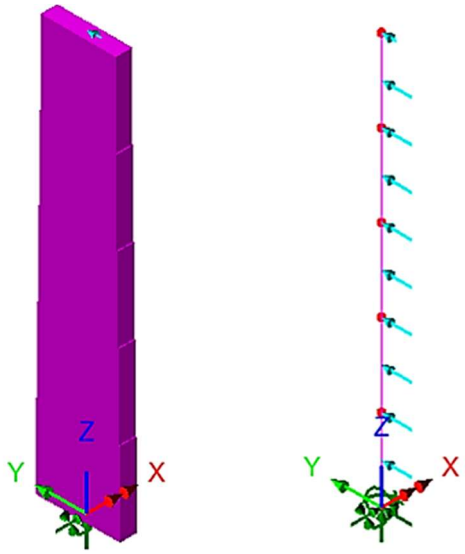

Figure 55: Model and applied load

The buckling load and the values of the deformations u_C and θ, were then calculated.

The results are as follows:

LUSAS

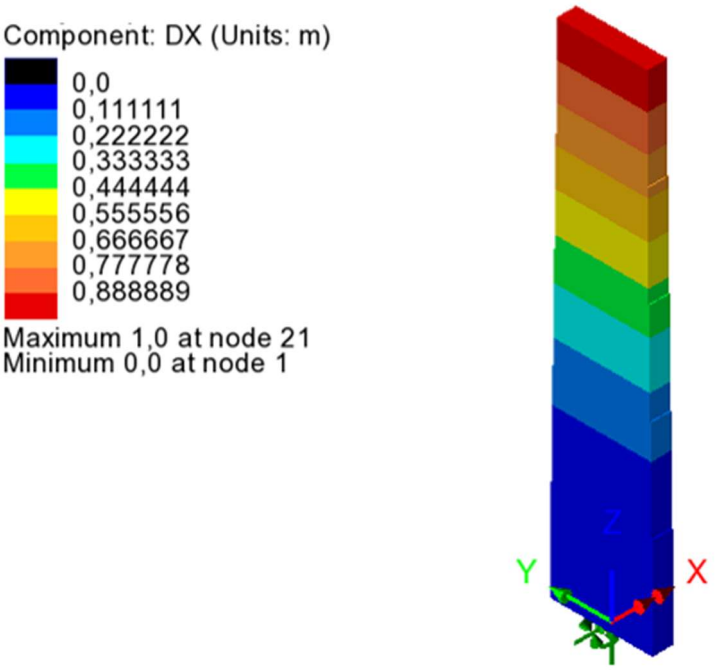

Figure 56: u_c computed by LUSAS software

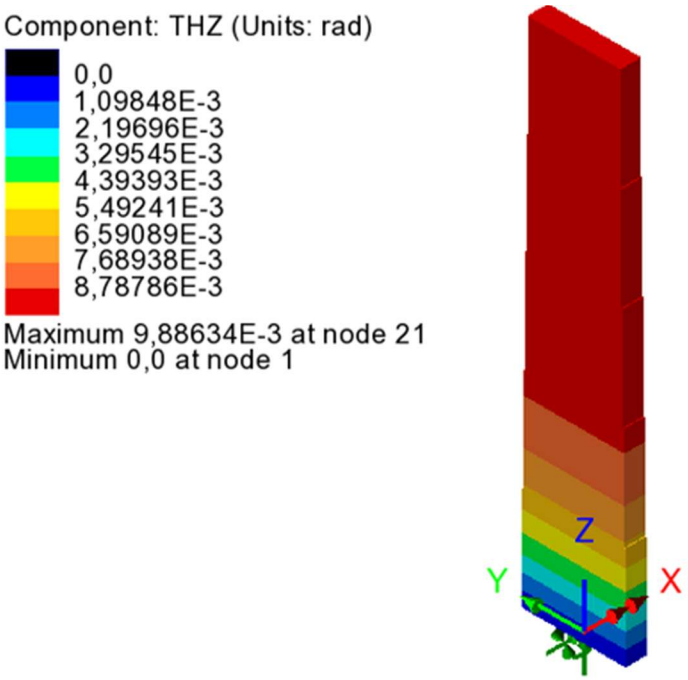

Figure 57: θ computed by LUSAS software

Initial load (total global distributed load): 100 N

Load amplification factor: 6.551 E+07

Buckling load: 6.551 E+09 N

MATLAB

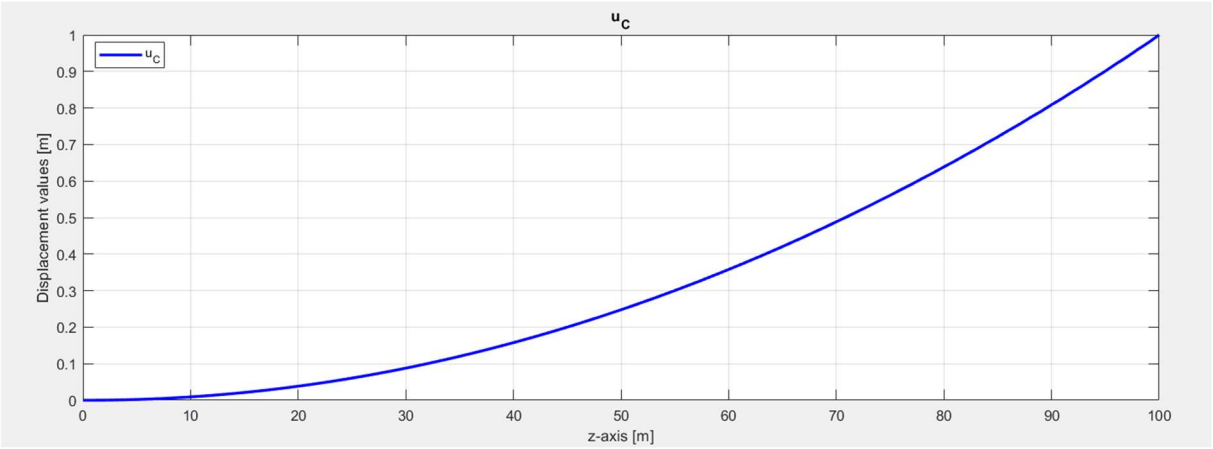

Figure 58: u_c displacement from Matlab analysis

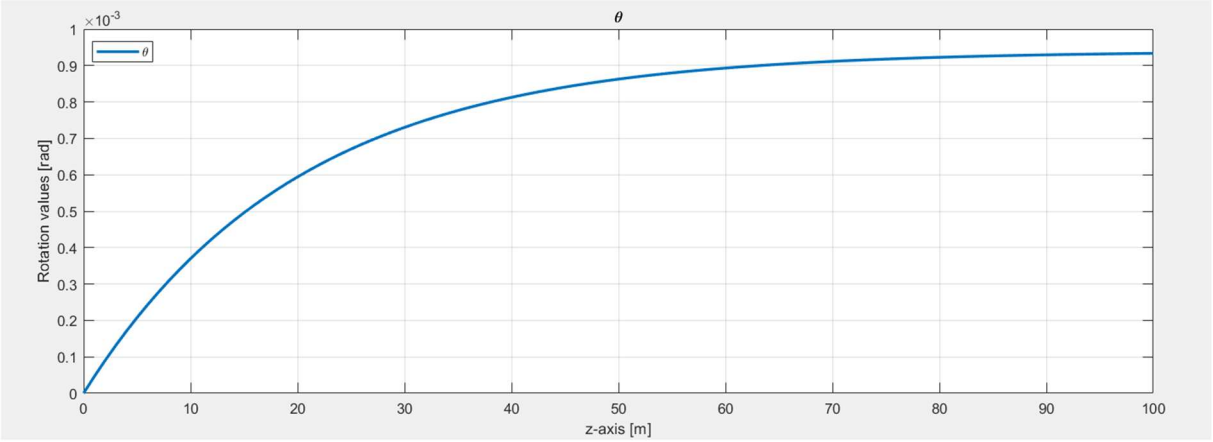

Figure 59: θ displacement from Matlab analysis

Initial load: 10 N/m

Load amplification factor: 6.39785 E*05

Buckling load: -6.3978 E+09 N

General results

Difference between the computed Buckling loads and displacements:

Percentage difference between buckling loads: 2,34%

Displacement along x:

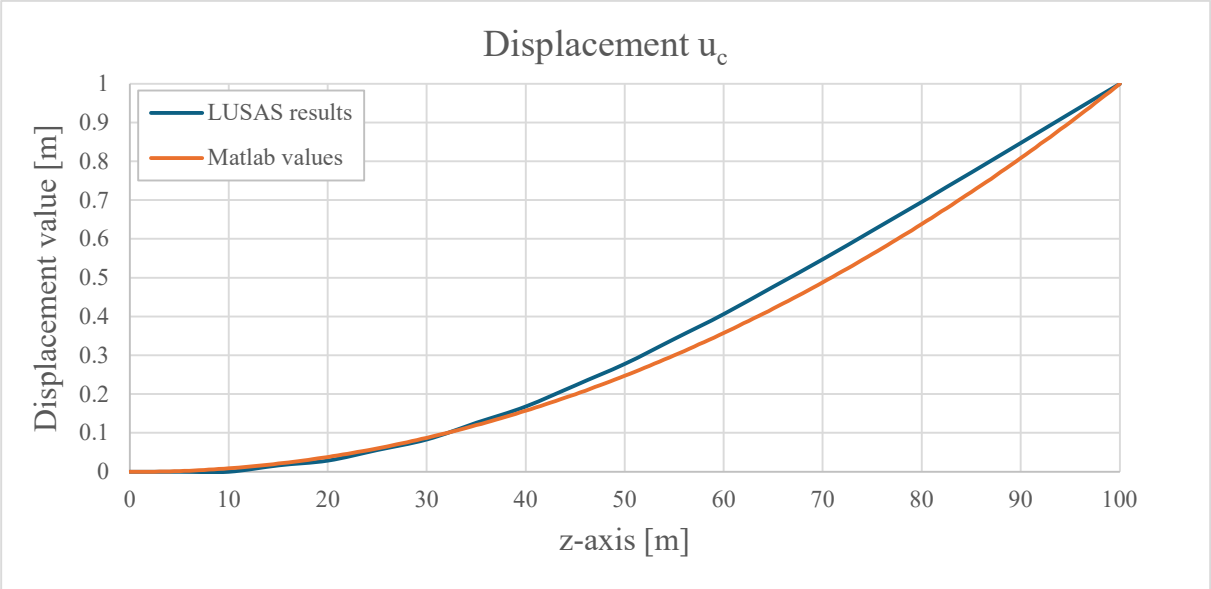

Figure 60: Comparison between LUSAS and Matlab results about u_c

Rotation about z:

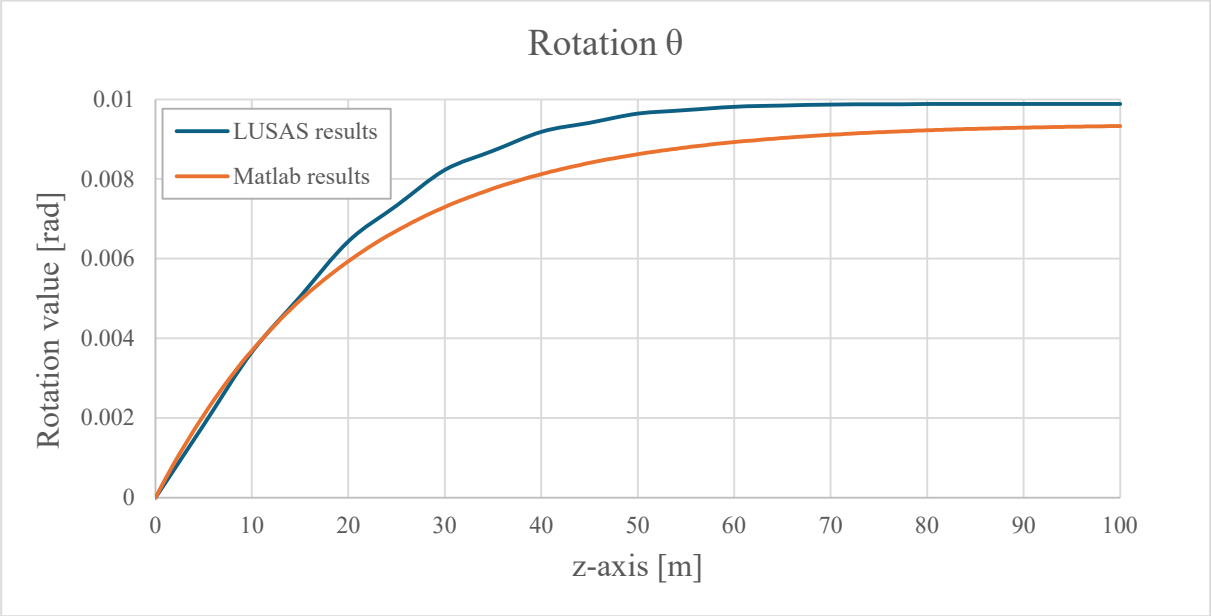

Figure 61: Comparison between LUSAS and Matlab results about θ

Through LUSAS, the total result of the movements was also highlighted

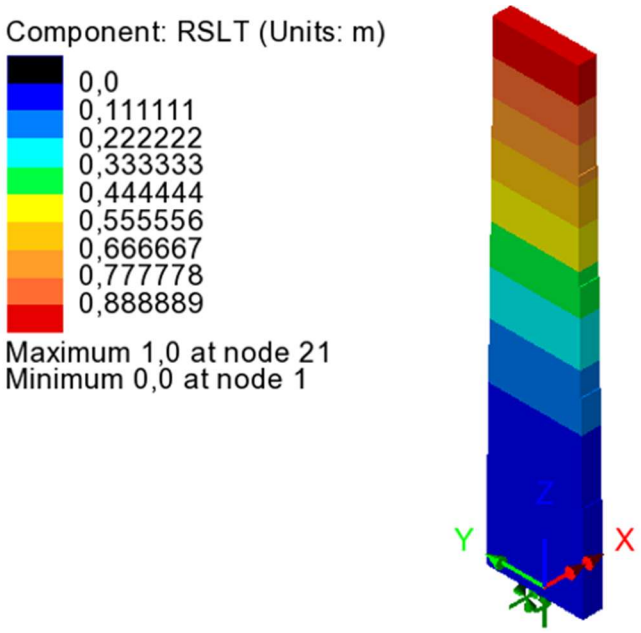

Figure 62: Total result of LUSAS analysis

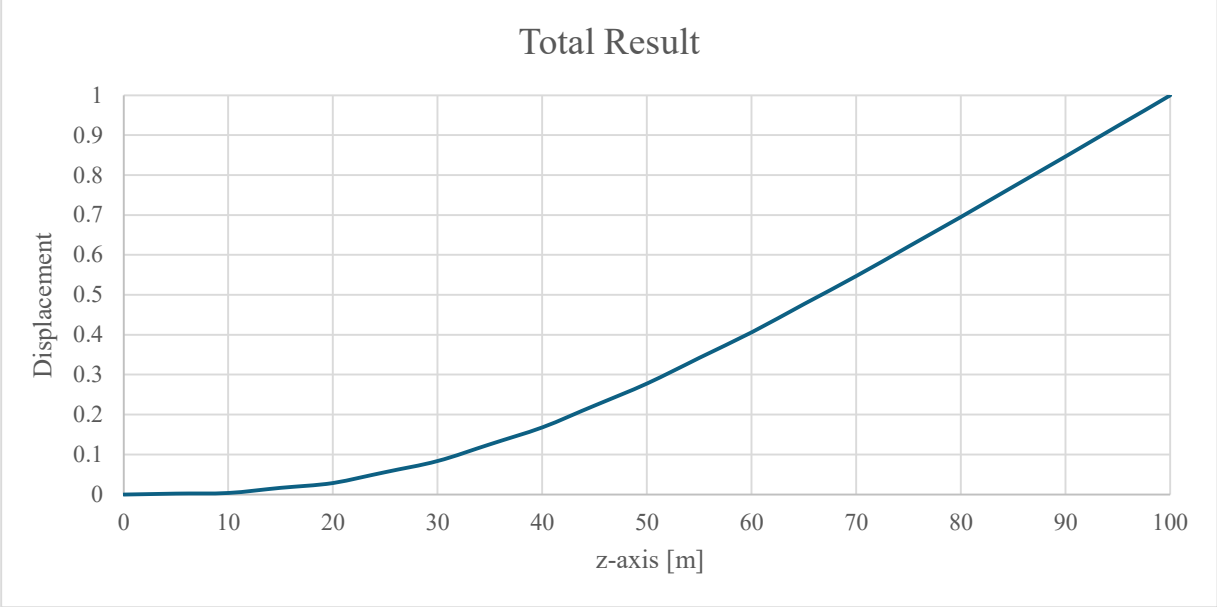

Figure 63: Total results of LUSAS analysis in graph form

7.15 Example 2: C-section

Defined along the *z*-axis a C-section and considering m = 50. The dimension of the section has been reported in *Fig. 64*:

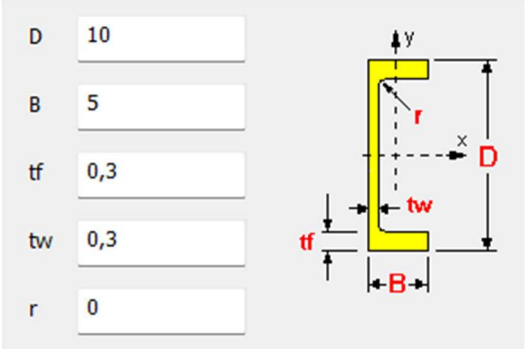

Figure 64: Characteristics of the section of the model

A distributed load has been applied.

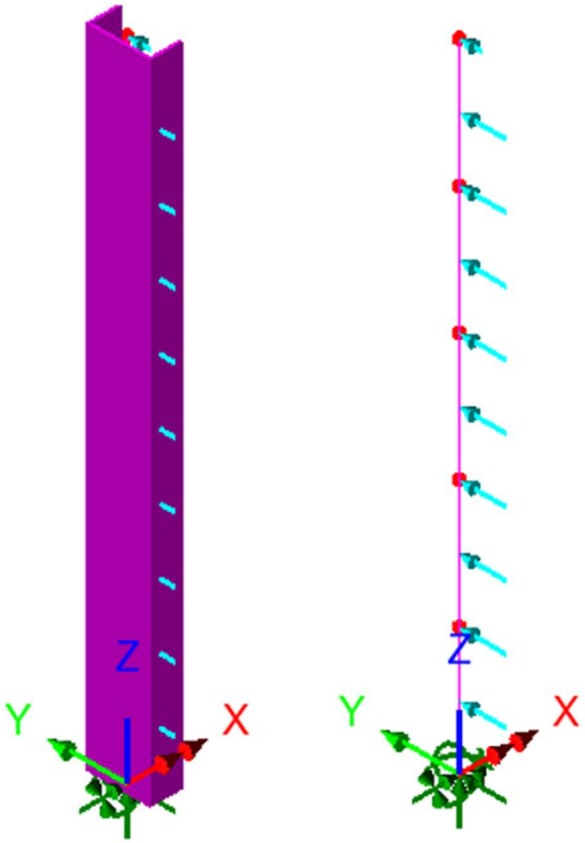

Figure 65: Model and applied load

The results are the following:

LUSAS

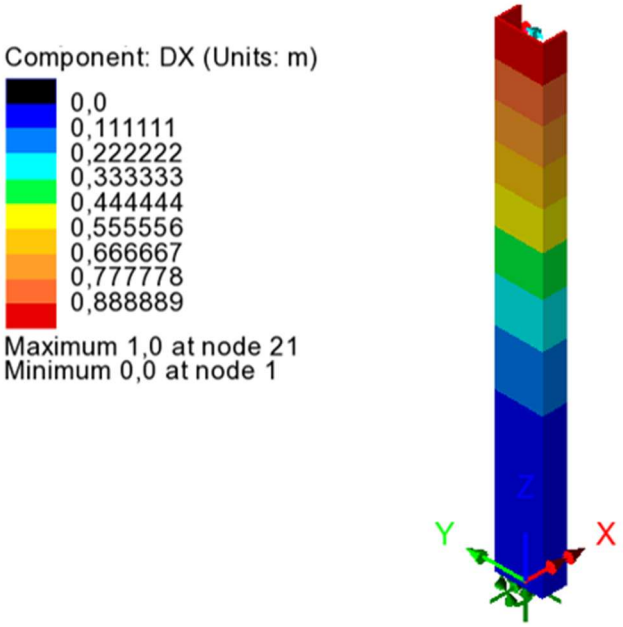

Figure 66: u_c computed by LUSAS software

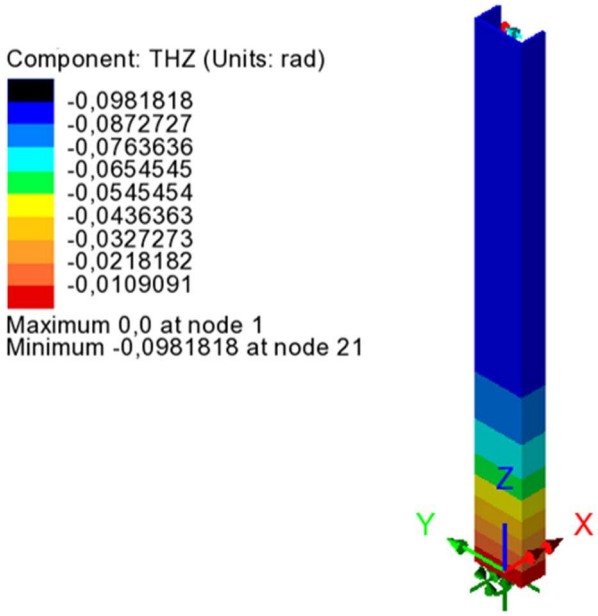

Figure 67: θ computed by LUSAS software

Initial load (total global distributed load): 1000 N

Load amplification factor: -1.40433 E+05

Buckling load: 1,40433 E+08 N

MATLAB

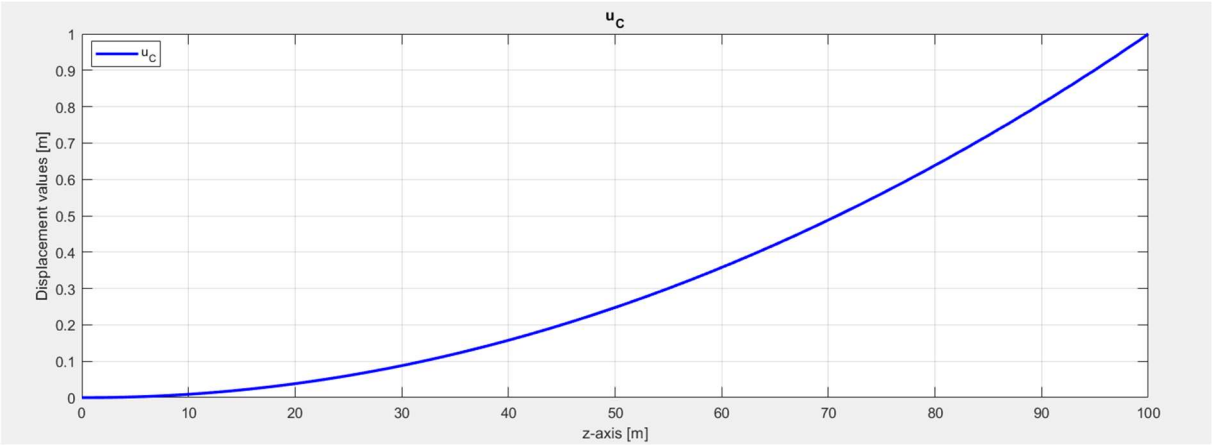

Figure 68: uc displacement from Matlab analysis

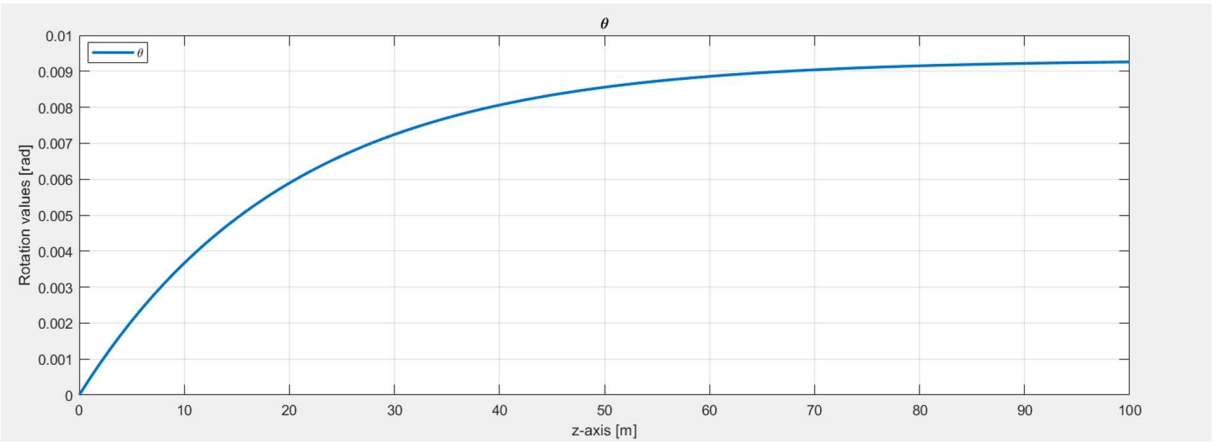

Figure 69: θ displacement from Matlab analysis

Initial load: 10 N/m

Load amplification factor: 1.38518 E+05

Buckling load: -1.3852 E+08 N

General results

Difference between the computed Buckling loads:

Percentage difference between buckling loads: 1,37%

Displacement along x:

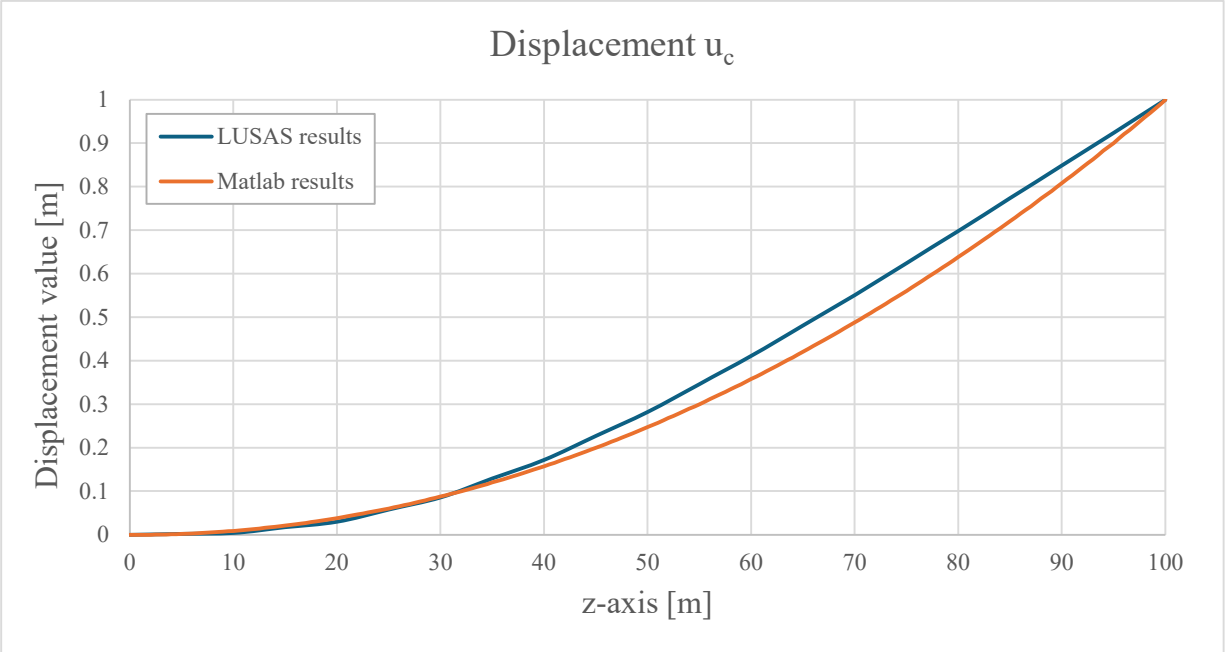

Figure 70: Comparison between LUSAS and Matlab results about uc

Rotation about z:

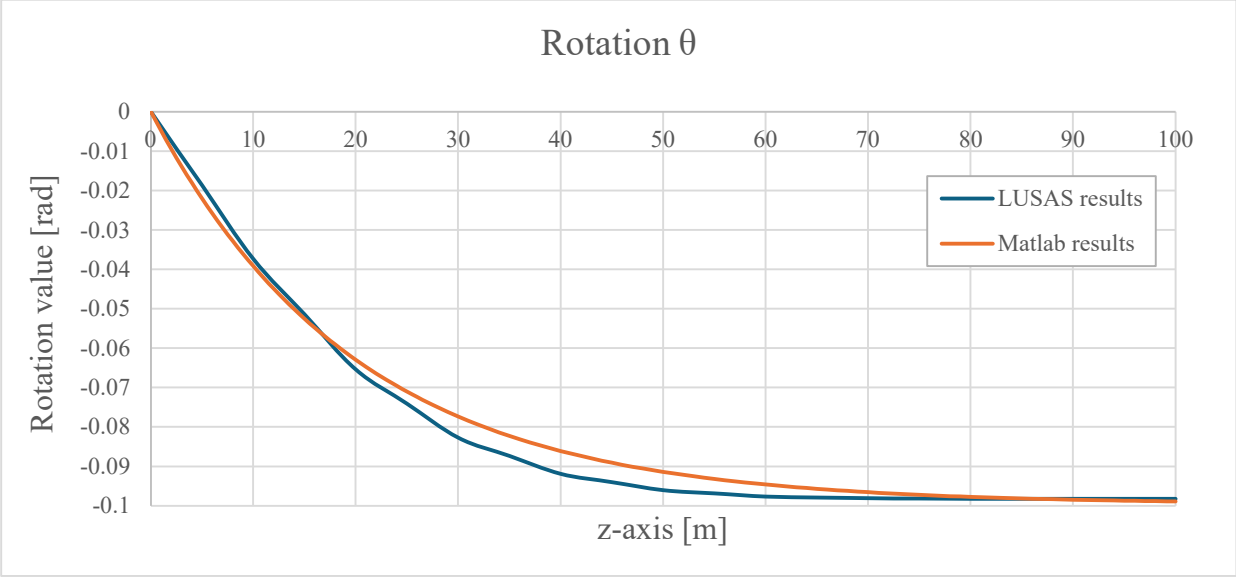

Figure 71: Comparison between LUSAS and Matlab results about θ

Through LUSAS, the total result of the movements was also highlighted

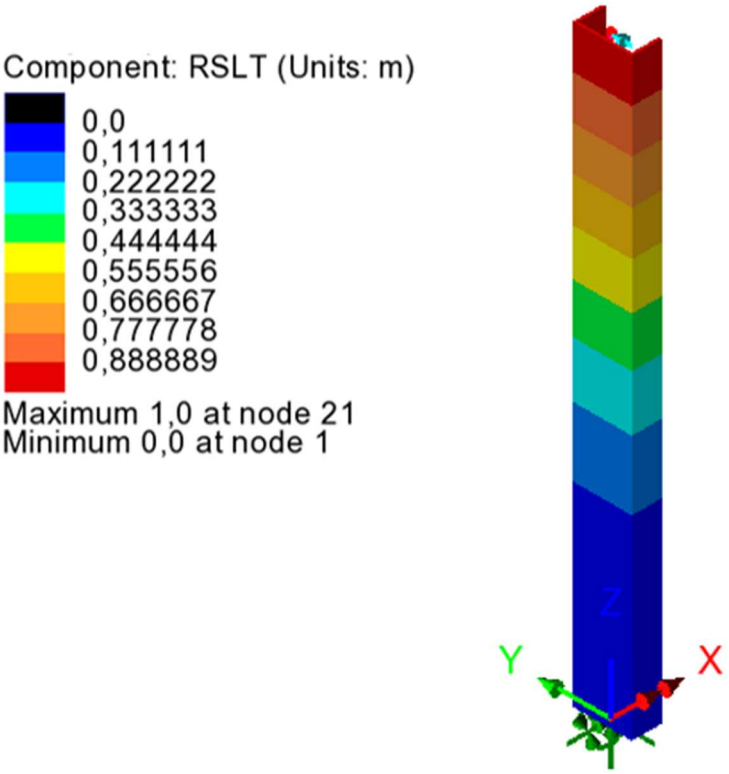

Figure 72: Total results of LUSAS analysis

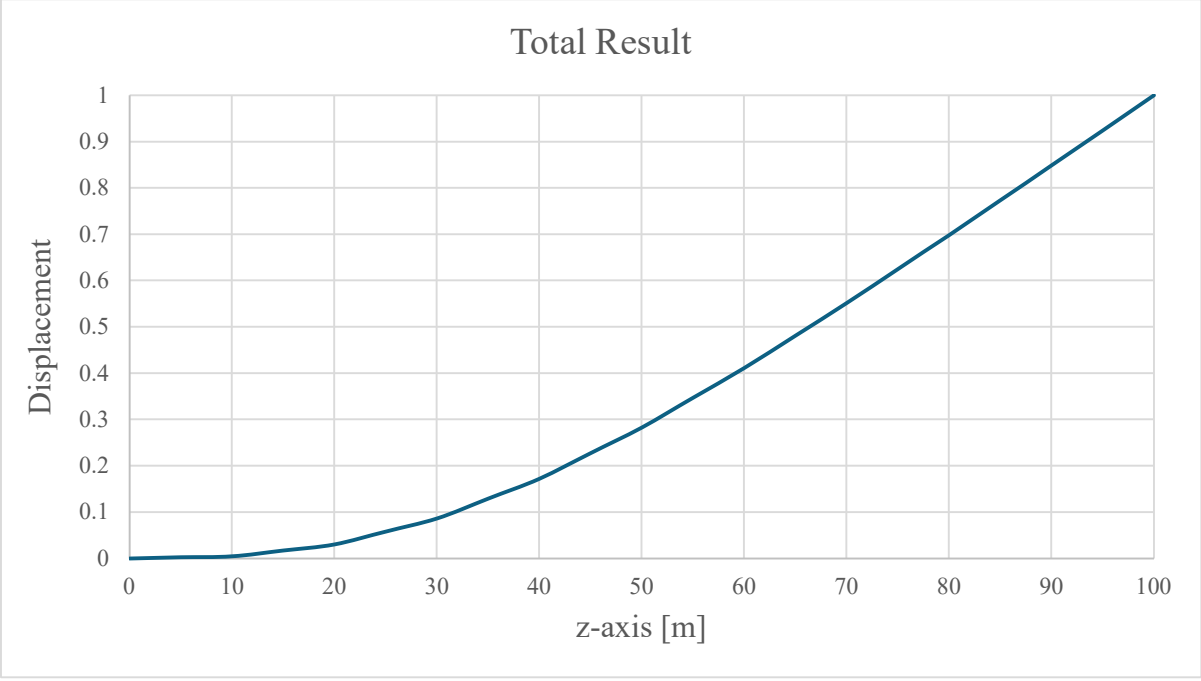

Figure 73: Total results of LUSAS analysis in graph form

7.16 Example 3: Circular Cross-Section

Defined along the *z*-axis a circular cross-section and considering m = 100. The dimension of the section has been reported in *Fig. 74*:

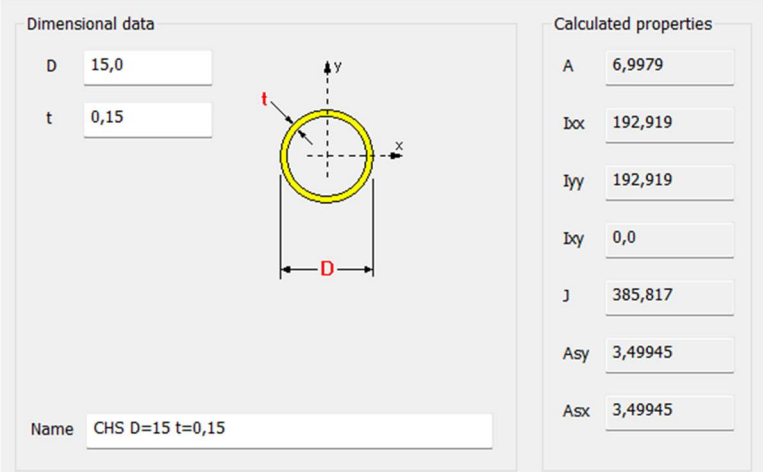

Figure 74: Characteristics of the section of the model

A distributed load has been applied.

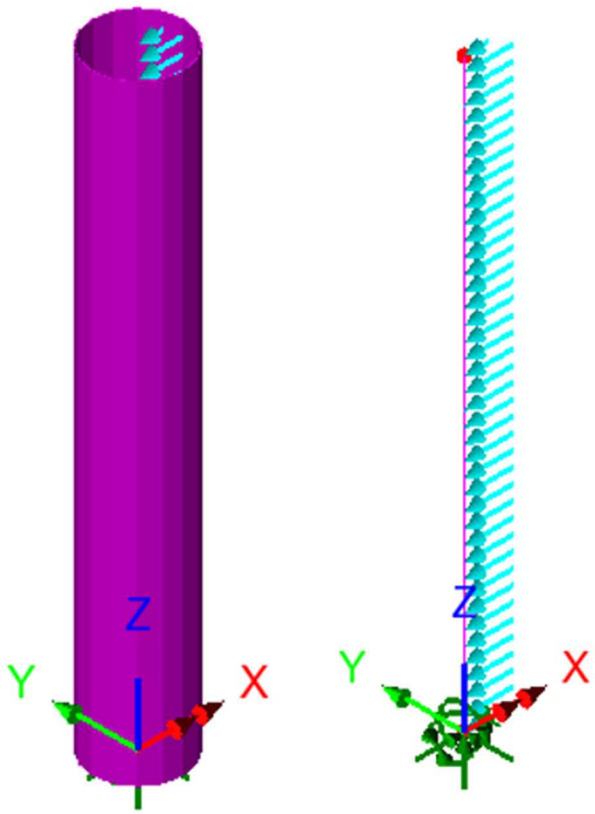

Figure 75: Model and applied load

The results are the following:

LUSAS

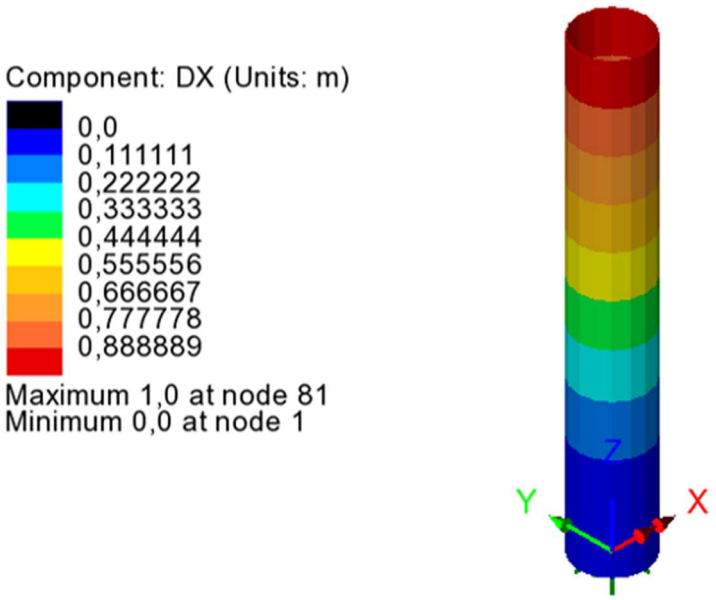

Figure 76: Uc computed by LUSAS software

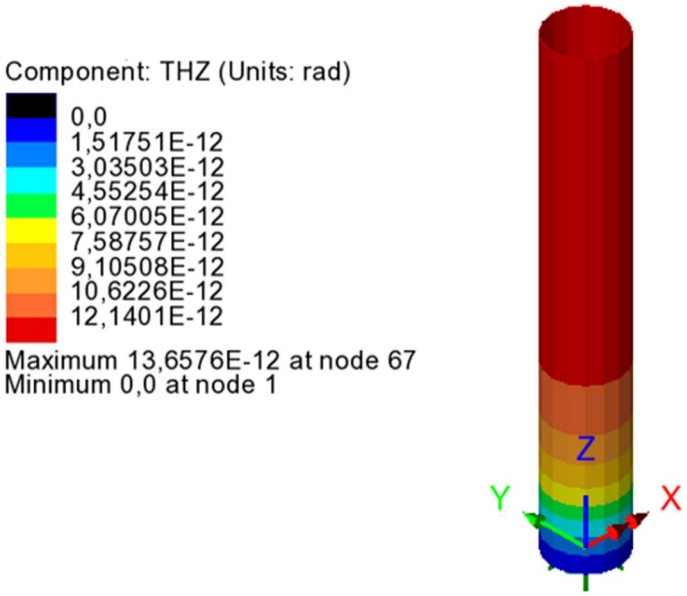

Figure 77: θ computed by LUSAS software

Initial load (total global distributed load): -10000 N

Load amplification factor: 7.14524 E+05

Buckling load: 7.14524 E+09 N

MATLAB

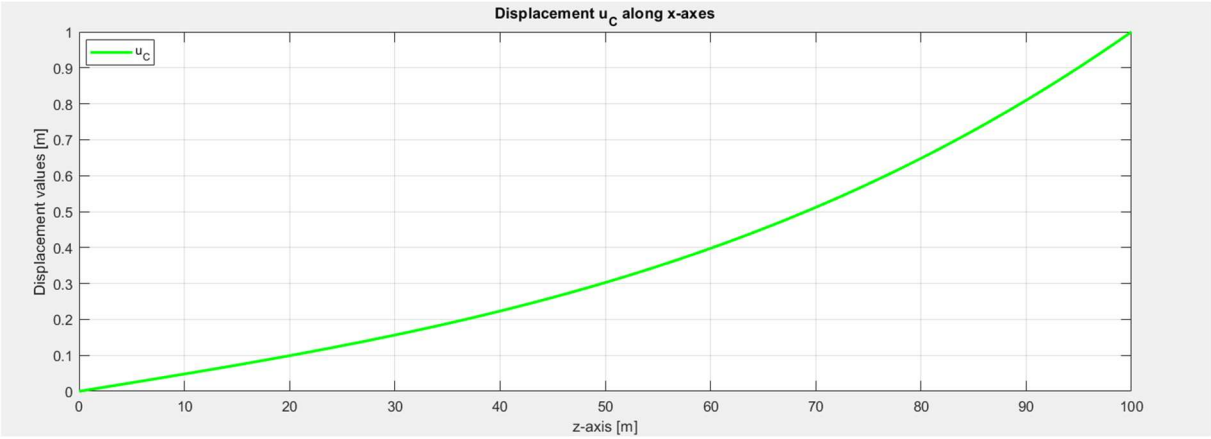

Figure 78: uc displacement from Matlab analysis

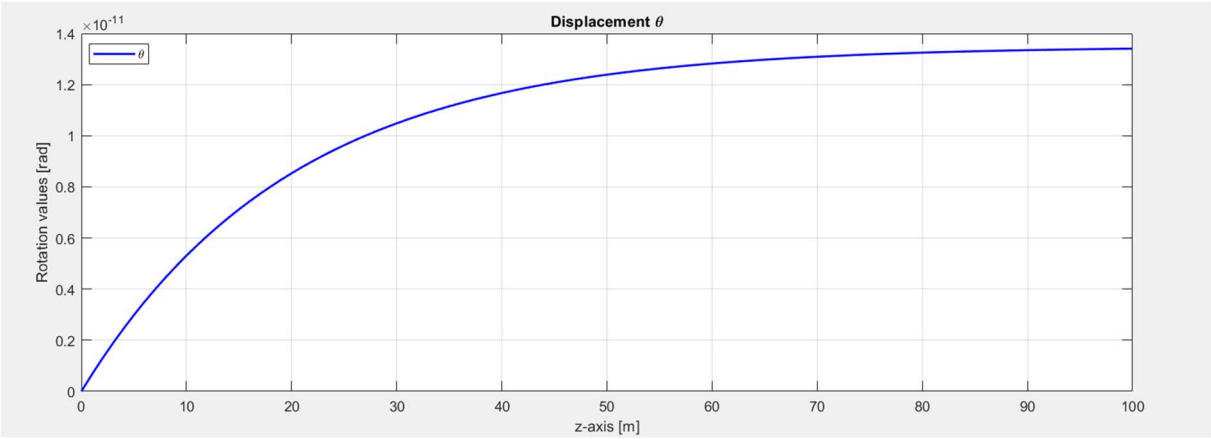

Figure 79: θ displacement from Matlab analysis

Initial load: 10 N/m

Load amplification factor: 7.14123 E+06

Buckling load: 7.14123 E+09 N

General results

Difference between the computed Buckling loads:

Percentage difference between buckling loads: 0,056%

Displacement along x:

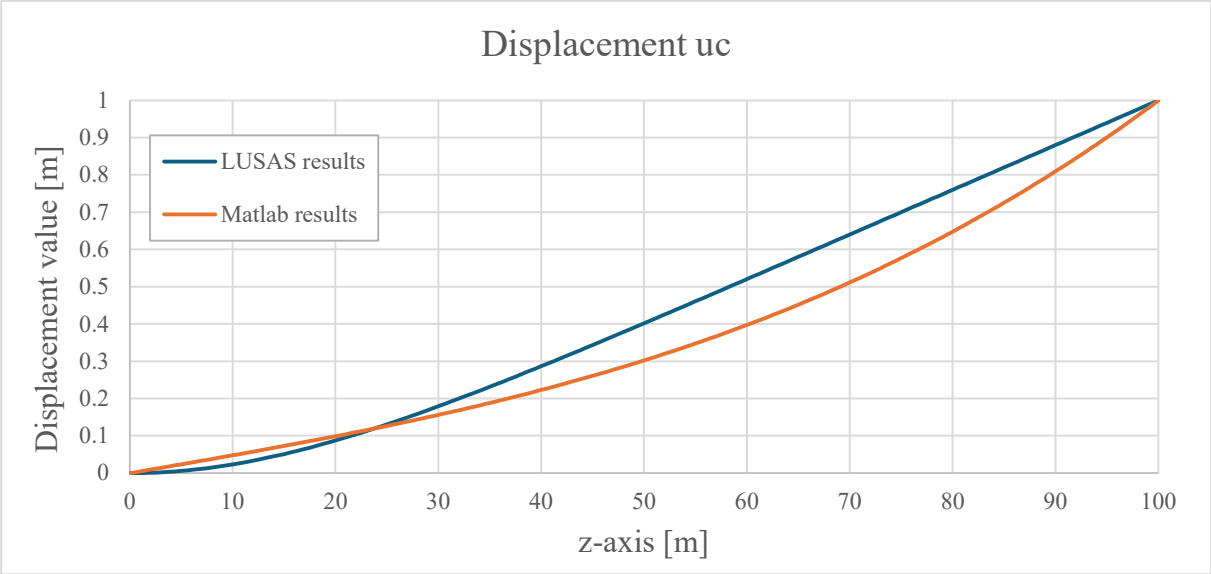

Figure 80: Comparison between LUSAS and Matlab results about uc

Rotation about z:

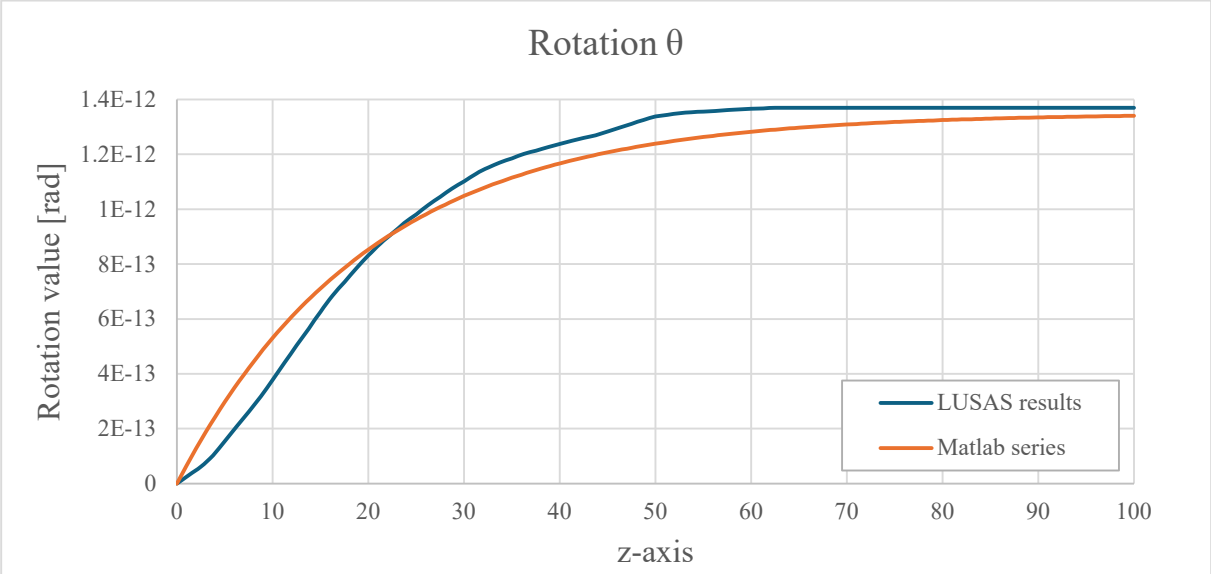

Figure 81: Comparison between LUSAS and Matlab results about θ

Through LUSAS, the total result of the movements was also highlighted

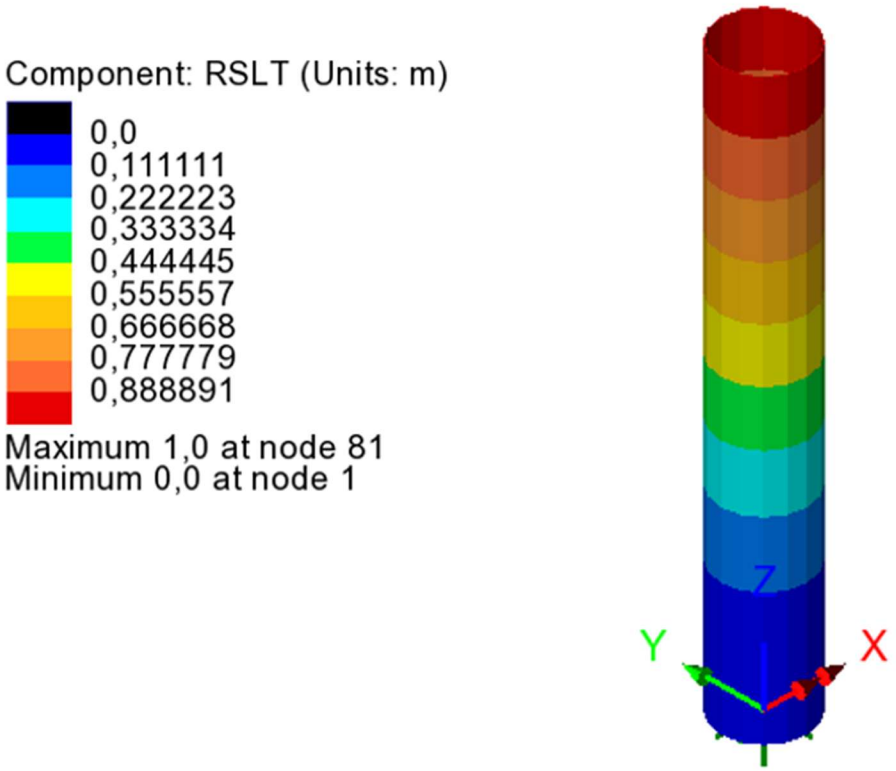

Figure 82: Total results of LUSAS analysis

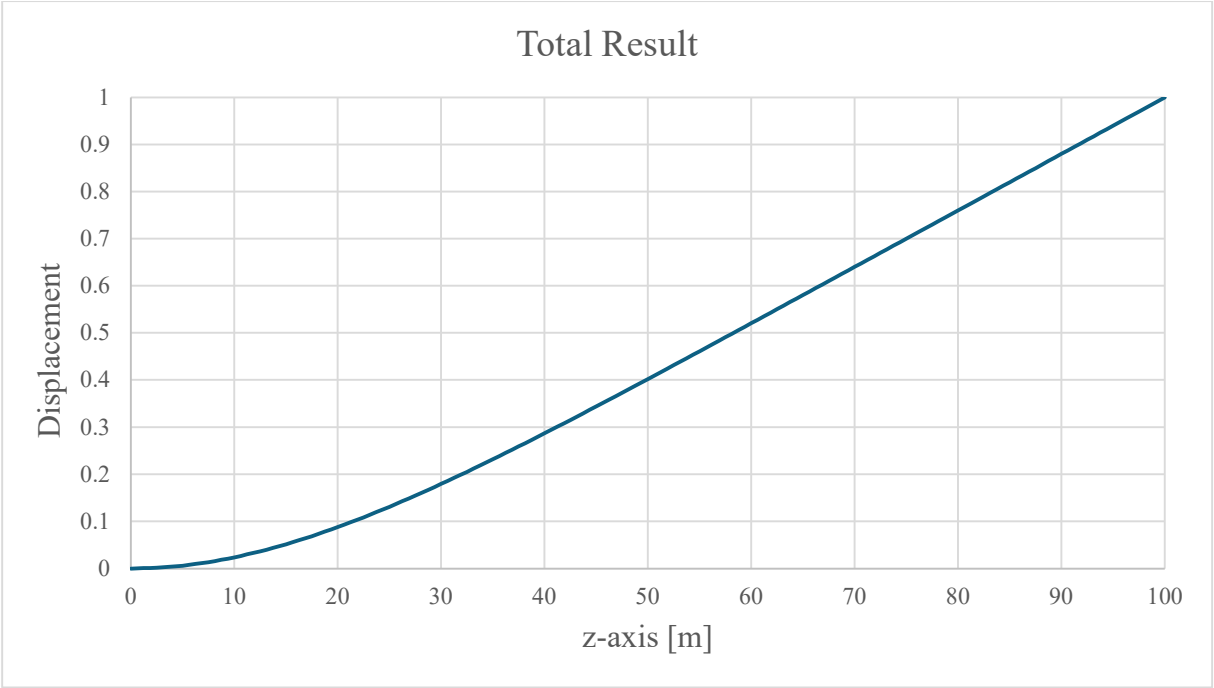

Figure 83: Total results of LUSAS analysis in graph form

7.17 Final Observations about the Results

The buckling analysis on the open thin sections, conducted using finite element analysis, allowed to determine the critical values of displacement u_c and rotation θ under a distributed horizontal load to simulate wind pressure.

The analyses confirmed structural deformation was fully consistent with the boundary conditions enforced, specific to the interlocked beam with no governing torsional restraints conditions also confirmed the fidelity of the FEM model back to the original initial condition.

It was demonstrated from the plots illustrated above, and at the paragraphs 6.4 to 6.8 on each occasion the values of u_c at point of critical state were always equal to and less than 1, as expected, indicating linear buckling analysis characteristic normalization, that was replicated in the Matlab code faithfully, where both values were intended to act as representations to the mode of buckling shape, based on a fixed maximum displacement value of 1 for ease of interpreting purposes: this value isn't a physical absolute amplitude, but rather a relative deformation to the critical load factor calculated.

As expected at this stage, it was demonstrated that the model was able to replicate critical behavior of open thin sections under distributed loads and provided adequate confidence to assess structural stability.

Future research could include the combinations of multiple level complexities and including torsion constraints, analysis of moving load systems, or other irregular or generic cross sections.

For example, a study could be done to characterize the difference in behavior between a wedged-free beam with a thin open C-section and a wedged-free beam that has a closed section locally, using the interfloors.

In this instance the model should be updated in several ways, such as considering potential differences of stiffness and materials between the C-section and the interfloors.

In addition to performing this analysis for this type of structure on LUSAS, a Modeling with plate elements should be performed and a section with different features than those of the beam should be defined to be assigned only in the summaries where the inter-storey is inserted.

An example of this kind of modeling would incorporate elements "flat thin shell".

The geometrical and material data are the following:

- Height: 100 m
- Flanges: 5 m
- Web: 10 m
- Elastic modulus: $210 \cdot 10^9$ N/mm^2.

Without inter-floor

Buckling load: 1212.9 N

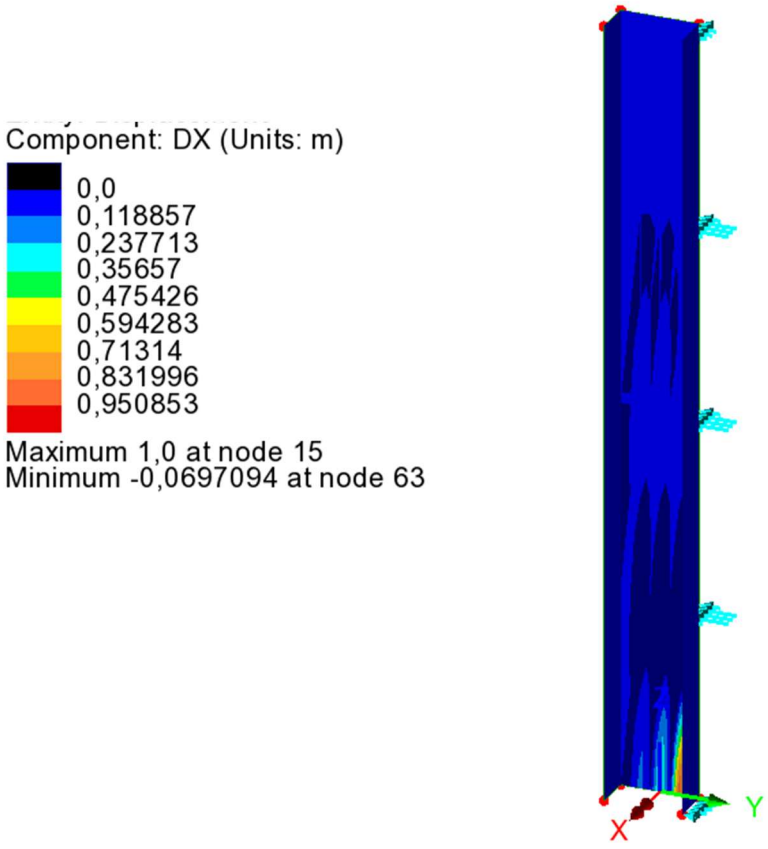

Figure 84: Deformation along x

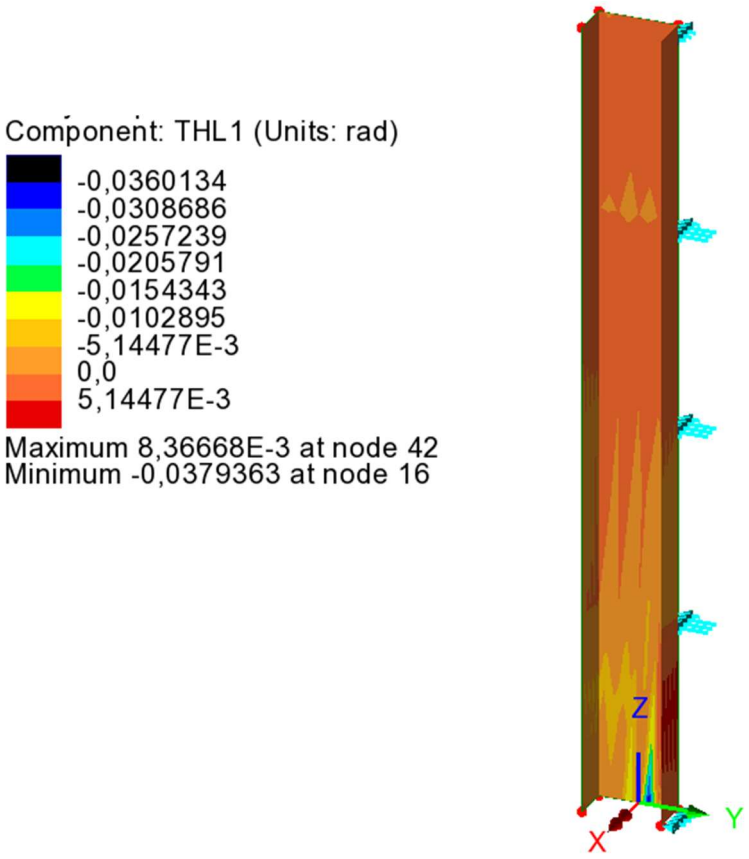

Figure 85: Rotation

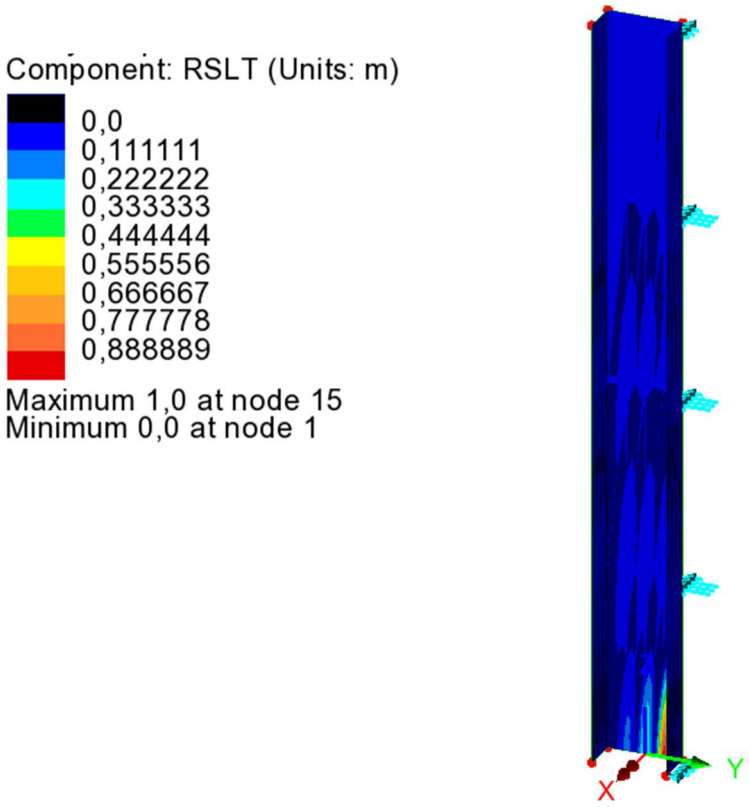

Figure 86: Total result of LUSAS analysis

One inter-floor at mid-span

Buckling load: 4825.48 N

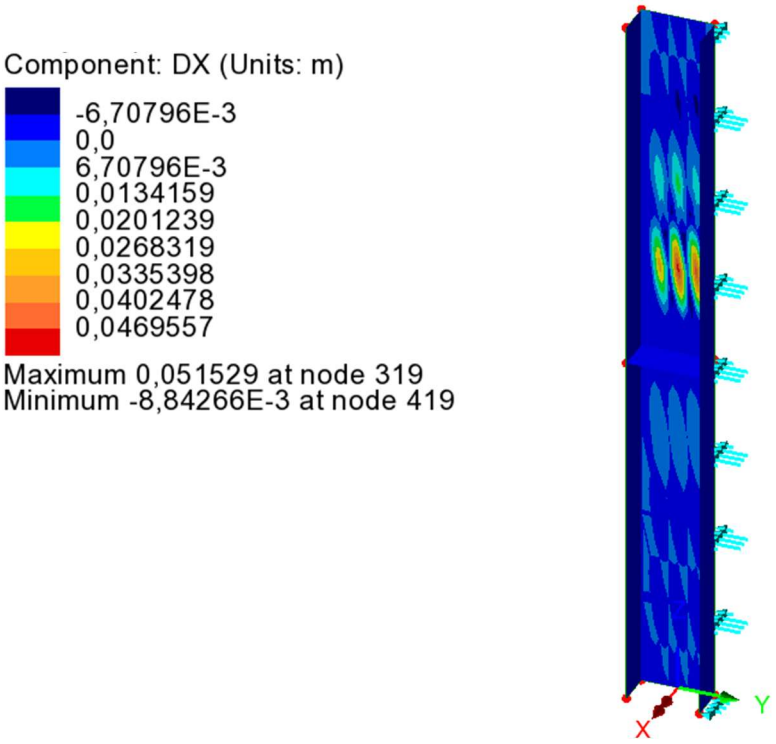

Figure 87: Displacement along x - one interfloor

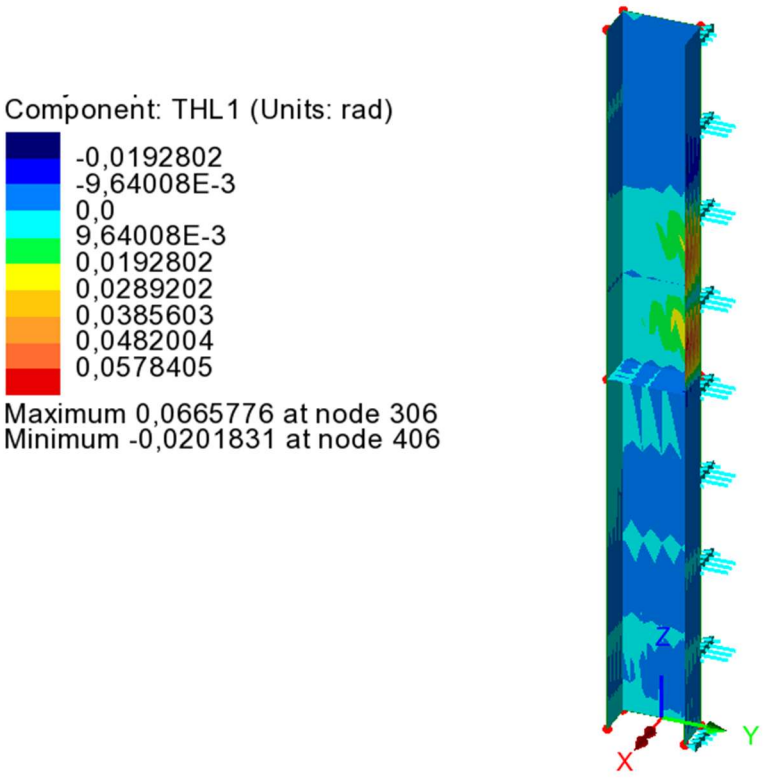

Figure 88: Rotation - one interfloor

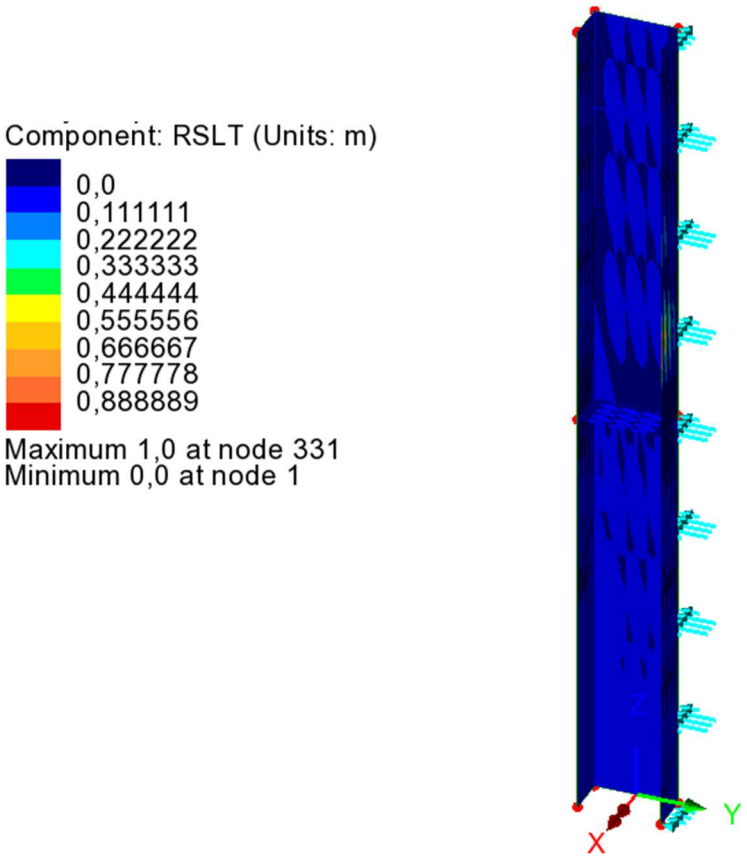

Figure 89: Total result of LUSAS analysis - one interfloor

The stiffer section decreases the free length of deflection and increases the overall stiffness and reduces the vulnerabilities of the member to global buckling.

The added stiffening also changes the mode of buckling; instead of buckling as one beam, the member is able to buckle into two independent segments with a node at the stiffening. This means a net result of more stiffness and less deflection overall.

The types of regional instability are:

- Wing Flaking: this is where the wings of the section may deflect laterally

- Core Flaking: this is where the core might deflect due to compressive load or shear

Finally, as the analysis is regarding a C-section, there is generally low torsional stiffness since it is an open section rather than a closed section, and therefore it is also vulnerable to torsional - flexural flexing.

The half-length stiffener applies an additional intermediate constraint on the free length to flex and thus increases overall stability.

The critical load can be increased by approximately 4 times on a single floor spacing with the single stiffener located at the centerline.

The next few pages outline two additional cases, one that includes the addition of a stiffener at the centerline and the top, and the second that has a stiffener every 25 m.

The results of both cases are outlined on the following pages.

Two inter-floors at mid-span and top

Buckling load: 9343.11 N

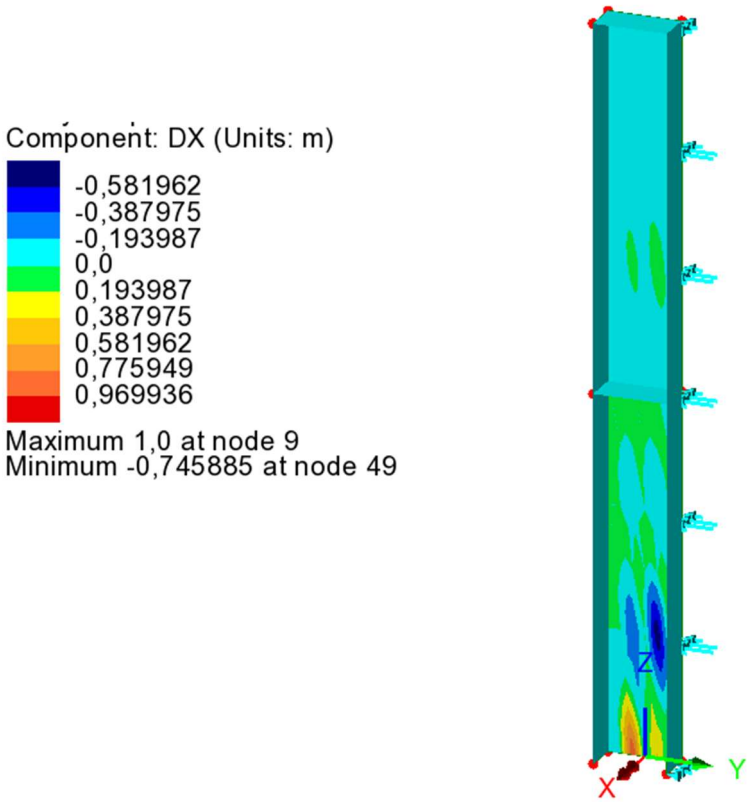

Figure 90: Displacement along x - two interfloors

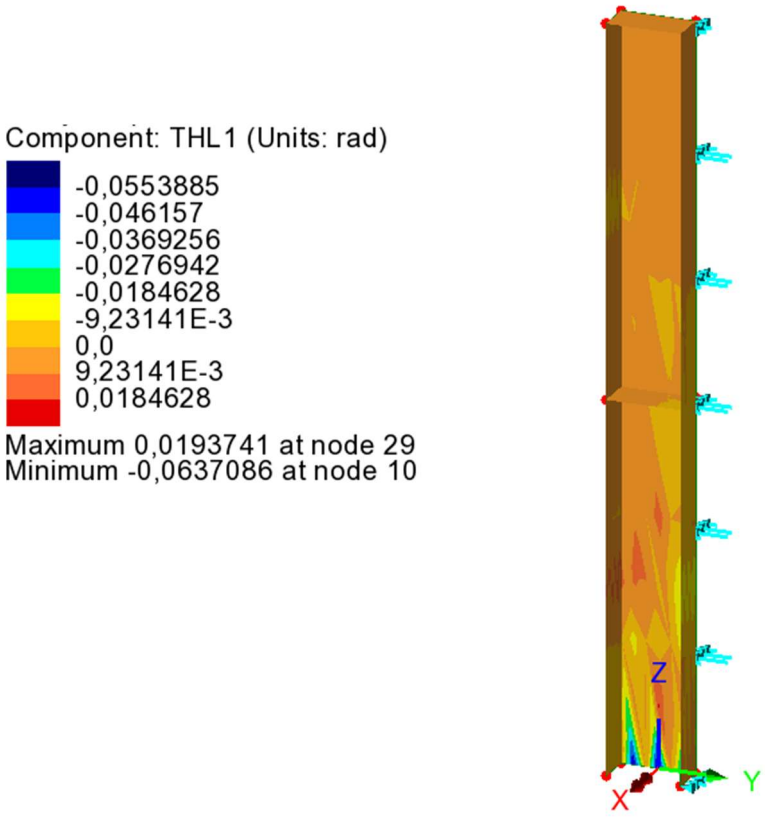

Figure 91: Rotation - two interfloors

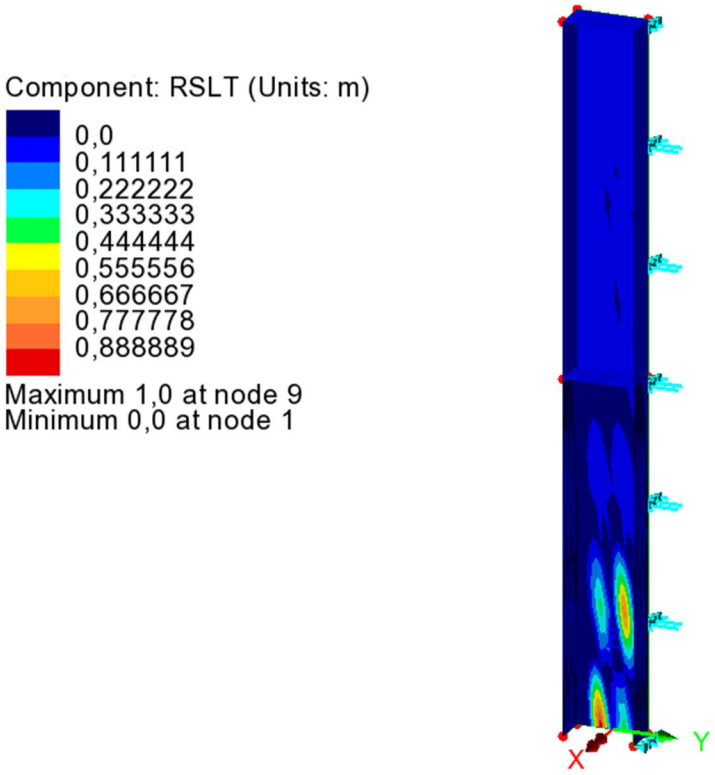

Figure 92: Total result of LUSAS analysis

Multiple inter-floors

Buckling load: 15722.5 N

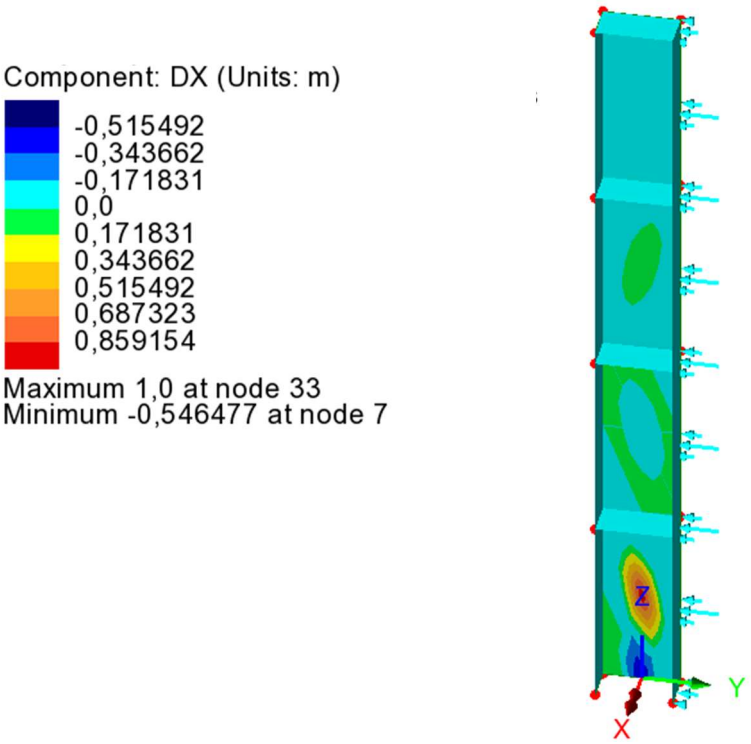

Figure 93: Displacement along x - four interfloors

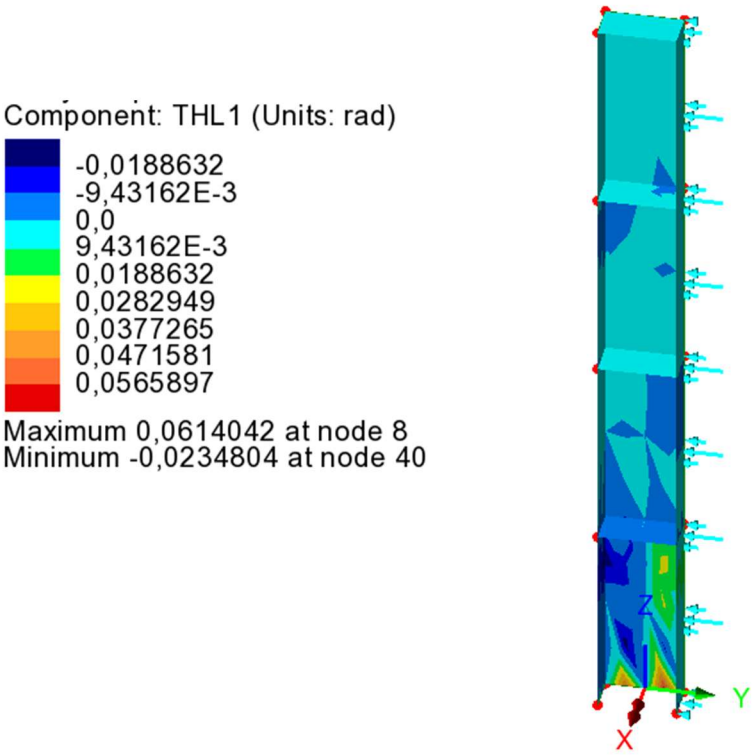

Figure 94: Rotation - four interfloors

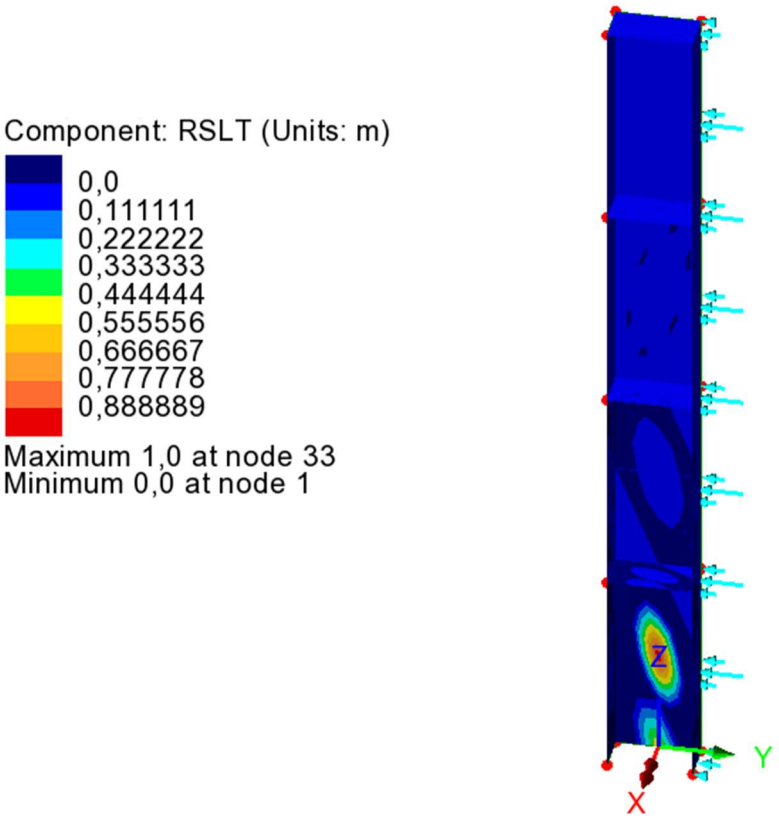

Figure 95: Total result of LUSAS analysis - four interfloors

The behavior of the beam structurally alters significantly with the addition of multiple stories to consider. With respect to the beam only, multiple stories are just more added constraints and distributed loads down through the height of the structure, which will change the structural behavior as follows:

- Increased Global Stiffness: each added floor adds additional rigidity to the overall structural system, as rigid diaphragms create more overall constructed rigidity, impacting the overall movement and the ability to resist bending and torsional stress.
- Load Distribution: each distributed load will now be distributed over multiple stories and therefore decrease the Stresses each individual story will see; however, there will now be considerably more expansive internal forces including shear forces and bending moments at the connections between stories and the beam.
- Local Effects: local effects i.e., concentrated stresses in the connection points or at the structural nodes etc., may become a concern from adding more stories and will need to be accounted for in a design if you want to mitigate instability or local failure.

- Changes in Modes of Vibration: as each added floor adds unsuspended mass, the vibration modes of the structure will be varied. More stories have a lower natural frequency which increases the dynamic behavior of the structure. The probability of the structure having sensitivity to some resonance phenomena or dynamic loading (wind load or seismic loading) will be more probable with more stories.

In conclusion, there are a number of ways the addition of multiple stories can change the structural behavior of the beam from mostly the increase in global stiffness, but complicating the issues of load distribution as well as considering local effects and overall dynamic behavior which will need adequate attention through the design and layering.

8. CONCLUSION

This Thesis, as mentioned above, aims to analyze structural stability, in particular when it involves thin-walled elements, e.g. C, L or Z profiles, widely used in lightweight structures due to their high strength/weight ratio, but which may be subject to buckling phenomena concerning local and global stability.

These types of sections are critical for designing slender structures such as skyscrapers; in fact, their vulnerability to global instability, such as the lateral or torsional instability, requires careful analysis to ensure safety and strength, as required by Eurocodes or other Standards, to avoid design errors and comply with safety requirements. In addition, under dynamic or seismic loads, these sections can be subject to amplified buckling, making the study of stability essential to prevent structural collapse.

Over time, several theories have been developed for the study of the stability of open thin sections, such as Vlasov's theory. Nowadays, it is possible to use new tools, like Finite Element Analysis, to solve these kinds of engineering problems. At the same time, simplified analytical and numerical models can help in the preliminary design phase as they can provide rapid, approximate solutions.

In connection to this, the Thesis focused on the implementation of a Matlab code to analyze buckling of uni-dimensional open thin-walled profiles subjected to various loading and boundary conditions; as an application, tall building structures were considered, providing a global view of the effects due to wind and seismic loads. The results obtained by the formulation implemented were compared with others available in literature or with those obtained with a commercial finite element program.

Thanks to the Finite Element Method, the buckling analysis of the open thin sections was conducted, allowing for the determination of the critical values of displacement and rotation under different loads, giving a structural deformation that was fully consistent with the boundary conditions enforced.

An aspect to take into account is that, in the context of linear buckling analysis, a characteristic normalization has been applied, so the values of u_c at the point of critical state were always equal to or less than 1; obviously, this value isn't a physical absolute amplitude, but rather a relative deformation to the critical load factor calculated.

As expected at this stage, it was demonstrated that the model was able to replicate critical behavior of open thin sections under different loads, providing adequate confidence to assess structural stability.

As regards tall building structures, the code was applied to analyze the elastic stability of a tapered stepped narrow rectangular section, of a uniform C-section, and of a uniform circular section, subjected to distributed transverse load.

It must be taken into account, however, that the limit of this type of analysis is that it can be difficult to implement the behavior of the structure and discretize in finite elements on calculation software such as Matlab, obtaining results from numerical analysis that could differ from analytical or real ones.

Furthermore, since analytic theories have basic simplifications and assumptions, when they are implemented on a numerical computing software such as Matlab, there is a risk of obtaining incorrect results due to the accumulation of approximations; in fact, the basic assumptions of the theory, such as linear elasticity or the absence of imperfections, are combined with the hypotheses and limitations of numerical algorithms, such as discretization and rounding errors, as well as convergence problems: all these problems can lead to results that do not accurately represent the real behavior of the system.

To conclude, in the last part of the Thesis, an analysis of the possible future development of the work has been performed. In particular, a code could be implemented to characterize the difference in behavior between a wedged-free beam with a thin open C-section and a wedged-free beam that has a closed section locally, using the interfloors, taking into account potential differences in stiffness and materials between the C-section and the interfloors.

In addition, future research development could involve the combination of various factors influencing structural behavior, such as the inclusion of torsional restraints under different loading conditions. Another interesting analysis could concern the response of systems subjected to moving loads, carrying out an investigation of the dynamic effects and their interaction with structural stability. Also, other possible developments could be to examine irregular or generic cross-sections, to better understand how unconventional shapes respond to various types of loads and constraints. These advances would contribute to a more comprehensive understanding of structural behavior under complex and realistic conditions.

ACKNOWLEDGMENTS

This thesis marks the conclusion of my academic journey and prompts me to reflect on the past five years.

They were, without a doubt, the strangest and most revolutionary years of my life: full of unexpected turns and continuous and radical changes that I never thought I could face.

University was a unique experience, for better or for worse.

“Engineering” changes you radically because, already after the first week you understand that the concept of “time” you had had up to that moment has suddenly lost its meaning and in order not to be left behind you change everything about yourself: your priorities, your mindset, your way of approaching life.

The university took everything I had: my hobbies, my friends, even a part of my personality. Yet, in what seemed to be a twist of fate, it also gave me the most important thing I have: the love of my life, the person without whom I would have given up everything a long time ago, my rock, my Home.

Precisely for this reason, first of all, I want to thank Gianluca, without whom I would not be here today, but probably I would not have been here in the future either. I am grateful to have experienced all this with you, for better or for worse. Above all, I am happy that, despite all the challenges we have had to face in the academic world, we managed to support each other, grow, and change on a personal level.
Thank you, I Love You.

A special thanks also goes to Gianluca's parents, who in recent years have been like a second family to me, who welcomed me from the first moment without hesitation.

I also want to thank my parents, without whom I would not have been able to face this path.

My gratitude also goes to my supervisors for their guidance and support during this work.

However, I don't feel like concluding this journey by simply celebrating the goal achieved, forgetting the obstacles I encountered along the way.

Most of the time, “Engineering” feels like a fight for survival, in which you have to fight with all your strength to achieve the goal.

I sincerely hope that in the future there will be a change and that the faculty of engineering will be structured in a way that allows students to maintain a balance between study and personal time.

Finally, I cannot conclude this journey without addressing an issue that remains largely overlooked: sexism, which continues to permeate our society.

In a field like civil engineering, where women are still significantly underrepresented, gender discrimination remains an undeniable reality, especially in the workplace.

However, I believe that the value of a person must be recognized for their skills, commitment and passion, rather than being influenced by prejudices.

It is necessary to continue working to build a more equitable society, in which everyone has the same opportunities to grow and contribute to the creation of a better, fairer and supportive world.

"It is not just about breaking the glass ceiling, but about changing the entire structure of the system." (Audre Lorde)

REFERENCES

[1] "Structural stability", STRUCTURAL ENGINEER, URL: https://www.thestructuralengineer.info/education/structural-analysis/struc stability, [Access: 25/11/2024]

[2] N. Augenti, *LEZIONI DI STABILITÀ DELLE STRUTTURE*, Napoli, IT: ILARDO & c. s.a.s., 1993.

[3] Prof. D. Zaccaria, *FONDAMENTI DI STABILITÀ DELLE STRUTTURE ELASTICHE*, Dipartimento di Ingegneria Civile, Università di Trieste, 31/05/2005.

[4] E. M. Lui, "Structural Stability", *STRUCTURAL ENGINEERING AND STRUCTURAL MECHANICS*, Department of Civil & Environmental Engineering, Syracuse University, Syracuse, NY 13244-1240 USA

[5] Edgard Sousa Junior, "ANÁLISE DA INTERAÇÃO ENTRE NÚCLEOS ESTRUTURAIS E LAJES EM EDIFÍCIOS ALTOS", Escola de Engenharia de São Carlos, da Universidade de São Paulo, como parte dos requisitos para obtenção do título de Doutor em Engenharia de Estruturas. São Carlos, 2001

[6] NTC2018

[7] A. ALSOFI, A GRAHN, *Design Methodology for Evaluation of Global Stability in Structural Systems*, Master's thesis in Structural Engineering and Building Technology, CHALMERS UNIVERSITY OF TECHNOLOGY Department of Architecture and Civil Engineering, Gothenburg, Sweden, 2017

[8] "What is Linear Analysis and Nonlinear Analysis: Introduction", Vedantu, URL: https://www.vedantu.com/jee-main/maths-difference-between-linear-and-nonlinear-analysis, [Access: 10/12/2024]

[9] "What is FEM in Structural Analysis?", SDC VERIFIER, URL: https://sdcverifier.com/structural-engineering-101/fem-in-structural-analysis/#:~:text=Finite%20Element%20Method%20(FEM)%20is%20a%20numerical%20approach%20that%20divides,behavior%20of%20the%20entire%20structure, [Access: 10/12/2024]

[10] “Bifurcation theory”, Wikipedia, 28 January 2025 21:24 UTC [Online], URL: https://en.wikipedia.org/wiki/Bifurcation_theory#:~:text=Most%20commonly%20applied%20to%20the,topological%20change%20in%20its%20behavior, [Access: 25/02/2025].

[11] A. Luongo, M. Ferretti, S. Di Nino, *Stability and Bifurcation of Structures (Statical and Dynamical Systems)*, 1st edition: Springer Nature Switzerland AG 2023

[12] G. Lacidogna, “STATIC AND DYNAMIC INSTABILITY OF STRUCTURES” slides, Static course material, DISEG, Politecnico di Torino, 2024.

[13] Università Mediterranea, “Edifici alti”, rif: 1464_2023_576_41919.pdf

[14] M, Zeeshan, M, Sadiq, M, Mazhar, A, Khan, “THE STABILITY OF HIGH-RISE BUILDINGS”, International Journal of Advance Research in Science and Engineering, Volume NO.07, Issue No.10, October 2018.

[15] RGM College of Engineering and Technology, “Shear Center” – https://www.rgmcet.edu.in/assets/img/departments/CIVIL/materials/R19/2-2/SM-II/unit-5.pdf

[16] E. Cacciamanni, *Torsional buckling of open thin-walled beams*, Università Politecnica delle Marche, Facoltà di Ingegneria, Corso di Laurea Triennale in Ingegneria Edile, A.A. 2018/2019.

[17] “La progettazione degli edifici a grande altezza”, ingenio (informazione tecnica e progettuale) URL: https://www.ingenio-web.it/articoli/la-progettazione-degli-edifici-a-grande-altezza/, [Access: 25/02/2025].

[18] T. K. Makarios and A. Athanatopoulou, “Center of Stiffness, Principal Axes and Principal Start Point of Thin-Walled Open-Sections of Cores: A New Modified Calculation Technique Based on Vlasov Torsion Theory”, Institute of Structural Analysis and Dynamics of Structures, School of Civil Engineering, Aristotle University of Thessaloniki, GR54124 Thessaloniki, Greece, MDPI, *Buildings* 2022, *12*(11), 1804, URL: https://doi.org/10.3390/buildings12111804

[19] “Travi Multimateriale”, Travi Complesse V1-6, [SCRIBD], URL: https://it.scribd.com/document/369358095/Travi-Complesse-V1-6, [Access: 03/03/2025]

[20] “SEZIONI A PARETE SOTTILE SFORZI TANGENZIALI E CENTRO DI TAGLIO”, Università degli Studi di Cagliari, URL: https://web.unica.it/static/resources/cms/documents/Traviaparetesottilecentroditaglioesforzitangenziali.pdf

[21] M. Ganz, “Finite Element Method I – Getting Started”, Department of Computer Science, Faculty of Science, University of Copenhagen, 11/01/2010, URL: http://image.diku.dk/ganz/Lectures/fem_slides_mel.pdf

[22] “Metodo degli elementi finiti”, Wikipedia, 22 December 2024 19:06, URL: https://it.wikipedia.org/wiki/Metodo_degli_elementi_finiti, [Access: 05/03/2025].

[23] A. Bacchetto, “INTRODUZIONE AL METODO DEGLI ELEMENTI FINITI E ALLA MODELLAZIONE FEM”, URL: https://www.ingegneriastrutturale.net/documenti/articoli/adepron13_0012.pdf.

[24] “FEM - Finite Element Method”, ingenio (informazione tecnica e progettuale) URL: https://www.ingenio-web.it/articoli/topic/fem-finite-element-method/?page=3, [Access: 05/03/2025].

[25] P. Mendis, T.Ngo, N. Haritos, A. Hira, B. Semali, J. Cheung, “Wind loading on tall buildings”, Electronic Journal of Structural Engineering, 2007, 7 pp. 41 – 54, 2007/12/01, URL: http://hdl.handle.net/10453/5822

[26] Franco Concli, “Il fenomeno dell’instabilità elastica”, ilprogettistaindustriale.it, 24/02/2023, URL: https://www.ilprogettistaindustriale.it/quaderni-di-progettazione-il-fenomeno-dellinstabilita-elastica/

[27] Michael Gremingher, “Calculating the Johnson-Euler Buckling Load”, The Official EngineeringPaper.xyz Blog, 29/06/2022, URL: https://blog.engineeringpaper.xyz/calculating-the-johnson-euler-buckling-load

[28] Università Mediterranea, “Elementi compressi”, rif: 1464_2014_377_20927.pdf

[29] “How can we determine stable and unstable equilibrium points from a potential energy versus displacement graph?”, PHYSICS, 4 June 2020, URL: https://physics.stackexchange.com/questions/384279/how-can-we-determine-stable-and-unstable-equilibrium-points-from-a-potential-ene [Access: 05/03/2025].